NON-INTRUSIVE EFFICIENCY ESTIMATION OF INVERTER-FED INDUCTION MACHINES

By

Mathews Chirindo

A thesis submitted to the department of Electrical Engineering, University of Cape Town, in complete fulfilment of the requirements for the degree of Doctor of Philosophy

October 2020

DECLARATION

This thesis is submitted to the Department of Electrical Engineering, University of Cape Town, in complete fulfilment of the requirements for the degree of Doctor of Philosophy. It has not been submitted before for any degree or examination at this or any other university. The author confirms that this thesis is based on his own work, save for which is duly referenced. A portion of this work has been published in a peer reviewed journal.

Signed: Signed by candidate Date: 18 October 2020

ABSTRACT

Motorised loads using induction machines use approximately 60% of the electricity globally. Most of these systems use three-phase induction motors due to their robustness and lower cost. They are often installed in continuously operating industrial plants/applications that require no operational interruptions. Whilst most of these induction machines are supplied from ideally sinusoidal supplies, applications are emerging where induction machines are fed from non-sinusoidal supplies. In particular, pulse width modulated inverters realize efficient control of induction machines in many automated industrial applications. From an energy management perspective, it is vital to continually assess the efficiency of induction machines in order to initiate replacement or economic repair. It is therefore of paramount importance that reliable and non-intrusive techniques for efficiency estimation of induction machines be investigated, that consider sinusoidal and non-sinusoidal supplies.

This work proposes a non-intrusive efficiency estimation technique for inverter–fed induction motors that is based on harmonic regression analysis, harmonic equivalent circuit parameter estimation and harmonic loss analysis using limited measured data.

Firstly, considerations for inverter-fed induction motor equivalent circuit modelling and parameter estimation techniques suitable for non-intrusive efficiency estimation are presented and the selection of one equivalent circuit for analysis is justified. Measured data is obtained from two different induction motors on a flexible 110kW test rig that utilises an HBM Gen 7i data acquisition system. By measuring voltage, current and input power at the supply terminals of the inverter-fed motor, the fundamental equivalent circuit parameters are estimated using population based incremental learning algorithm and compared with those obtained from the IEC 60034-2-1 Standard. The harmonic parameters are estimated using the bacterial foraging algorithm basing on the input impedance of the motor at each harmonic order. A finite harmonic loss analysis is carried out on the tested induction motors. The proposed techniques and harmonic loss analysis provide accurate efficiency estimates of within 1.5% error when compared to the direct method.

Lastly, a related non-intrusive efficiency estimation technique is proposed that caters for a holistic loss contribution by all harmonics. The efficiency results from the proposed techniques are compared to those obtained from the IEC-TS 60034-2-3 Technical

Specification and a direct method. The estimated efficiencies are comparable to those measured by the Technical Specification and a direct method within 2% error when tested on 37kW and 45kW PWM inverter-fed motors across the loading range.

Furthermore, this work conducts a comprehensive non-intrusive rotor speed estimation comparative analysis in order to recommend the best technique(s), in terms of intrusiveness, accuracy and computational overhead. Errors of less than 1% have been reported in literature and experimental verification when using vibration analysis, Motor Current Signature Analysis (MCSA), Rotor Slot Harmonic (RSH) and Rotor Eccentricity Harmonic (REH) analysis techniques in inverter-fed IMs.

ACKNOWLEDGEMENTS

The author would like to thank the following:

My supervisors, Professor Azeem Khan and Professor Paul Barendse for their guidance and support for the entire duration of the research study.

To Jamlick Murimi and John Mushenya for development of a specialised 110kW test rig and setting up for experimental data acquisition respectively.

To my family for unconditional love, support and patience while I used your precious time to pursue this study.

To National Research Foundation (NRF) for funding the research.

To Francois Kapp, NRF-SARAO Electronics Manager, thanks for your support of this organizational initiative.

TABLE OF CONTENTS

LIST OF FIGURES

LIST OF TABLES

LIST OF SYMBOLS

D_{max}	-	is the maximum amplitude value at the position of f_r
ε_{η}	-	is the relative error of the measured efficiency
ε_{Pi}	-	is the relative error of the measured input power
ε_{Po}	-	is the relative error of the measured output power
err	-	is the estimation error
ε_S	-	is the relative error of the measured speed
ε_T	-	is the relative error of the measured torque
f	-	is the frequency
f_{low}	-	is the lower boundary frequency
f_{syn}	-	is the synchronous frequency
f_r	-	is the rotor frequency
FR	-	is the frequency resolution
f_1	-	is the fundamental supply
f_h	-	is the hth order harmonic frequency
f_{sh}	-	is the rotor slot speed dependent harmonic frequency component
f_{ecc}	-	is the dynamic eccentricity harmonic frequency component
H	-	skin effect conductor height
h	-	is subscript for harmonic order
i_a	-	is the instantaneous phase current at phase a
i_b	-	is the instantaneous phase current at phase b
i_c	-	is the instantaneous phase current at phase c
IC_{Pi}	-	is the influence coefficient of input power
IC_S	-	is the influence coefficient of speed transducer
IC_T	-	is the influence coefficient of torque transducer
I_{meas}	-	is the measured line to line current
I_m	-	is the magnetic core phase current
$I_{m,est}$	-	is the estimated magnetic core phase current
I_r	-	is the rotor phase current
$I_{r,est}$	-	is the estimated rotor phase current
I_{rated}	-	is the rated current

$I_{no-load}$	-	is the no-load current
I_s	-	is the stator phase current
$I_{s,est}$	-	is the estimated stator phase current
I_{load}	-	is the machine load current
k	-	is 234.5 for 100% IACS conductivity copper, or 225 for aluminium, based on a volume conductivity of 62%
k_{ad}	-	is the assumed value of stray load loss recommended by IEEE 112
K_c	-	is classical eddy current loss constant
K_{exc}	-	is excess eddy current loss constant
k_{FW}	-	is the friction and windage constant
k_h	-	is a constant at the hth harmonic order
K_h	-	is hysteresis loss constant
K_{TH}	-	is the thermal coefficient in $°C/W$
L_{DC}	-	is the DC inductance
L_{AC}	-	is the AC inductance due to skin effect
m	-	is the number of phases
N_r	-	is the rotor speed in revolutions per minute
n_r	-	is the rotor speed in revolutions per second
N_{data}	-	is the number of data points
N_{low}	-	is the rotor speed in revolutions per minute at f_{low}
n_d	-	is the eccentricity order.
P	-	is the number of poles
P_c	-	is classical eddy current loss
P_{exc}	-	is excess eddy current loss
P_{FW}	-	is the friction and windage losses
$P_{FW,rated}$	-	is the rated friction and windage losses
$P_{FW,load}$	-	is the friction and windage losses at machine load
$P_{FW,no-load}$	-	is the friction and windage losses at no-load
P_{HL}	-	is the total harmonic losses
P_i	-	is the electrical input power
$P_{i,est}$	-	is the estimated electrical input power
$P_{i,meas}$	-	is the measured electrical input power
$P_{i,no-load}$	-	is the input power at no-load

$P_{i,PWM}$ - is the input power using PWM inverter supply

P_k - is the constant losses

$P_{k,harm}$ - is the constant additional harmonic losses

$P_{k,PWM}$ - is the constant losses using PWM inverter supply

P_{losses} - is the machine total losses

$P_{losses,fund}$ - is the machine total losses due to the fundamental component

$P_{losses,PWM}$ - is the machine total losses using PWM inverter supply

P_o - is the mechanical output power

$P_{o,rated}$ - is the rated output power

P_r - is the total rotor loss

$P_{r,harm}$ - is total harmonic rotor loss

P_s - is the total stator loss

P_{SLL} - is the stray load loss

$P_{SLL,fund}$ - is stray load loss at fundamental frequency

$P_{SLL,harm}$ - is total harmonics stray load loss

$P_{SLL,PWM}$ - is the stray load loss using PWM inverter supply

$P_{s,no-load}$ - is the total stator loss at no-load

R_{AC} - is the AC resistance due to skin effect

R_{DC} - is the DC rotor bar resistance

r_{HL} - is the harmonic loss ratio

R_m - is the core loss equivalent resistance

R_r - is the rotor resistance

R'_r - is the corrected rotor resistance

R_s - is the stator resistance

R'_s - is the corrected stator resistance

R_{SLL} - is the stray load loss resistance

s - is the machine slip

s_{meas} - is the measured machine slip

s_{rated} - is the rated machine slip

SR - is the sampling rate

s_{load} - is the slip in per unit., measured at stator winding temperature, T_{load}

T - is the torque

T_{ag}	-	is the air gap torque
T_{amb}	-	is the ambient or reference temperature
T_{load}	-	is the temperature of the winding at machine load to which the resistance is to be corrected (in ℃)
$T_{load,est}$	-	is the estimated temperature of the winding at machine load
T_{meas}	-	is the measured shaft torque
$T_{no-load}$	-	is the winding temperature at no-load
V_{meas}	-	is the measured line to line voltage
$V_{no-load}$	-	is the no-load voltage
V_{rated}	-	is the rated voltage
$v_{ca}, v_{ab}\ v_{bc}$	-	are the instantaneous line-to-line voltages
V_s	-	is the supply phase voltage
X_s	-	is the base stator leakage reactance
X_r	-	is the base rotor leakage reactance
X_m	-	is the base core leakage reactance
$\vec{Y}_s$	-	is the complex stator admittance
$\vec{Y}_r$	-	is the complex rotor admittance
$\vec{Y}_c$	-	is the complex core admittance
$\overline{Z}_b$	-	is the complex base input impedance
$\vec{Z}_s$	-	is the complex stator impedance
$\vec{Z}_r$	-	is the complex rotor impedance
$\vec{Z}_c$	-	is the complex core impedance
η	-	is the motor efficiency
δ	-	is the skin effect depth
ξ	-	is the ratio of conductor height to skin depth in skin effect
β	-	is the Steinmetz constant
α	-	is the temperature coefficient of resistance
z	-	is the number of rotor slots
λ	-	is the order of the space harmonic
ΔT	-	is the rated temperature minus ambient temperature
ω_1	-	is the supply fundamental frequency in radians per second
ω_r	-	is the rotor speed in radians per second

$\omega_{r,meas}$	-	is the measured rotor speed in radians per second
$\omega_{r,load}$	-	is the rotor speed at machine load in radians per second

NOMENCLATURE

A	Ampere(s)
AC	Alternating Current
BFA	Bacterial Foraging Algorithm
BFOA	Bacterial Foraging Optimization Algorithm
dB	Decibel(s)
CDMs	Complete Drive Modules
DC	Direct Current
DTC	Direct Torque Control
EASA	Electrical Apparatus Service Association
EISA	Energy Independence and Security Act
EMF	Electro-motive Force
EPAct	Energy Policy Act
FEA	Finite Element Analysis
FEM	Finite Element Method
FOC	Field Orientation Control
FFT	Fast Fourier Transform
GA	Genetic Algorithm
HBM	Hottinger Baldwin Messtechnik
Hz	Hertz
IACS	International Annealed Copper Standard
IEC	International Electrotechnical Commission
IEC-TS	International Electrotechnical Commission Technical Specification
IEEE	Institute of Electrical and Electronics Engineers
IEPE	Integrated Electronics Piezo Electric
IM	Induction Motor
JEC	Japanese Electrotechnical Committee
kS/s	Kilo Samples Per Samples
kW	Kilo Watt(s)
MCSA	Motor Current Signature Analysis
MCFT	Maximum Covariance method for Frequency Tracking

MEE	Maximum Error Estimation
MMF	Magneto Motive Force
MSA	Minor Space Analysis
MSE	Mean Square Error
MS/s	Mega Samples Per Samples
MUSIC	Multiple Signal Classification
NEMA	National Equipment Manufacturers Association
NI	Non-Intrusive
NIEE-PWM	Non-Intrusive Efficiency Estimation – Pulse Width Modulation
OHME	Ontario Hydro Modified Method E
PBIL	Population Based Incremental Learning
PDSs	Power Drive Systems
PSO	Particle Swarm Optimization
PWM	Pulse Width Modulation
REE	Realistic Error Estimation
REH	Rotor Eccentricity Harmonic
RLS	Recursive Least Squares
RMS	Root Mean Square
rpm	Revolutions Per Minute
RSH	Rotor Slot Harmonic
STFT	Short Time Fourier Transform
THD	Total Harmonic Distortion
V	Volt(s)
VDF	Voltage Distortion Factor
VSD	Variable Speed Drive

Chapter 1

INTRODUCTION

1.1. Background

Motorised systems consume approximately 60% of the electricity globally in various applications. Most of these systems use three-phase induction motors due to their robustness and lower cost. It is therefore important, from an energy management point of view, to continually assess the efficiency of induction machines.

Legislative bodies, in some instances, enforce the use of efficient induction machines in various sectors, for instance, the Energy Independence and Security Act (EISA), 2007 [1] is a new legislative policy that regulates, among other things, the efficiency of motors that can be legally bought or sold in the United States. The EISA builds on the previous Energy Policy Act (EPAct) of 1992 [2], and updates mandated standards from 1 hp to 500 hp that are manufactured for sale in the United States.

Existing induction machine efficiency testing standards are accurate at the expense of their intrusive nature. Besides, they are targeted for use on mains fed machines. However, the need for inverter-fed machines is growing in most automated systems. The impact of these inverter supplies is that additional losses are incurred in the induction machine due to voltage and current harmonic components contained in the non-sinusoidal waveforms. The motivation for this research is the need to investigate these additional losses due to inverter supplies in order to determine inverter-fed induction machine efficiency, non-intrusively.

1.2. Problem Statement

The efficiency of induction machines have been determined by use of standard procedures such as IEEE 112, IEC 34-2-1, JEC 37 [3], [4]. These testing standards are ideal for induction machines fed from purely sinusoidal supplies. At the time of writing this thesis, there is no standard for determining the rated efficiency of inverter-fed induction machines. The IEC 61800-9-2:2017 Standard [5] allows evaluation of power losses of Complete Drive Modules (CDMs) and Power Drive Systems (PDSs) which is beyond the scope of this research. The IEC-TS 60034-2-3 [6], which focusses on the efficiency of inverter-fed machines is still a draft awaiting qualification to a standard. However, this Technical Specification and all the standard procedures require the machine to be tested under laboratory conditions with rigorous intrusive operations in order to determine

efficiency. This is not suitable for efficiency measurement/estimation of in-service induction motors. It is therefore imperative that new non-intrusive procedures be developed to estimate the efficiency of induction machines fed from inverter supplies. The development of a non-intrusive efficiency estimation technique for inverter-fed machines paves an opportunity to understand the machine harmonic losses. This can be utilized to develop even better techniques based on this knowledge base.

1.3. Research Questions

The main research question associated with this thesis is:

"How can the efficiency of an induction machine fed from a PWM inverter supply be determined in a non-intrusive manner?"

This question will be addressed through detailed consideration of each of the following secondary research questions:

- Which efficiency estimation technique(s) of an induction motor (IM) can be used non-intrusively with acceptable accuracy? This question is addressed in Chapter 2 of this thesis.
- How can the rotor speed be estimated in a non-intrusive manner when an induction machine is fed an inverter supply? This question is addressed in Chapter 3 of this thesis.
- How can the machine parameters be estimated in a non-intrusive manner when an induction machine is fed from an inverter? This question is addressed in Chapter 4 of this thesis.
- How can the additional harmonic losses be quantified in an inverter-fed induction machine? This question is addressed in Chapter 4 of this thesis.
- How can the operating temperature of an induction machine be suitably determined in a non-intrusive manner in order to suitably correct the stator and rotor resistances? This question is addressed in Chapter 4 of this thesis.
- Can the same developed efficiency estimation technique(s) of an induction machine be suitably used when the machine is fed from a sinusoidal supply and a PWM inverter supply? This question is addressed in Chapter 4 and Chapter 5 of this thesis.

- How does the efficiency results obtained from developed efficiency estimation technique(s) compare with those obtained from IEC-TS 60034-2-3? This question is addressed in Chapter 5 of this thesis.

1.4. Objectives

The objectives of this thesis are to:

- Conduct an extensive literature survey on efficiency estimation of inverter-fed IMs including the quantification and impact of additional losses caused by harmonics in the inverter supply.
- Investigate, compare and recommend an appropriate rotor speed estimation technique(s) suitable for non-intrusive efficiency estimation of IMs based on literature review and experimental verification.
- Investigate and implement the appropriate parameter estimation technique suitable for non-intrusive efficiency estimation based on experimental data and equivalent circuit models of IMs.
- Perform harmonic analysis, determine harmonic parameters and present harmonic loss analysis based on experimental data from inverter-fed IMs.
- Develop and implement non-intrusive efficiency estimation technique(s) suitable for inverter-fed IMs and compare the results to those obtained using IEC-TS 60034-2-3 Technical Specification.
- Draw conclusions and make recommendations based on the findings presented in the thesis.

1.5. Scope and Limitations

Due to time and equipment constrains, this research focusses on the non-intrusive efficiency estimation of inverter-fed motors operated at rated frequency and the inverter operating at one switching frequency. The estimation of fundamental and harmonic parameters including fundamental and harmonic loss analysis thereof is performed for two inverter-fed induction motors. Rotor speed estimation is performed using data obtained from three different induction motors. The comparative efficiency estimation

analysis in Chapter 5 is limited to IEC-TS 60034-2-3 Technical Specification which focusses on the power losses of inverter-fed machines rather than IEC 61800-9-2:2017 Standard [5] which allows evaluation of power losses of complete drive modules and power drive systems.

1.6. Thesis Contributions

The main contribution of this thesis is to provide a practical non-intrusive online efficiency estimation solution of inverter-fed IMs through stochastic search and evolutionary based optimisation algorithms and harmonic loss analysis, using only measured values.

The specific contributions per chapter are as follows:

Chapter 2

- Provides important considerations for non-intrusive efficiency estimation of inverter-fed induction motors, focusing on the quantification of additional losses based on different harmonic equivalent circuits. The effect of voltage and current harmonics on the performance of IMs is discussed.
- Provides analysis of the existing efficiency estimation methods and recommends techniques for state-of-the-art methods.

Chapter 3

- Presents a review and analysis of the different speed estimation techniques in terms of intrusiveness, relative accuracy and computational overhead when the motor is fed by an inverter supply. Based on the analysis of reported results and those from experimental verification, potential techniques are recommended for state-of-the-art non-intrusive rotor speed estimation of inverter-fed IMs.
- Conducts a sensitivity analysis to assess the robustness of the non-intrusive speed estimation techniques during small changes in the frequency of the inverter supply.

Chapter 4

- Presents equivalent circuit parameter estimation of induction motors based on fundamental values and rms values of the PWM inverter supply. The estimated

parameters are compared against those obtained from IEC 60034-2-1 procedures of no-load and locked rotor tests.

- Presents harmonic parameter estimation and segregation of harmonic loss analysis of inverter-fed induction motors following a linear regression based harmonic analysis technique of the PWM inverter supply voltages, currents and power factors.

Chapter 5

- Presents a development of a non-intrusive efficiency estimation technique of inverter-fed induction motors that caters for a holistic harmonic loss based on the analysis of PWM losses and fundamental losses. The proposed technique can be used for both sinusoidal and inverter-fed machine efficiency estimation.
- Provides a comparative analysis of the machine efficiencies obtained from the proposed non-intrusive efficiency estimation techniques and those obtained from the IEC-TS 60034-2-3 Technical Specification and a direct method.

Journal papers published or submitted:

M. Chirindo, M. A. Khan and P. S. Barendse, "Considerations for non-intrusive efficiency estimation of inverter-fed motors," *IEEE Trans. Ind. Electron*., vol. 63, no. 1, pp. 741-749, 2016.

M. Chirindo, M. A. Khan and P. S. Barendse, "Analysis of non-intrusive rotor speed estimation techniques for inverter-fed induction motors," *Submitted to IEEE Trans. Energy. Convers*., 17 Jan. 2020.

1.7. Thesis Outline

This thesis is organized as follows:

Chapter 2 reviews and provides considerations on non-intrusive efficiency estimation of inverter-fed IMs. It focuses on the quantification of additional losses for different

harmonic equivalent circuits and the effect of voltage and current harmonics on the performance of these motors. Based on the analysis of the existing efficiency estimation methods, recommended techniques are proposed for state-of-the-art methods. This chapter is based on [7] which have been published by the author of this thesis.

Chapter 3 provides a detailed review of non-intrusive rotor speed estimation techniques for inverter-fed IMs. Some techniques are implemented to provide a comparative analysis in terms of intrusiveness, relative accuracy, sensitivity and computational overhead. Based on the analysis of results, potential techniques are recommended for state-of-the-art non-intrusive rotor speed estimation of inverter-fed motors.

Chapter 4 reviews and provides considerations for inverter-fed IM equivalent circuit modelling and parameter estimation techniques suitable for non-intrusive efficiency estimation. Parameter estimation results obtained from a PBIL algorithm based on experimental data are compared with those obtained from the IEC 60034-2-1 standard procedures of no-load and locked rotor tests. In this chapter, harmonic analysis of voltage and current experimental data is performed. The harmonic voltage and current data are used to estimate harmonic parameters based on the BFO algorithm. Harmonic loss analysis is performed to implement segregation of harmonic losses of the induction motors.

Chapter 5 presents a non-intrusive efficiency estimation technique of inverter-fed IMs that caters for a holistic loss contribution by all harmonics using only a set of measured values plus an iterative algorithm. The results are compared with those obtained from the Technical Specification IEC-TS 60034-2-3, the proposed method in Chapter 4 and a direct method. The technique can be used for both grid and inverter supplied machine efficiency estimation. Error analysis and repeatability tests are conducted to test the accuracy and the reliability of the efficiency estimation technique(s).

Chapter 6 draws conclusions based on the findings of the research and make recommendations for future work.

Chapter 2

NON-INTRUSIVE EFFICIENCY ESTIMATION METHODS AND QUANTIFICATION OF HARMONIC LOSS IN INVERTER-FED INDUCTION MOTORS

2.1. Introduction

The study of non-intrusive efficiency estimation of inverter-fed induction machines necessitates a thorough discussion of the main efficiency estimation methods as well as an assessment of these methods in terms of their intrusiveness and their suitability for use with inverter-fed machines. This chapter provides a detailed overview of the main efficiency estimation methods (section 2.2), including work towards the efficiency estimation specifically for inverter-fed machines (section 2.4). Section 2.5 provides some considerations for the quantification of additional losses due to voltage and current harmonics from inverter supplies. Section 2.6 discusses the effects of voltage and current harmonics on the performance of induction machines while section 2.7 recommends techniques particularly suitable for non-intrusive efficiency estimation of inverter-fed machines. Section 2.8 provides some concluding remarks.

2.2. Review of Efficiency Estimation Methods

Although there is no precise distinction between an intrusive measurement operation and a non-intrusive measurement operation, it is possible to describe the level of intrusiveness as either intrusive or non-intrusive. An intrusive measurement operation at its extreme involves a complete shutdown of the motor in order to install sensors, which adversely affects the operation process in which the motor is embedded. If the type of data or its collection process entails the shutting down of the motor, such an operation renders the entire measurement intrusive. On the other hand, a non-intrusive efficiency measurement operation at its extreme involves no interference with the operation of the motor. However, in most cases, a non-intrusive measurement operation results in less accurate measurements than an intrusive operation. The accuracy of an intrusive or non-intrusive efficiency measurement is determined with reference to the direct efficiency measurement technique. In this technique the efficiency is calculated from shaft torque and rotor speed as follows:

$$\eta = \frac{P_o}{P_{i,meas}} \qquad (2\text{-}1)$$

and

$$P_o = T_{,meas} \cdot \omega_{r,meas} \qquad (2\text{-}2)$$

where:

η	-	is the motor efficiency
P_o	-	is the mechanical output power at the shaft
$P_{i,meas}$	-	is the measured electrical input power
T_{meas}	-	is the measured shaft torque
$\omega_{r,meas}$	-	is the measured rotor speed

Whilst there are numerous IM efficiency estimation methods, most of them can be classified in one or more of the following categories: nameplate methods, slip methods, current methods, equivalent circuit methods, segregated loss methods, torque methods and optimisation methods [8]-[22].

The application of these methods is mostly relevant to IMs fed by sinusoidal mains supply. Their use in inverter-fed motors only allows rough estimates of efficiency since most of them rely on root mean square (RMS) values of measured quantities without quantifying harmonic losses. The methods are discussed here for completeness of the efficiency estimation analysis. Some of these methods are highly intrusive, involving operations such as no-load tests, variable voltage no-load tests and multiple loading tests.

2.2.1. Nameplate Method

The nameplate method assumes that the efficiency of the machine is constant and equal to the nameplate value. Although this method is the least intrusive, it is only valid if the efficiency versus load characteristic is fairly constant over the entire load range. In [8] the potential accuracy of the nameplate method is evaluated using typical efficiency versus load curves for motors having various number of poles and horsepower ratings. It is concluded that the nameplate method may be applicable for some motors but could result in substantial inaccuracies for other motor types.

This method is potentially unreliable because of the following reasons.

1) The nameplate data may be provided according to a method other than IEEE 112B Standard.
2) The motor may have been repaired and additional uncertainties could be introduced which invalidates the nameplate data. Changes in the stator coil wire gauge may affect the stator coil resistance, hence stator loss. Tempering with the lamination insulation may result in changes in the core loss. After the rewind process, the new efficiency of

the motor will therefore be slightly lower than the one derived from the nameplate data. However, a different opinion [23] indicates that the efficiency should not be reduced if the rewinding follows Electrical Apparatus Service Association (EASA) Standards.

3) The practical field environment in which motors are installed are often worse in terms of voltage unbalance, over/under voltage (but balanced conditions) and harmonic content than that from which the nameplate data was derived. Clearly, in most cases, the nameplate data does not cater for the effect of unbalanced supplies and inverter supplies (rich in harmonics) on overall motor efficiency.

From [9], it can be deduced that different motor efficiency standards give rise to different efficiencies of the same motor. Thus, the same motor can be stamped with different nameplate data as measured according to different testing standards. The most common testing standards are, the National Equipment Manufacturers Association (NEMA) that uses the IEEE 112 Standard, the JEC-37 and the IEC 34-2-1 as mentioned in section 1.2.

2.2.2. The Slip Methods

The slip methods rely on speed measurements to estimate the motor efficiency. It is assumed that the percentage load is proportional to the ratio of the measured slip to the full load (rated) slip. The main merit is simplicity. However, these methods suffer major drawbacks that render them unsuitable for accurate efficiency estimation. Slip methods have a few variations which strive to improve accuracy. These variations are: standard slip method, Ontario-Hydro modified slip method and upper bound slip method. These methods are explained below.

2.2.2.1. Standard Slip Method

This is the simplest slip method. The motor efficiency is approximated as:

$$\eta = \frac{s_{meas}}{s_{rated}} . \frac{P_{o,rated}}{P_{i,meas}} \qquad (2\text{-}3)$$

where:

s_{meas} - is the measured slip

s_{rated} - is the rated slip

$P_{o,rated}$ - is the rated output power

The standard slip method is an improvement over the nameplate method especially when the motor efficiency versus load curve is not constant. However, it relies on the accurate measurement of motor speed, and uses the assumption that rated slip and rated output power are based on rated, balanced and pure sinusoidal supplies. This assumption is not realistic in the harsh industrial environments in which the majority of these motors are installed.

2.2.2.2. Ontario-Hydro Modified Slip Method

In order to improve the standard slip method, the Ontario-Hydro modified slip method corrects the nameplate speed against variations in supply voltages especially when the efficiency versus load curve is not constant. The efficiency is thus approximated as:

$$\eta = \frac{s_{meas}}{s_{rated}} . \frac{P_{o,rated}}{P_{i,meas}} . \left(\frac{V_{meas}}{V_{rated}}\right)^2 \qquad (2\text{-}4)$$

where:

V_{meas} - measured input voltage

V_{rated} - rated input voltage

Despite the voltage variation correction, Ontario-Hydro modified slip method still suffers a relatively large error, since the accuracy of the nameplate (rated) speed is allowed to deviate up to 20% of the actual speed according to NEMA MG1 Standard [24].

A more accurate version of equation (2-4) was proposed in [10] which is claimed to better reflect the relation between the slip and load of the machine is shown in (2-5) as:

$$\eta = \frac{P_{o,rated}}{P_{i,meas}} . \frac{s^2}{{s_{rated}}^2} . \left(\frac{V_{meas}}{V_{rated}}\right)^2 \qquad (2\text{-}5)$$

This method is only more accurate than the preceding slip methods, but it still suffers relatively high inaccuracies because of the generic drawbacks of slip methods as indicated at the end of this subsection.

2.2.2.3. Upper Bound Slip Method

The simplest and original upper bound slip method assumes the stator loss to be zero according to [25]. The efficiency is given as shown in equation (2-6).

$$\eta \leq (1 - s_{meas}) \quad (2\text{-}6)$$

However, it is well known that the stator loss accounts for about 40% of the total losses in a typical motor. This method can be improved by including stator loss as in 2-7 [11].

$$\eta = (1 - s_{meas}).\left(1 - \frac{3(I_S)^2 R_S}{P_{i,meas}}\right) \quad (2\text{-}7)$$

where:

I_s - is the stator phase current

R_s - is the stator resistance

The resulting efficiency from this slip method is always higher than the actual efficiency since it neglects rotor losses, core losses, friction and windage losses and stray load losses. Besides the stator losses, it is assumed that the rated, balanced and pure sinusoidal three phase supplies are used. The stator resistance also changes with temperature. There is no indication of whether this is a cold stator resistance or operating temperature resistance.

To summarise the discussion on the slip methods considered above, it can be mentioned that they have low intrusion level but relatively low accuracy because of the following reasons:

1) The slip is not linearly proportional to the load over the entire range.
2) Rated motor slips that comply with NEMA MG-1 Standard allows for up to 20% error of the actual slip value. The resulting efficiency will therefore be very inaccurate. NEMA MG-1 Standard states a tolerance of ±20% of rated slip, which should be measured at rated voltage, frequency, and load, after thermal equilibrium is reached with an ambient temperature of 25ºC.

   IEC 60034-1 Standard [26] states a tolerance of ±30% of rated slip, for motors with rated power lower than 1 kW, and ±20% of rated slip, for motors with rated power equal or higher than 1 kW.
3) Speed measurement errors contribute to overall efficiency inaccuracy.
4) The slip is affected by temperature changes in the motor. This has not been accounted for in the slip methods.
5) The effect of additional losses due to harmonics in non-sinusoidal supplies is not accounted for in the slip methods.

2.2.3. Current Methods

In general, the current methods presume that the percentage load is proportional to the ratio (in percent) of measured current to full load current. Like the slip methods, the main merit of the current methods is simplicity but they suffer major drawbacks as a result of inaccuracies experienced. The current methods available include: standard current method, the modified current method and the voltage compensated current method. These methods are discussed below:

2.2.3.1. Standard Current Method

The standard current method estimates the efficiency of a motor according to (2-8). This is a low-intrusive method where only the current measurement, input power and the manufacturer's data are required to estimate the efficiency.

$$\eta = \frac{I_{meas}}{I_{rated}} . \frac{P_{o,rated}}{P_{i,meas}} \qquad (2\text{-}8)$$

where

I_{meas} - is the measured current

I_{rated} - is the rated current

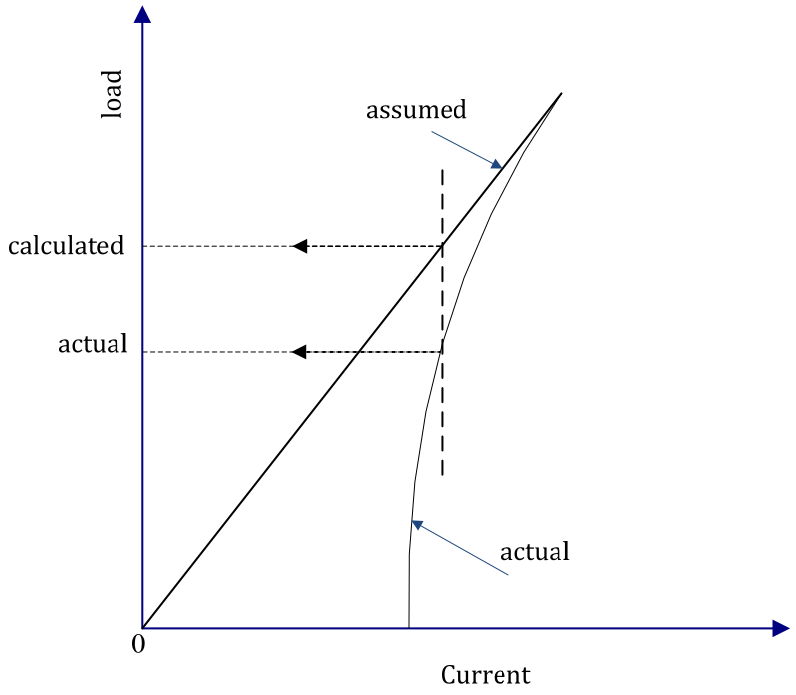

Figure 2-1. Induction machine assumed and actual current-load curve [8].

The accuracy of this method is however compromised because, in reality, the current versus load curve is slightly non-linear [12].

The source of error in using equation (2-8) is shown in Figure 2-1 [8]. The assumed curve indicates no (zero) current flow under no-load conditions which is not the case in practice. It can be seen from Figure 2-1 that the load is overestimated for a specific amount of current. The error becomes significantly higher when light loads are considered.

2.2.3.2. Modified Current Method

In order to improve the accuracy of the current method, equation (2-9) is used to estimate the motor efficiency.

$$\eta = \frac{I_{meas} - I_{no-load}}{I_{rated} - I_{no-load}} \cdot \frac{P_{o,rated}}{P_{i,meas}} \qquad (2\text{-}9)$$

where:

$I_{no-load}$ - is the no-load current

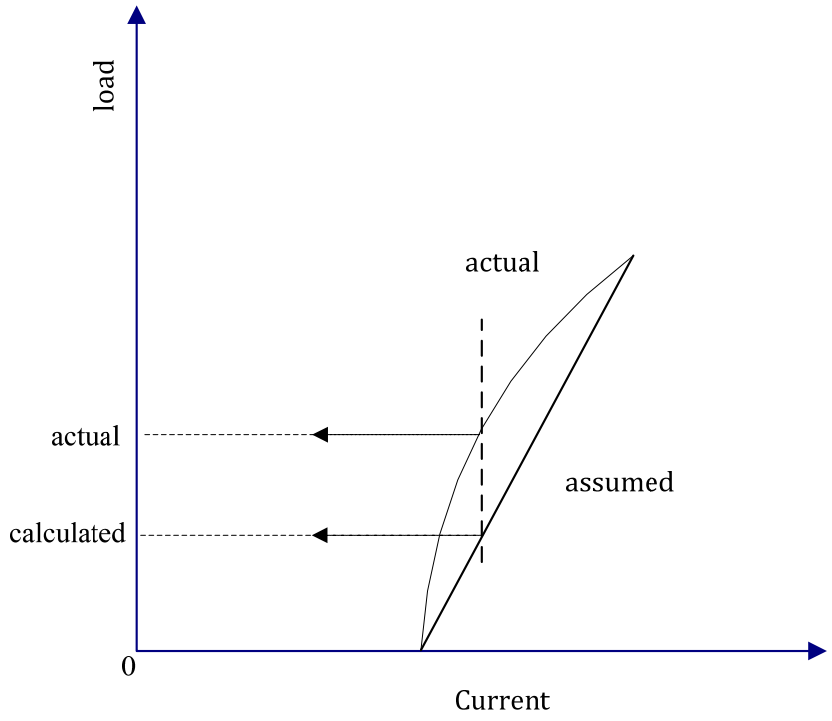

Figure 2-2. Modified induction machine assumed and actual current-load curve.

Figure 2-2 shows the resulting source of error when equation (2-9) is used. Although the modified current method is an improvement to the standard current method, it still suffers some substantial error due to the non-linearity of the actual curve versus the assumed curve. It can be seen from Figure 2-2 that the load is underestimated. Furthermore, the requirement of a no-load current measurement in (2-9) introduces high intrusiveness to this method.

To further reduce the error, equation (2-10) [8] is used that accounts for the slightly non-linear current versus load curve. However, the requirement of a no-load current measurement is not eliminated.

$$\eta = \frac{2I - I_{no-load}}{2I_{rated} - I_{no-load}} \cdot \frac{P_{o,rated}}{P_{i,meas}} \qquad (2\text{-}10)$$

From the discussion above, it is apparent that the current methods are not suitable for non-intrusive, accurate efficiency estimation because of the following reasons:

1) In reality, the current versus load curve is not linear as assumed by these methods.
2) NEMA MG-1 Section 12.47 states that, when operated at rated voltage, rated frequency and rated horsepower, the input current shall not vary from the nameplate value by 10%. The possibility that it can vary by up to 10% introduces an additional source of error.
3) No-load tests in modified current method are highly intrusive.
4) Nameplate specifications are not reliable when the condition of the motor changes due to repairs, rewinds or operating environment.
5) No considerations are made for motor supply voltage unbalances and harmonics effects on losses.

2.2.4. Equivalent Circuit Methods

The equivalent circuit methods estimate the efficiency of the IM from its equivalent. The main merit of the equivalent circuit methods is that they provide efficiency estimation for a motor operating under load conditions other than those at which measurements are made. However, the equivalent circuit parameter values can change a great deal when the

motor speed varies between standstill and no-load due to skin effect and magnetic saturation. Different equivalent circuit methods are briefly discussed below:

2.2.4.1. Standard Equivalent Circuit (IEEE Standard 112 Method F/F1)

This method is based on the standard equivalent circuit defined in [3] and shown in Figure 4-1. It requires an impedance test, no-load test, locked rotor test and variable voltage test. The stray load loss is measured through an additional removed rotor and reverse rotation test. These tests are too intrusive for in-service motors because an interruption in operation is required.

2.2.4.2. Ontario Hydro Modified Method F (OHMF)

This is a modified version of the IEEE 112 Standard Method F1 proposed by Ontario Hydro [13]. Although a variable voltage test is not required, both no-load and full-load tests at rated voltage must be conducted. Line voltage, input power, line current, power factor and stator resistance are measured while operating at no-load and full-load. The slip is measured at full load. This modified method is so highly intrusive for in-service efficiency determination.

2.2.4.3. Nameplate Equivalent Circuit Method (ORMEL96)

It is also a modified version of IEEE 112 Standard, Method F, in which an extra parasitic resistance is added in series with the rotor circuit to account for stray load losses, since they are mostly dependent on rotor current. The motor equivalent circuit is derived from the nameplate data. The stator resistance is also estimated from the nameplate data according to defined algorithms by Oak Ridge National Laboratory [13]. There is need to measure the rotor speed only. The estimation of stator resistance from the nameplate data however compromises accuracy because the resistance is dependent on temperature. Although it is a low-intrusive method, the parameters are solved from assumed load conditions derived from nameplate information which may have up to 20% error according to NEMA MG-1 [24].

2.2.4.4. Reliance Motor Efficiency Wizard Method

This method was proposed by Reliance Electric, where estimated efficiency accuracy is claimed to be within 1%. The efficiency is estimated by measuring input power, voltage,

current, speed, stator resistance, stator temperature and frequency at two load points. Although it appears to be a low-intrusive method, no consideration is given to supply harmonics in this method. Moreover, accurate stator resistance requires removal of stator supply voltage. This disrupts operations, which makes this method unsuitable for continuously in-service motors.

2.2.4.5. Locked Rotor Method

The equivalent circuit for this method has two rotor loops to allow for the influence of rotor eddy currents on the torque of single-cage motors [14]. The parameters of the circuit are obtained from locked rotor tests. In addition, no-load tests must be conducted. These procedures make this method too intrusive for in-service efficiency estimation.

2.2.4.6. Standstill Frequency Response Method

The equivalent circuit for this method also uses two rotor loops. The parameters of the circuit are derived by measuring the impedance of the motor over a frequency range 0.01Hz to 500Hz with its rotor stationary. The merits of this method lie in the use of low voltage with no-load tests required. However, it is still inherently a high intrusive method.

2.2.5. Segregated Loss Methods

The determination of machine efficiency by segregated loss methods involves separating different losses of the machine into stator copper loss, rotor copper loss, core loss, friction and windage loss and stray load loss. The shaft power would then be equal to input power minus total losses. The variations of the segregated loss methods are briefly described below.

2.2.5.1. Standard Segregated Loss Method (IEEE Standard 112, Method E/E1)

In this method [3], the stray load loss is determined by direct measurement (Method E), which involves removed rotor and reverse rotation tests for fundamental frequency and high frequency stray load losses, respectively. In addition, no-load tests are required. This renders this method highly intrusive for in-service efficiency estimation.

The simpler version of this method (Method E1) uses an assumed value of stray load losses as shown in Table 2-1. This avoids the measurement of stray load loss. However, this version is still complicated and intrusive for in-service efficiency estimation, since it

requires variable voltage no-load and multiple loaded tests. The repeatability of Method E1 is improved by the adjustment of all resistance and slip measurements to a specified temperature.

Table 2-1. Assumed values for stray load loss.

Machine Rating (kW)	Stray-Load Loss (% of Rated Load)
0.7457-90	1.80%
91-375	1.50%
376-1850	1.20%
1851 and greater	0.90%

2.2.5.2. Ontario Hydro Modified Method E (OHME)

The IEEE 112 Standard, Method E1 is simplified by Ontario Hydro [12] by combining the friction, windage and core losses and assuming it to be 3.5% – 4.2% of rated input power. The stray load loss is estimated from Table 2-1. The stator resistance is based on the simple approximation using motor current to estimate temperature rise. The only required measurements are input power and rotor speed. Although this is a low intrusive method with good accuracy (±2% - 3% error) [8], no considerations for the effect of unbalanced supplies and harmonics are made.

2.2.6. Torque Methods

Motor efficiency estimation by torque methods is based on the following relationship, in terms of shaft torque, air gap torque and rotor speed [15]:

$$\eta = \frac{T_{meas} \cdot \omega_{r,meas}}{P_{i,meas}} \qquad (2\text{-}11)$$

$$\eta = \frac{T_{ag} \cdot \omega_{r,meas} - P_{FW} - P_{SLL}}{P_{i,meas}} \qquad (2\text{-}12)$$

where:

T_{ag} - is the air gap torque

P_{FW} - is the friction and windage losses

P_{SLL} - is the stray load loss

A discrepancy in equation (2-12) was noted in [16] that the core loss is not contained in the air gap torque. A more accurate equation was proposed as follows:

$$\eta = \frac{T_{ag} \cdot \omega_{r,meas} - P_{FW} - P_c - P_{SLL}}{P_{i,meas}} \qquad (2\text{-}13)$$

where:

P_c - is the core loss.

By measuring the input power and the rotor speed, the efficiency can be determined if the shaft torque is known. The following torque methods are based on this principle:

2.2.6.1. Shaft Torque

This is the most straightforward and most accurate torque method of efficiency determination obtained by directly measuring the shaft torque and the rotor speed. The efficiency is then calculated by (2-11). The drawbacks of this method are:

1) It is highly intrusive. Machine downtime is required for preparing and replacing shaft torque couplings.
2) The high cost of torque transducers makes this method too expensive for most industrial applications.
3) The accuracy of the method depends on the quality of the torque transducer, the signal noise and the quality of the shaft alignment of the motor and its load.

2.2.6.2. Air Gap Torque (AGT) Method

By measuring the line voltages and currents supplying the motor, its air gap torque can be estimated from equation (2-14) which was first proposed by [15]. The efficiency would then be calculated using equation (2-13).

$$T_{ag} = \frac{P}{2\sqrt{3}}\{(i_a - i_b).\int[v_{ca} - R_s(i_c - i_a)]dt - (i_c - i_a).\int[v_{ab} - R'_s(i_a - i_c)]dt\} \qquad (2\text{-}14)$$

where:

P - is the number of poles

i_a, i_b, i_c - are the instantaneous phase currents at phases a, b, c

v_{ca}, v_{ab} - are the instantaneous values of line-to-line voltages

R'_s - is the corrected stator resistance according to (2-22)

When the air gap torque is known, it is possible to find the shaft power and hence efficiency from (2-13). The advantages of this method are that it is generally highly accurate (within ±0.5% to ±1% error) [17] and that it accounts for losses associated with unbalanced motor supplies when estimating the air gap torque. This is very relevant to most industrial installations.

However, this method requires no-load tests to be performed in order to estimate friction and windage, core and stray load losses. This makes it highly intrusive and unsuitable for in-service motor efficiency estimation.

The formulation of equation (2-14) brings forth some errors due to some assumptions and simplifications briefly described in [15].

2.2.6.3. Non-Intrusive Air Gap Torque (NAGT) Method

In order to overcome the intrusiveness associated with the conventional AGT method described above, a NAGT method was proposed in [16]. In this method, no-load tests are avoided by assuming empirical values for no-load losses according to OHME and ORME96 methods. Stray load losses are calculated according to a fixed allowance, as described in the IEEE 112 Standard. These assumptions pose potential sources of error in the efficiency estimation process. The estimation of stator resistance by the dc injection technique [18] introduces some degree of intrusiveness since machine operation must be halted in order to install the required circuitry.

2.2.7. Optimization Methods

Numerous optimization techniques have been proposed to estimate parameters and hence efficiency of induction machines. These techniques rely mostly on iterative search algorithms to estimate parameters of the IM equivalent circuit. Once the motor parameters are known, it is possible to estimate the motor efficiency at any operating point.

A detailed survey of the optimization methods for parameter estimation is provided in Chapter 4, Section 4.2.3.3.

2.3. Basics of Voltage and Current Harmonics in Non-Sinusoidal Waveforms

The main cause of additional losses in the inverter-fed machines is the voltage and current harmonics present in the non-sinusoidal supply waveforms. Therefore, it is important to review the mathematical background from which these quantities come.

The harmonic content of a non-sinusoidal waveform can be assessed by the use of Fourier analysis. However, in order for the Fourier analysis to be feasible, the following conditions must be satisfied by the non-sinusoidal waveform.

1) The waveform must be periodic, that is, $f(x) = f(x) \pm 2\pi)$ and completely integrable over the period.
2) The waveform must have a finite number of maxima and minima.
3) The waveform must have a finite number of discontinuities.

Having satisfied the above conditions, the Fourier series of a non-sinusoidal waveform $f(x)$ is given by (2-15).

$$f(x) = \frac{a_0}{2} + \sum_{n=1}^{\infty}(a_h \cos nx + b_h \sin nx) \qquad (2\text{-}15)$$

where:

a_0 - is the dc component

a_h - $\frac{2}{L}\int_{-L}^{L} f(x)cos(hx)d\,x \qquad h \geq 0 \qquad (2\text{-}16)$

b_h - $\frac{2}{L}\int_{-L}^{L} f(x)sin(hx)d\,x \qquad h \geq 1 \qquad (2\text{-}17)$

L - is the period of the waveform

h - is the *hth* harmonic in the waveform

a_0, a_h, b_h are the Fourier coefficients as defined above.

In [27], a non-sinusoidal supply voltage output from a PWM inverter can be expressed in a general form as:

$$v(t) = \sqrt{2}\,[V_1 Sin\,\omega t + \sum_{h=2}^{\infty} V_h Sin\,(h\omega t + \theta_h)] \qquad (2\text{-}18)$$

where:

V_1 - is the fundamental supply voltage

ω - is the angular speed in radians per second

t - is the time in seconds

V_h - is the *hth* order harmonic voltage

θ_h - is the *hth* order harmonic phase angle

To analyse the harmonic content of a non-sinusoidal waveform, it is essential to review the harmonic measurement terminology as below [28].

2.3.1. Total Harmonic Distortion (THD)

The THD of non-sinusoidal voltage waveform is given by:

$$\text{THDv}(\%) = \sqrt{\frac{Sum\ of\ squares\ of\ amplitudes\ of\ all\ harmonic\ voltages}{Square\ of\ the\ amplitude\ of\ fundamental\ voltage}}$$

$$= \frac{\sqrt{\sum_{h=2}^{\infty} {V_h}^2}}{V_1} \text{ x } 100\% \qquad (2\text{-}19)$$

The THD of non-sinusoidal current waveform is given by:

$$\text{THDi}(\%) = \sqrt{\frac{Sum\ of\ squares\ of\ amplitudes\ of\ all\ harmonic\ currents}{Square\ of\ the\ amplitude\ of\ fundamental\ current}}$$

$$= \frac{\sqrt{\sum_{h=2}^{\infty} {I_h}^2}}{I_1} \text{ x } 100\% \qquad (2\text{-}20)$$

According to IEEE Standard 159 [29], the Total Harmonic Distortion limit on industrial power supplies less than 69 kV is 5% for normal operation, that is, for conditions lasting for more than one hour. This information is shown in Table II.

2.3.2. Voltage Distortion Factor (VDF)

The amount of voltage distortion due to the *hth* order harmonic is measured by the Voltage Distortion Factor as follows [28]:

$$\text{VDF}(\%) = \sqrt{\frac{Square\ of\ amplitude\ of\ the\ kth\ order\ harmonic\ voltage}{Square\ of\ amplitude\ of\ the\ fundamental\ voltage}}$$

$$= \frac{V_h}{V_1} \text{ x } 100\% \qquad (2\text{-}21)$$

The Voltage Distortion Factor is more useful when analysis of individual harmonics is required. The IEEE 519 Standard specifies limits of VDF for networks with several voltage levels as shown in Table 2-2.

Table 2-2. Voltage distortion limits [29]

Bus Voltage at PPC	Individual Voltage Distortion (%)	Total Voltage Distortion THD %
69 kV and below	3.0	5.0
69.001 kV through to 161 kV	1.5	2.5
161.001 kV and above	1.0	1.5

2.4. Review of Efficiency Estimation of Inverter-Fed Machines

Most of the IMs installed in industrial plants are fed by sinusoidal voltage supplies. However, the use of non-sinusoidal voltage supplies such as inverters is growing fast. There are a number of benefits associated with the use of inverters for this purpose. In particular, the use of Pulse Width Modulated (PWM) inverters realises efficient and fast control of IMs in many automated industrial applications. This is achieved through control of the supply voltage and frequency to optimise motor operation at various load conditions.

Despite the benefits of using inverters to drive IMs, the use of inverters introduces additional losses in the motor as a result of voltage and current harmonics which impact negatively on the motor efficiency. It is therefore important that considerations be made regarding the quantification of these additional losses [30] due to voltage and current harmonics in order to estimate the efficiency of inverter-fed motors. The inverter-fed motor losses can be considerably reduced in normal operation by using multilevel inverter drives [31]-[33] that offer a good trade-off by reducing the switching frequency and the harmonic content, since low switching frequency decreases the inverter losses while low harmonic content decreases the motor losses. Alternatively, the inverter-fed motor losses can be reduced by using efficiency optimization control techniques [34], [35] that always aim to operate the motor at its maximum efficiency point. However, for

completeness of all the advances in reducing motor losses, it is still necessary to quantify the losses as a measure of the effectiveness of the methods used.

In order to evaluate the overall loss due to harmonics in an inverter-fed IM, it is necessary to develop IM models that can be used to analyse individual losses due to these harmonics. In some cases, the losses are estimated separately [36] and suitably combined using the superposition theorem in order to obtain the total losses. These losses are mainly calculated based on different harmonic equivalent circuits. However, the accuracy of the methods used will depend on the assumptions made when modelling the harmonic equivalent circuits. Moreover, the analysis of the harmonic content of inverter supplies requires thorough treatment if the loss calculation is to be reasonably accurate. In other cases, sinusoidal supplies are deliberately corrupted by certain harmonic voltages [28], [37] for loss analysis. This approach is only for laboratory work and not suitable for automating the efficiency estimation process.

Reference [38] specifically focusses on non-intrusive efficiency estimation of inverter-fed IMs at various frequencies and loads using measured data. The motor equivalent circuit parameters at any load were evaluated using measured values in conjunction with a Genetic Algorithm (GA). This method appears very promising for non-intrusive efficiency estimation of inverter-fed IMs, but it is not suitable for practical implementation since some known harmonic voltages were injected in the supply.

Work has been carried out to investigate the effect of voltage and current harmonics on the performance of IMs [28]. It has been claimed that voltage and current harmonics from inverter supplies result in additional losses in IMs that cause reduced efficiency. The additional motor losses due to harmonic currents result in an increased motor temperature rise [39], [40]. It is important to accurately estimate the motor temperature in order to correct for parameters such as stator and rotor resistance, particularly in efficiency estimation methods based on equivalent circuits.

2.5. Quantifying Additional Losses Due to Voltage and Current Harmonics from Inverter Supplies

Different equivalent circuit models of the IM have been developed to take account of additional losses due to voltage and current harmonics. The harmonic loss analysis is mainly performed based on these IM equivalent circuit models. A detailed analysis of the different equivalent circuit models is presented in Chapter 4, Section 4.2.1. This section explores some key principles for quantifying additional losses due voltage and current harmonics based on the standard equivalent circuit with a stray load resistor added in the rotor circuit as shown in Figure 4-2.

2.5.1. Stator Loss

The harmonic currents contribute to an increase in the total RMS current, hence power loss in the stator. This increase in loss causes increased temperature rise in the stator windings. Correction of the stator resistance for the increased temperature rise is therefore mandatory for accurate efficiency estimation. The corrected stator resistance, R'_s (in ohms) can be determined using (2-22) according to the winding temperature class (using IEEE 112-2017 standard [3]).

$$R'_s = \frac{R_S(T_{load}+k)}{T_{amb}+k} \qquad (2\text{-}22)$$

where:

R_s - is a measured winding (stator) resistance (in ohms) at temperature, T_{amb} (in °C)

T_{load} - is the load temperature to which the resistance is to be corrected (in °C)

k - is 234.5 for 100% IACS conductivity copper, or 225 for aluminium, based on a volume conductivity of 62%

The estimation or measurement of stator loss is complicated by the determination of the harmonic content of different practical waveforms and the impact of skin effect on the stator conductors. Skin effect in the stator may be neglected if the height of the stator conductor is small.

The total stator loss, P_s due to the fundamental and harmonic currents according to Figure 4-2 is given by:

$$P_s = mR'_s[(I_{s1})^2 + \sum_{h=2}^{\infty}(I_{sh})^2] \qquad (2\text{-}23)$$

where m is the number of phases.

The cold stator resistance R_s needs to be measured in order to use equation (2-22). This is usually an intrusive operation that entails the shutdown of the motor.

In some cases, [41], [42] the stator loss is simply computed based on the measured RMS current, I_s according to:

$$P_s = m(I_s R_s) \qquad (2\text{-}24)$$

In this case, $I_s = \sqrt{\left[\left({I_{s1}}^2\right) + \sum_{h=2}^{\infty}\left({I_{sh}}^2\right)\right]}$ and the knowledge of individual harmonic magnitudes is not required. The high frequency effects are then neglected.

Figure 2-3 shows an example spectrum of line current of an induction machine fed by a PWM inverter supply at a switching frequency of 5 kHz [43]. The additional stator loss due to harmonic currents is very marginal since the largest additional current component is 30 dB below the fundamental component according to Figure 2-3.

Moreover, these IM harmonic losses become even less as the order of PWM sidebands increases, assuming a simple stator resistance without skin effect. The low order harmonic distortions due to magnetic saturation and slotting are less evident in PWM supplies than sinusoidal supplies.

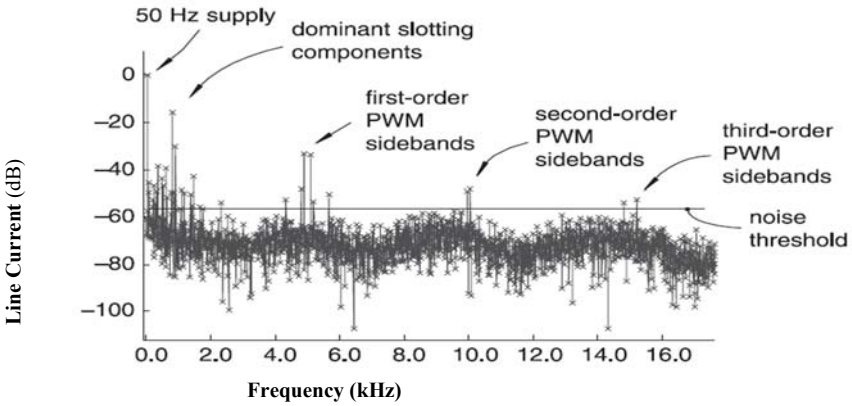

Figure 2-3. Example of line current spectrum of an induction machine fed by a PWM supply [43].

2.5.2. Rotor Loss

The fundamental rotor I^2R loss is due to rotor current flowing through the base resistance of the rotor conductive bars. Furthermore high frequency harmonic rotor

currents flow in the rotor bars, causing substantial additional rotor loss. This loss is mainly due to the skin effect in the rotor bars owing to their relatively large depths. In most cases, this loss is difficult to consider due the variations in rotor bar shapes and sizes especially in installed motors. This poses a challenge where efficiency estimation of inverter-fed motors needs to be conducted non-intrusively. Several analytical methods to evaluate the skin effect in rotor bars can be found in literature, but they are mainly based on regular rotor slot shapes, such as rectangular, trapezoidal or round [44], [45].

An analysis of rotor resistance as a function of frequency and conductor height for a rectangular conductor with open slots is conducted in [45]. The dependence of bar resistance $\varphi_R(\xi)$ and bar inductance $\varphi_L(\xi)$ on frequency is also given as in (2-25) and (2-26). The variable ξ is equal to $\frac{H}{\delta}$, where H is the conductor height and δ is the skin depth, which is a function of frequency.

$$\varphi_R(\xi) = \frac{R_{AC}}{R_{DC}} = \frac{\sinh(2\xi)+\sin(2\xi)}{\cosh(2\xi)-\cos(2\xi)} \qquad (2\text{-}25)$$

where:

R_{DC} - is the DC resistance

R_{AC} - is the AC resistance due to skin effect

$$\varphi_L(\xi) = \frac{L_{AC}}{L_{DC}} = \frac{3}{2\xi}\frac{\sinh(2\xi)-\sin(2\xi)}{\cosh(2\xi)-\cos(2\xi)} \qquad (2\text{-}26)$$

where:

L_{DC} is the DC inductance

L_{AC} is the AC inductance due to skin effect

These mathematical models are only valid when some variables such as rotor bar height and skin depth are known. As a result, they attract very little or no interest in non-intrusive efficiency estimation.

In literature such as in [42] and [46], the rotor equivalent circuit for skin effect analysis is represented by a series of LR circuits where in [46] the frequency response of the IM is required in order to model the skin effect. In [42], the effect of harmonics on stray load was not considered for loss analysis.

Like the stator resistance, the corrected rotor resistance R'_r is according to machine temperature is given by:

$$R'_r = \frac{R_r(T_{load}+k)}{T_{amb}+k} \quad (2\text{-}27)$$

where:

R_r - is the rotor resistance to be corrected

The total rotor loss P_r, with reference to Figure 4-2 is given by:

$$P_r = m\frac{R'_r}{s_h}[(I_{r1})^2 + \sum_{h=2}^{\infty}(I_{rh})^2] \quad (2\text{-}28)$$

Because of the variation of rotor resistance with frequency, the total rotor harmonic loss, $P_{r,harm}$ with reference to Figure 4-2 can be substantial and is given by:

$$P_{r,harm} = m\sum_{h=2}^{h=\infty}(I_{rh})^2 R'_{rh} \quad (2\text{-}29)$$

where:

R'_{rh} - is the effective rotor resistance at harmonic order, h at the operating temperature.

The harmonic slip s_h is very close to 1 as motivated in section 2.6.2 and given by (2-39) and (2-40).

2.5.3. Core Loss

The total core loss, P_{core} in soft ferromagnetic materials under non-sinusoidal magnetization are normally separated into the hysteresis loss, P_h, and the eddy current loss, P_e given by:

$$P_{core} = P_h + P_e \quad (2\text{-}30)$$

$$P_h = K_h f B_m^{\beta} \quad (2\text{-}31)$$

$$P_e = P_c + P_{exc} \quad (2\text{-}32)$$

$$= K_c \frac{1}{T}\int_0^T \left(\frac{dB^2}{dt}\right) dt + K_{exc}\frac{1}{T}\int_0^T \left(\frac{dB^{1.5}}{dt}\right) dt \quad (2\text{-}33)$$

where:

P_c and P_{exc} - are classical and excess eddy current loss components, respectively [47]

K_h, K_c and K_{exc} - are hysteresis constant, classical eddy current constant and excess eddy current constant respectively

β - is the Steinmetz constant, typically equal to 2

However (2-31) may underestimate the hysteresis loss since it omits Laver's correction factor [43] which accounts for the presence of minor loops in the B-H curve mainly caused by the high frequency switching of the inverter. Moreover, hysteresis loss may not be considered in most non-intrusive efficiency estimation methods since these methods are mostly current based. Although the core loss (eddy current) is proportional to frequency squared, it is the decrease in flux amplitude with increase in frequency (due to excitation of an inductive circuit and lack of deep penetration into the lamination) that accounts for the overall decrease in loss. The estimation of the harmonic equivalent circuit in Figure 4-4 neglects the core loss since it is a small fraction of the total loss. However, its magnitude must be closely monitored in some parts of the cores such as stator tooth tips as it can be substantial due to concentrated flux densities in those regions. Moreover, in [19], the core loss resistors (and the stray load resistors) are accounted for in the stator and rotor of an IM in a so called iron-loss equivalent circuit.

Despite their small values relative to the total loss, references [47]-[52] seek to estimate the core loss suffered by IMs when fed by non-sinusoidal supplies. The methods employed are too intrusive. In most cases, knowledge of the magnetic core material is required in order to obtain the values of the *K* constants in equations (2-31) and (2-33), which is not always available in installed motors. Formulae have also been used in [47] and [51] that require the inverter supply waveform data such as the average rectified voltage. The inverter supply waveform data may not available for efficiency estimation of in-service motors. However, the inclusion of core losses improves the efficiency estimation accuracy.

2.5.4. Stray Load Loss

The stray load loss consists of many loss components within the stator and rotor, involving variations of the winding distribution, number of slots, slot opening shape, rotor construction, skewing and saturation, irregularities and mechanical imperfection in the air gap [53].

Stray load losses vary with the load conditions and are assumed to vary closely with the square of the applied load torque [3]. They are very small in magnitude compared to the

total losses. This makes it extremely difficult to quantify experimentally. However, successful estimation of the loss have been achieved only in simulations using Finite Element Analysis (FEA) [54], [55]. With reference to the equivalent circuit based loss estimation approach, a stray load loss representative resistance is added in the rotor circuit (see Figure 4-2) to allow for the variation of stray load loss with load. The fundamental stray load loss resistance R_{SLL1} is given by (2-34) based on Figure 4-2 and assumed values of the stray load loss recommended by IEEE-112-2017 Standard [3].

$$R_{SLL1} = k_{ad}.\left(\frac{1-s_{rated}}{s_{rated}}\right).R_{r1} \qquad (2\text{-}34)$$

where k_{ad} is obtained from assumed values of the stray load loss recommended by [3]. k_{ad} only takes the percentage value of the assumed stray load loss. Since the Since R_{SLL1} is added as a resistance in the rotor circuit, it changes with the loading condition as implied (by 2-34).

The stray load loss can be estimated from the IEC-60034-2-1-2007 Standard [26] as in [16], [56]. In this standard, the stray load loss representative resistance is in the stator circuit since the loss is considered as a proportion of the input power.

It is mentioned in [56] that the variation of harmonic stray load resistor R_{SLLn} with frequency is extremely complex and highly variable. However, it is assumed to be proportional to $h^{0.8}$, with sufficient accuracy as follows:

$$R_{SLLh} = h^{0.8} \times R_{SLL1} \qquad (2\text{-}35)$$

where R_{SLL1} is found from (2.33).

The total stray load loss is given by:

$$P_{SLL} = {I_{r1}}^2 R_{SLL1} + \sum_{h=2}^{\infty}(I_{rh})^2 R_{SLLh} \qquad (2\text{-}36)$$

2.5.5. Friction and Windage Losses

These losses are not directly related to harmonic currents. However, an increase in supply frequency, as in the case of Variable Speed Drives (VSDs), results in an increase in the rotor speed and hence an increase in the friction and windage losses. In addition, the vibration of the rotor due to pulsation torques from positive and negative sequence supply harmonics in inverter-fed motors may increase the friction losses on the bearings and hence reduce the lifespan of the bearings [28]. In most non-intrusive efficiency

estimation cases [58]-[60], the friction and windage losses are assumed to be 1.2% of rated input power. However, the standard is based on a sinusoidal supply input where the effect of the increase in rotor speed or pulsation torques due to harmonic current is not considered. Further discussion and formulation of the friction and windage losses are found in 5.2.3.5.

2.6. Effects of Voltage and Current Harmonics on the Performance of IMs

The harmonic components in the supply of an IM reduce its performance and efficiency due to different harmonic effects. Some of these harmonic effects on the IM are discussed in more detail in the following subsections.

2.6.1. Temperature Rise

The additional motor losses due to harmonic currents result in increased motor temperature [56]. It is important to accurately estimate the motor temperature in order to correct for parameters such as stator and rotor resistance in efficiency estimation methods based on equivalent circuits. The corrected stator resistance is found from (2-22) in accordance with the IEEE-112-2017 Standard [3]. The accuracy of the method depends on strategic placement of temperature sensors on the stator windings to obtain a correct stator winding temperature. Since the rotor resistance is directly related to slip, the corrected value of slip s can be used to determine the I^2R loss in accordance with IEEE 112-2004 Standard. The corrected slip is given by:

$$s = \frac{s_{load}(T_{amb}+k)}{(T_{load}+k)} \qquad (2\text{-}37)$$

where:

s_{load} - is the slip in per unit, measured at stator winding temperature, T_{load}

The temperature rise of the motor due to additional loss results in an increase in thermal stress of the stator winding insulation which shortens the lifespan of the motor. Under this condition, it is necessary to derate the motor in order to prolong its life span depending on its design class [28], [62], [63]. The effect of different harmonic orders on the temperature rise of an IM was investigated in [28] and it was shown that the lower order harmonics below 5 affect the performance of an IM more severely than the

harmonic orders above 5. This is due to their relatively higher magnitudes compared to higher order harmonics.

Various temperature estimation techniques have been proposed in the literature. The simplest technique is to use discrete thermal sensors mounted directly on the stator windings. This configuration is too intrusive, increases cost and reduces reliability of the drives due to these additional components. Alternatively, there are temperature estimation techniques based on thermal models [64] [65]. Thermal models usually calculate power loss inside the motor based on terminal measurements and then estimate the temperature at specific locations within the motor using a thermal model to represent heat flow. However, the accuracy of this method depends on the accurate representation of the heat flow by the proposed models and the correct estimation of the initial temperature. Moreover, the calculated power loss of the motor depends on the accurate determination of the motor parameters.

The temperature of the windings at machine load T_{load} can also be estimated from the stator resistance by using the linear relationship between temperature and resistance of conductors in (2-38).

$$T_{load} = \frac{(T_{amb}+(R\prime_S - R_{amb}))}{\alpha R_{amb}} \qquad (2\text{-}38)$$

where:

α - is the temperature coefficient of resistance

However, the measurement of stator resistance, R'_s at machine load is extremely difficult and potentially intrusive.

Some methods [40], [16], [66] inject a test signal to determine resistance whilst other methods [67] use the fundamental excitation and the motor model to estimate resistance. The former requires additional hardware and introduce torque distortions in the motor, whilst the latter is sensitive to motor parameters and its performance depends on the operating point of the motor.

In [19] and [20] a temperature estimation technique is proposed that is based on the total losses dissipated by a machine, the machine thermal coefficient and an iterative algorithm. This technique sounds very promising for non-intrusive efficiency estimation.

The only other requirement is the initial temperature. Further details of this technique are found in section 4.2.4.3.

From the discussion above, it is necessary to estimate/measure the machine temperature for the following reasons:

1) To correct the resistive parameters at the operating temperature for efficiency estimation.
2) To monitor the machine temperature in order to avoid thermal stress and degradation of the motor performance.

It is also evident that the most non-intrusive temperature estimation technique is based on the calculation of the machine power loss, which requires accurate estimation of the machine parameters and correct representation of the heat flow in a thermal model.

2.6.2. Motor Rotor Vibration

The motor rotor vibration originates from pulsation torques caused by positive and negative sequence time harmonics in the motor current. Positive sequence time harmonics (4^{th}, 7^{th} ….$3k+1$, for $k = 1, 2 \ldots \ldots$) have the same phase sequence (e.g A-B-C) as the fundamental and therefore produce a rotating Magneto-Motive Force (MMF) in the same direction as that produced by the fundamental. Therefore, the nett torque developed is a positive torque. Negative sequence time harmonics (2^{nd}, 5^{th} ….$3k-1$, for $k = 1, 2 \ldots \ldots$) have an opposite phase sequence (e.g C-B-A) to the fundamental and therefore produce a rotating MMF in the opposite direction to that produced by the fundamental. The torque developed is therefore negative. Zero sequence harmonics (3^{rd} and its entire integer multiples (6^{th}, 9^{th} ……)) are in phase and produce no rotating MMF and therefore no torque. The hth harmonic slip is given as:

$$s_h = \frac{(h \pm (1 - s_1))}{h} \qquad (2\text{-}39)$$

where s_h is the slip at the hth harmonic frequency and s_1 is the slip at the fundamental frequency. In [56], equation (2-39) is simplified to (2-40) assuming a fundamental slip of essentially zero for an IM running under normal load conditions.

$$s_h = \frac{(h \pm 1)}{h} \qquad (2\text{-}40)$$

It can be seen from (2-40), that the harmonic slips are very close to unity and since they are always positive, the resultant torque is always positive with respect to the rotation of the stator MMF. A plus sign represents a backward revolving field and a minus sign represents a forward revolving field. Consequently, higher order harmonics will generate additional losses which are approximately independent of the actual operating point [61].

In addition to the time harmonics from non-sinusoidal supplies, space harmonics are also present in the air gap due to the finite spatial distribution of stator slots and rotor eccentricity that cause a non-sinusoidal air gap MMF waveform. The combined effect of these time and space harmonics is to cause distortions in the electromagnetic torque. These distortions are analysed using a developed model for an induction motor fed by sinusoidal and non-sinusoidal sources in [68]. Reference [69] uses measured phase currents to calculate the forces causing the main dynamic disturbances, taking into consideration the air gap eccentricity and saturation levels. It is claimed that the harmonic current from static inverters can produce high stator vibration and that the degree of severity of this phenomenon is related to motor air gap eccentricity, saturation level and rotor unbalance. However, the validity of all these observations and claims from [68] and [69] depends on the accuracy of the models used to quantify these torque pulsations.

2.7. Recommended Techniques for Non-Intrusive Efficiency Estimation of Inverter-fed IMs

Following the analysis of non-intrusive efficiency estimation of inverter-fed IMs conducted and from Table 2-3 and from Figure 2-4, recommended techniques for different methods of efficiency estimation are outlined based on the current trend.

Figure 2-4 shows a rough estimation of potential accuracies for different techniques for loads between half load and full load. The general comment is that the least accurate method is the nameplate method which has the worst accuracy of 10% for loads between half and full load. The best accuracy is provided by the shaft torque method which has an accuracy of 1%. All the other methods that are partially involved with either nameplate

data and/or statistical values fall in between these two extreme basic methods. The inaccuracies, in general, are worse below 50% load. It can be seen that the level of intrusion increases as the level of accuracy increases.

However, based on literature review, the current trend in non-intrusive efficiency estimation follows loss segregation using IM equivalent circuits. Since some motor parameter values depend on harmonic frequency, it is preferred that a modified conventional equivalent circuit such as that in Figure 4-2 (with a stray load equivalent resistance) be used to estimate the fundamental and harmonic component losses. The estimated parameters from this equivalent circuit can be reasonably compared to those obtained by IEC 60034-2-1 Standard which uses a similar equivalent circuit.

The parameters of the IM equivalent circuit model need to be estimated in a non-intrusive manner. These parameters were estimated using optimisation techniques such as the GA in [20], PBIL in [19], and Bacterial Foraging Algorithm (BFA) in [70], all based on limited measurements.

The temperature of the IM can be found non-intrusively by a technique that is based on the total losses dissipated by a machine, the machine thermal coefficient and an iterative algorithm [19], [20]. It is then possible to use (2-22) and (2-27) to find the corrected resistance of the stator and rotor respectively. The initial value of stator resistance at a specific ambient temperature can be measured once-off when the motor is shutdown.

The total stator loss due to the fundamental and harmonic currents can be calculated using (2-23). The total rotor and stray load losses can be calculated using (2-28) and (2-36) respectively based on the equivalent circuit in Figure 4-2. The harmonic core loss is derived from the harmonic loss characteristic curve for a particular motor [165] based on measured (or calculated) harmonic loss factors and curve fitting (see equation (4-58) subsection 4.3.3). The friction and windage losses can be empirically estimated to be 1.2% of the input power. It can also be corrected to any speed (hence load) by using (5-7) in Chapter 5.

The above techniques and methodologies for different aspects of non-intrusive efficiency estimation of inverter-fed IMs are recommended. However, there is still a need to

perform detailed harmonic loss analysis in the IM to account for the segregation of harmonic losses based harmonic analysis and harmonic parameter estimation techniques.

2.8. Concluding Remarks

Following the consideration and analysis in this chapter, it can be concluded that the current and future trend in non-intrusive efficiency estimation of inverter fed motors focusses on segregation of motor losses based on equivalent circuits whose parameters are estimated by optimisation techniques using limited measured values. The accuracy in quantifying additional losses due to high frequency harmonic currents depend on the assumptions made when modelling the harmonic equivalent circuits to account for skin effects as well as core and stray load losses. Efficiency estimation errors at normal loads of within 1% and up to 1.2% based on PBIL using standard and iron loss equivalent circuits respectively have been reported [19]. An efficiency estimation error of 2% using BFA was reported in [70]. The techniques based on these optimisation algorithms present suitable candidacy for the development of non-intrusive efficiency estimation of inverter-fed motors in Chapter 4 and Chapter 5. However, further techniques still need to be proposed to be able to analyse harmonic voltages and currents, perform harmonic parameter estimation and harmonic loss analysis. Chapter 3 focusses on non-intrusive rotor speed estimation for inverter-fed motors.

Table 2-3. Summary table required tests and resources for most of the efficiency estimation techniques.

Method	No-Load test	Rated load test	Variable Supply	Stator Resistance	Speed	Torque	Nameplate data
Standard Nameplate Method	X	X	X	X	X	X	✓
Standard Slip Method	X	X	X	X	✓	X	✓
Ontario Hydro Modified Slip Method	X	X	X	X	✓	X	✓
Upper Bound Slip Method	X	X	X	✓	✓	X	✓
Standard Current Method	X	X	X	X	X	X	✓
Modified Current Method	✓	X	X	X	X	X	✓
Equivalent Circuit Method-IEEE 112 F1	✓	X	✓	✓	✓	X	X
Ontario Hydro Simplified Method F1	✓	✓	X	✓	✓	X	X
Segregated Loss Method-IEEE 112 E1	✓	✓	✓	✓	✓	X	X
The Ontario Hydro Modified Method E1	X	X	X	✓	✓	X	X
Air Gap Torque Method	✓	X	X	✓	✓	X	X
Non-Intrusive Air Gap Torque Method	X	X	X	X	X	X	X
Shaft Torque Method	X	X	X	X	✓	✓	X
Optimization Methods (PBIL, GA, BFA)	X	X	X	X pre-measured	X estimated	X	✓ non-intrusive

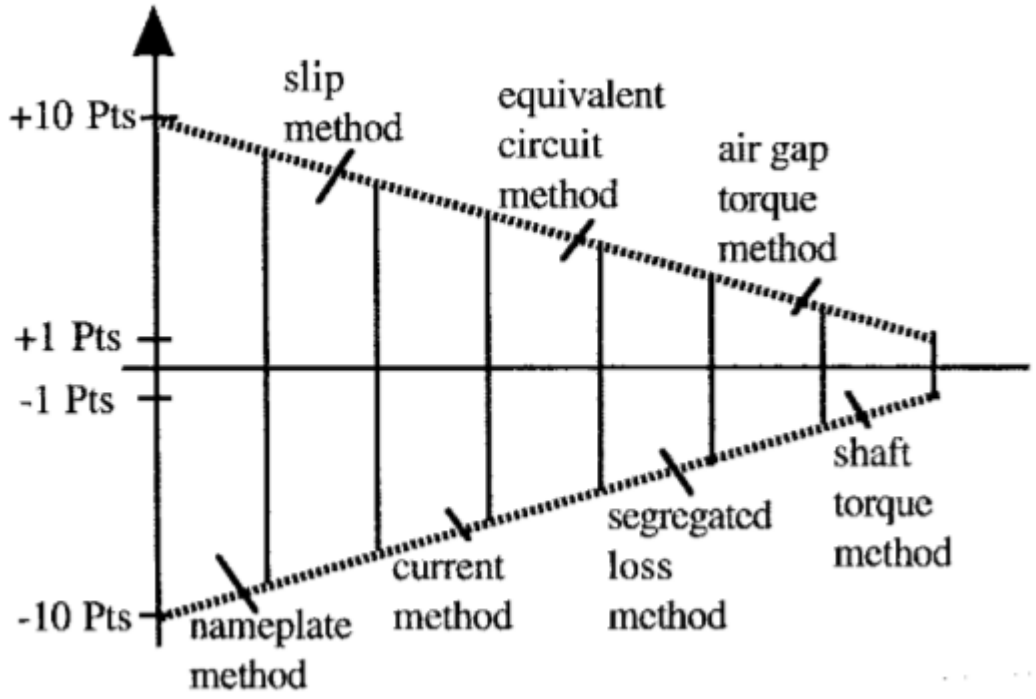

Figure 2-4 Potential accuracies for different techniques for loads between half load and full load [8]

Chapter 3

ANALYSIS OF NON-INTRUSIVE SPEED ESTIMATION TECHNIQUES FOR INVERTER-FED INDUCTION MOTORS

3.1. Introduction

Most non-intrusive IM efficiency estimation methods rely on the machine slip to compute the output power and efficiency. To maintain the overall non-intrusive nature of the entire process, it is vital to utilize a reliable and non-intrusive rotor speed measurement technique in order to obtain the slip of an in-service motor.

A number of rotor speed estimation techniques have been proposed in literature [71]-[117] with varying degrees of intrusiveness and accuracy. This chapter presents a review and analysis of the different speed estimation techniques in terms of intrusiveness, relative accuracy and computational overhead when the motor is fed by an inverter supply. Furthermore, an experimental accuracy and sensitivity analysis of some vibration and motor current based techniques is carried out to check the accuracy trend reported in literature and the robustness of these techniques. Based on the analysis results, potential techniques are recommended for state-of-the-art non-intrusive rotor speed estimation of inverter-fed motors.

3.2. IM Rotor Speed Estimation Techniques

The rotor speed of IMs has been estimated using different techniques. The following subsections outline and analyze some of the common techniques that were mostly applied to inverter-fed motors.

3.2.1. Shaft Based Speed Measurement/Estimation

Traditional speed measurement methods such as shaft mounted transducers or optical tachometers [38], [71] have been used. These sensors are generally very costly and are susceptible to wear, while their accuracy greatly reduces in harsh industrial environments. In addition, such devices are very difficult to mount, thus increasing the intrusiveness of the measuring process. In some cases, the shaft may not even be accessible. However, these methods are quite accurate (relative to other techniques discussed in the following subsections) when operated within normal environments and their results are often used as a reference when the other techniques are analyzed.

Reference [72] presents a speed estimation technique using electrostatic sensors coupled with autocorrelation signal processing algorithms and tested on different shaft sizes. In

this technique, the period of the rotating motion is equal to the transit time of the autocorrelation of the signal. The location of the dominant peak on time axis is the period. For large diameter rotors, dual electrostatic sensors are used and the time taken by the rotor to pass through the two sensors (separated by a small angular spacing) as determined by the cross correlation [72] of the two signals is used to compute speed. This technique is reported to have maximum errors of $\pm 1.2\%$ over the speed range of 600 to 3000 rpm when using a single electrostatic sensor and $> 10\%$ over the speed range of 100 to 3000 rpm when using dual electrostatic sensors. Clearly, this technique has limitations on low speed measurement. Besides, the reliability improves with increase in shaft size. This makes the technique unsuitable for general applications especially on in-service motors with different size and material type rotors. The installation of the electrostatic sensors is highly intrusive, and the sensors are also highly affected by operating environmental conditions.

Visual Based Measurement (VBM) for rotor speed has been reported [73], [74]. The principle lies in the capturing of image frames of the naturally reflected light from a rotating object (rotor) with a simple mark stuck on its cross section at a given frame rate (in frames per second). In [74] the similarity of image frames is achieved by two image processing algorithms, namely structural similarity (SSIM) and two-dimensional correlation (CORR2). The frequency of the dominant peak signal is determined by Chirp-Z transform.

The VBM rotor speed measurement looks very promising as a non-intrusive technique especially for inverter-fed machines since it is completely unaffected by supply harmonics. However, VBM techniques require long computational time to process the image signals and they require a mark to be placed on the rotor, thus rendering the entire process as intrusive.

3.2.2. Observer based Modelling Techniques

Observer-based modelling techniques estimate the rotor speed from the measured voltage and current based on IM models [75]-[87]. Some variations of these techniques [77], [78] calculate and estimate the magnetising current from the back-emf (due to rotor

flux) to formulate speed observers. However, in these and many other observer-based modelling techniques, sensorless speed estimators have been developed which suffer weakened results when considered for speed estimation at low speed and they require specific and accurate information about the operating parameters of the motor [7].

Some developments [79]-[81] were made to specifically improve speed estimation performance at low speed. In [81] the rotor speed was estimated using stator current based Model Reference Adaptive System (MRAS) with neural network observer. This is reported to have yielded some improvement in performance at low speed with acceptable stability even when the motor is in regeneration mode. However, this performance was not tested on the whole speed range. Various adaptive speed estimators based on MRAS and Kalman filters are reported [82]-[87]. Most of them depend on electromagnetic properties of the machines and are mainly applied to machine control systems.

3.2.3. Vibration Signature Analysis

The estimation of rotor speed of an IM using vibration signature analysis is applied in [16], [19]. It is indicated that the vibration signal of a motor contains a frequency component at the mechanical speed of the rotor. The vibration in electric motors occurs as a result of mechanical and magnetic forces acting upon the machine structure and the mounting of the motor [88]. Mechanical forces are due to unbalance in the rotating assembly which consists of the rotor, the shaft and the bearings. The magnetic forces are from the fluxes in the air gap which act radially on both the stator and the rotor.

The vibration signal of a motor contains a large amplitude component at rotor rotating frequency, which can be obtained using Fast Fourier Transform (FFT) and a peak detection algorithm. The search area can be narrowed by selecting the lower and upper boundaries based on the nameplate rated speed. These boundary values are obtained using equation (3-1):

$$f_{low} = \frac{n_{low}}{60}, \qquad f_{syn} = \frac{f_1}{p} \tag{3-1}$$

where:

n_{low} - is the rotor speed (in rev/sec) at the lower boundary frequency f_{low},

which is set to be either the speed at maximum torque or at 90% of the rotating magnetic field.

f_{syn} - is the frequency of the rotating magnetic field and p is the number of pole pairs.

The frequency of the rotor f_r is obtained by using the position of the harmonic current component having maximum amplitude value, D_{max} multiplied by the frequency resolution, FR.

$$f_r = D_{max} \times FR \ , \qquad n_r = f_r \times 60 \qquad (3\text{-}2)$$

Where:

n_r - is the rotor speed (in rpm). The frequency resolution FR is given by:

$$FR = \frac{SR}{N_{data}} \qquad (3\text{-}3)$$

where:

SR - is the sampling rate and

N_{data} - is the number of data points.

The vibration analysis technique records a relatively high accuracy with an error of less than 1% and less than $\pm 0.1\%$ in [16] and [19] respectively. It is apparently not directly affected by the motor supply conditions and therefore may be ideal for inverter-fed motors. However, vibrations caused by positive and negative torques due to harmonic components may degrade the performance of this technique. The vibration signal component due to the rotor frequency is easy to detect as it is always of high amplitude across all loading points and is available in both used and new machines. The rotor frequency is always lower than the motor supply frequency making it possible to use low sampling rates and achieving high resolution without long sampling times. This implies that the algorithm will have less computational overhead when compared to other advanced signal processing algorithms. Unlike the observer-based techniques, the vibration signature analysis technique is not dependent on motor parameters.

The performance of the vibration sensor also depends on the mounting method. Typical mounting methods are; stud mount, adhesive mount and magnetic mount in their order of frequency response (highest to lowest). In general, the looser the mounting connection,

the lower the measurable frequency limits. The choice of an accelerometer (vibration sensor) depends on the application. Single axis accelerometers are used to measure mechanical vibration levels while tri-axial accelerometers can be used to determine the type of vibration, such as lateral, transverse, or rotational.

3.2.4. Motor Current Based Analysis Techniques

The motor current based analysis techniques has found numerous applications in machine fault diagnostics such as detecting broken rotor bars and shorted turns in three phase IM drives [89], [90] including VSDs. The technique also finds application in rotor speed estimation [91]-[117]. In both applications, motor current is sampled and analyzed to detect specific sub-harmonic components that are dependent on certain mechanical/electrical faults or rotor speed. In this subsection, the rotor speed estimation of an IM using motor current based analysis is explored. The rotor speed signatures to be detected are mainly due to rotor frequency referred to as Motor Current Signature Analysis (MCSA), rotor slots and rotor eccentricity as described in the following paragraphs.

3.2.4.1. Detecting Rotor Frequency (MCSA)

The principle behind this scheme is that, a three-phase stator winding fed from a power supply generates a resultant forward rotating magnetic field at synchronous speed which induces voltages in the rotor windings. The voltage induced in each rotor phase winding depends on the rotor speed relative to the rotating magnetic field. The resulting rotor currents produce an effective magnetic field, which induces small currents in the stator windings at sub-harmonic frequencies of the rotating magnetic field. The rotor frequency can thus be detected from the stator current spectrum, which allows the rotor speed to be estimated [91].

From the description above, it can be clearly seen that the frequency component relating to rotor speed amplitude-modulates the supply frequency carrier. This implies that a demodulation process is required to extract the speed information from the supply current. A Fast Fourier Transform (FFT) is performed on the extracted signal to

determine the frequency component with maximum amplitude within the spectrum of interest. The basic algorithm is shown in Figure 3-1.

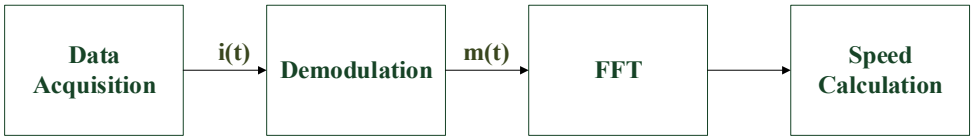

Figure 3-1. Speed estimation using rotor frequency MCSA [91].

The stator current, $i(t)$ is given in (3-4) [92] as:

$$i(t) = cos(2\pi f_1 t) \quad (3\text{-}4)$$

where: $m(t) = k_1 + \sum_{m=2} k_m cos(2\pi f_m t)$ and is the amplitude of the stator current.

k_1 - is the fundamental constant

k_m - is the mth order harmonic constant

f_1 - is the fundamental supply and

f_m - is the mth order harmonic frequency.

The demodulation process involves squaring the stator current $i(t)$ and filtering out $\frac{1}{2}m(t)^2$ from the resulting equation (5).

$$i(t) = \frac{1}{2}m(t)^2 + \frac{1}{2}\cos(2 \times 2\pi f_1 t)\, m(t)^2 \quad (3\text{-}5)$$

An FFT is done on $\frac{1}{2}m(t)^2$ in order to find the position of the maximum amplitude value. This component must be determined from the position of frequency between the lower boundary f_{low} and the upper boundary f_{syn} as in (3-1). The frequency of the rotor and hence the speed in rpm are obtained from (3-2).

The MCSA technique provides a non-intrusive way to estimate the rotor speed without the need for any additional information of equivalent circuit parameters, structures of the machine, switching frequency and switching pattern [93], besides the sampled motor current data. Accuracies of within 2% error (for inverter-fed IM) and less than 1% error (for line-fed IM) are reported in [91] and [93], respectively. However, this technique requires a large number of data points to achieve a high frequency resolution. This makes it unsuitable for use with fast response systems such as Field Oriented Control (FOC) and Direct Torque Control (DTC).

3.2.4.2. Detecting the Rotor Slot Harmonic (RSH)

Rotor slot harmonics detected in the motor current have been used to estimate the rotor speed of IMs [94]-[106]. The rotor slots of a squirrel cage IM produce a regular variation of the radial air gap permeance which interacts with the fundamental magnetising component of the air gap MMF. Since this occurs when the slip of the machine is zero, loading the machine (s≠0) causes the rotor slot MMF harmonics to further interact with the fundamental of the air gap flux. Therefore, the air gap flux is modulated by the passing rotor slots producing two harmonic components. The resulting flux density equation is given in [94]. The ripple in the air gap flux will induce corresponding current harmonics in the stator windings. In general, two or more speed dependent harmonics will appear for each harmonic in the air gap flux density whose frequencies, ω_{sh} are determined by:

$$\omega_{sh} = \frac{z}{p}\omega_r \pm \alpha\omega_1 \qquad (3\text{-}6)$$

where α = 1, 3,…., is the order of the air gap flux harmonic,

z - is the number of rotor slots,

p - is the number of pole pairs,

ω_r - is the rotor speed and

ω_1 - is the supply frequency.

The rotor frequency f_r is then given by:

$$f_r = \frac{P}{z} f_{sh} \pm \alpha f_1 \qquad (3\text{-}7)$$

The spectral components of the rotor slot harmonics that can be observed in the stator current signature in terms of the motor slip is given in (3-8).

$$f_{sh} = \left[(\lambda z \pm n_d)\left(\frac{(1-s)}{p}\right) + \alpha\right] f_1 \qquad (3\text{-}8)$$

where λ= 0, 1, 2,…., is the order of the space harmonic and n_d= 0, 1…., is the eccentricity order.

The Principal Slot Harmonic (PSH) is the first and prominent harmonic in the rotor slot harmonic series for an IM which is obtained when $\lambda = 1$, $\alpha = 1$ and when the static and dynamic eccentricities are neglected ($n_d = 0$). Equation (3-8) simplifies to:

$$f_{sh} = \left(\frac{z}{P}(1-s) \pm 1\right) f_1 \qquad (3\text{-}9)$$

Whilst most of the FFT based RSH speed estimation methods [94]-[96] reported are ideal for steady state operation, it is claimed that the method in [97] can operate in transient conditions. However, its practical implication and error analysis were not furnished as concluding remarks in that paper.

Fairly recent signal processing techniques to detect RSH in the motor current are further reported [99]-[104] as follows:

A technique based on frequency demodulation used at dynamic and steady state conditions [99] and a Maximum Covariance method for Frequency Tracking (MCFT) based on the statistical analysis of the motor current signal in the time domain [100] are presented.

Despite the good results obtained by [99], the speed estimation process can fail when motors operate at no-load or close to no-load condition. Moreover, this approach is only applicable for IMs operated from fixed-frequency power supplies.

A technique that uses Minor Space Analysis (MSA) EXIN neural networks based on classical Multiple Signal Classification (MUSIC) spectrum estimation theory is presented in [101]. The RSH related to the rotor speed is first extracted from the stator phase current using two cascaded adaptive linear elements. The frequency of the RSH and hence rotor speed is estimated using Minor Space Analysis (MSA) EXIN neural networks, which work on-line to iteratively compute the frequency of the slot harmonics based on classical Multiple Signal Classification (MUSIC) spectrum estimation theory. The MUSIC using MSA provides high frequency resolution from a short data record signal buried in noise and mitigates the long computation time when the dimension of the autocorrelation matrix increases. However, the performance of the algorithm is a trade-off between computational complexity and estimation accuracy.

Another technique that uses the Short Time Least Square Prony's method to estimate and track the PSH frequencies is presented in [102], [103]. It provides a linear-time frequency representation with high frequency resolution and adjustable time resolutions using few data samples. This reduces considerably the computational time and data storage requirements. However, the implementation of the techniques in real time applications is not fully discussed.

The rotor speed estimation using rotor slot harmonics is fairly accurate (within 5rpm) [96] even at very low and zero speed. The accuracy of the method used depends on how it is designed to obtain the requirements of high frequency resolution and short observation time. The trade-off between these requirements is difficult to achieve. The success of the trade-off determines the computational overhead of the algorithms used. Based on the analysis of this section, it is clear that knowledge of the number of rotor slots is required when the rotor speed is to be estimated from the spectral analysis of the stator current. This information may not be available for most of the installed machines. However, it is possible to implement automatic tests at different frequencies to determine the rotor slot number [94]. The signal strength of the RSH depends on some combinations of pole-pairs and number of rotor slots. Satisfying equations were derived for strong, weak and very weak RSH signal for different combinations [105].

3.2.4.3. Detecting the Rotor Eccentricity Harmonic (REH)

The estimation of rotor speed of IMs using harmonics caused by air gap eccentricity has been reported [96], [107]-[117]. Air gap eccentricity can be static or dynamic. Static eccentricity is due to stator core ovality or incorrect positioning of the rotor or stator during assembly. This results in a fixed level of static eccentricity. On the other hand, dynamic eccentricity results when the center of the rotor is not concentric with the center of rotation. This causes a minimum air gap to rotate with the rotor [107].

The frequency of the speed dependent harmonics due dynamic eccentricity, f_{ecc} is derived from (8) by making $\lambda = 0$, $n_d = \pm 1$ and $\alpha = 1$. It is then given by:

$$f_{ecc} = \left(1 \pm \left(\frac{1-s}{p}\right)\right) f_1 \qquad (3\text{-}10)$$

Unlike other methods where the accurate and specific machine parameters and/or number of rotor slots are required to estimate speed, this technique requires only the number of poles.

Different signal processing methods have been employed to extract the eccentricity harmonic for rotor speed estimation. Reference [112] uses Zero Crossing Times (ZCT) while reference [113] uses Short Time Fourier Transform and dichotomy interpolation

to detect the speed dependent harmonic from Space Vector Angle Fluctuation (SVAF) signal. In [114], the Teager-Kaiser Energy Operator (TKEO) and Interpolated FFT (IFFT) are used respectively to demodulate the stator current and to extract the eccentricity harmonic. The Hilbert transform was used to demodulate the stator current while the eccentricity harmonic detection was performed using IFFT [115] and interpolated Goertzel algorithm [116]. Most of these methods were applied to induction motors fed from sinusoidal supplies [113]-[115]. The difficulty of extracting the rotor eccentricity speed dependent harmonic in the inverter supplied stator current is aggravated in [116] by analyzing the supply side current of the inverter. However, this technique cannot be reliably used on the motor stator current where the supply side of the inverter is not accessible.

3.3. Fundamental Component Extraction

In the motor current spectrum analysis for speed estimation, the speed dependent harmonics are very small compared to the fundamental component. The fundamental frequency component is often extracted in order to accurately estimate the frequency of the speed dependent component from the residual signal. Earlier techniques [107], [108] used analogue notch filtering to extract fundamental component. Analogue filtering is prone to inaccuracies due to noise, changes in temperature and changes in supply frequency. The use of switched capacitor filters to track changes in supply frequency was presented in [108]. The filtering circuit can be very complicated if the supply frequency range is large. However, analogue filtering presents no computational overheard as the processing is done in real time.

Some methods use demodulation techniques to suppress the fundamental component [112]-[116]. Most of these techniques lack the adaptive frequency capability which is crucial for inverter-fed machines. In [109] the fundamental extraction is performed using an adaptive frequency tracking algorithm. A block diagram of the base algorithm is shown in Figure 3-2.

The formulation of the algorithm detailed in [110] is based on the gradient descend method and it tracks the desired sinusoidal component by minimizing the least square of the error function $e(t)$ defined by:

$$e(t) = i(t) - y(t) \qquad (3\text{-}11)$$

where $i(t)$ is composite input signal and $y(t)$ is the output (extracted fundamental) signal.

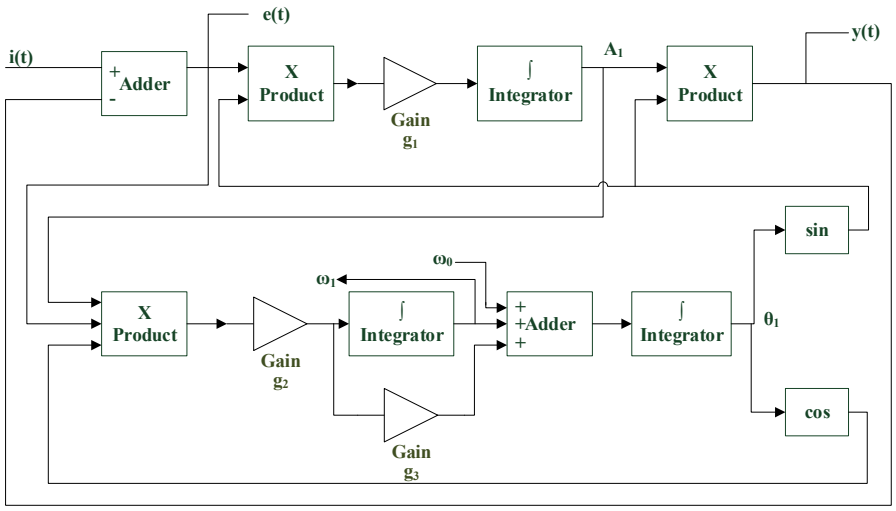

Figure 3-2. Block diagram of the adaptive sinusoid tracking algorithm.

The adaptive frequency tracking algorithm is governed by a set of differential equations below:

$$\frac{dA(t)}{dt} = 2g_1 e(t) sin\,\theta(t) \qquad (3\text{-}12)$$

$$\frac{d\omega(t)}{d(t)} = 2g_2 e(t) A(t) \cos\theta(t) \qquad (3\text{-}13)$$

$$\frac{d\theta(t)}{d(t)} = \omega(t) + g_3 \frac{d\omega(t)}{d(t)} \qquad (3\text{-}14)$$

where g_1, g_2 and g_3 are constants that determine the convergence speed and the steady state error of the algorithm, g_1 determines the convergence speed while g_2 and g_3 determine the steady state error. The choice for values of these constants is a compromise between the convergence speed and the steady state error. $A(t)$, $\omega(t)$ and $\theta(t)$ are the instantaneous amplitude, angular frequency and phase values respectively.

3.3.1. Performance of the Algorithm

To ensure that the adaptive sinusoid tracking algorithm extracts and tracks the fundamental component of the motor supply reliably, it is important to verify its performance in terms of convergence, transient response and noise immunity. Figure 3-3 through to Figure 3-8 show some simulation results obtained from Matlab/Simulink. The algorithm converges and tracks the 50Hz fundamental component within 0.1seconds (less than 5 cycles) as can be seen from the relationship between the input and output signals in Figure 3-3.

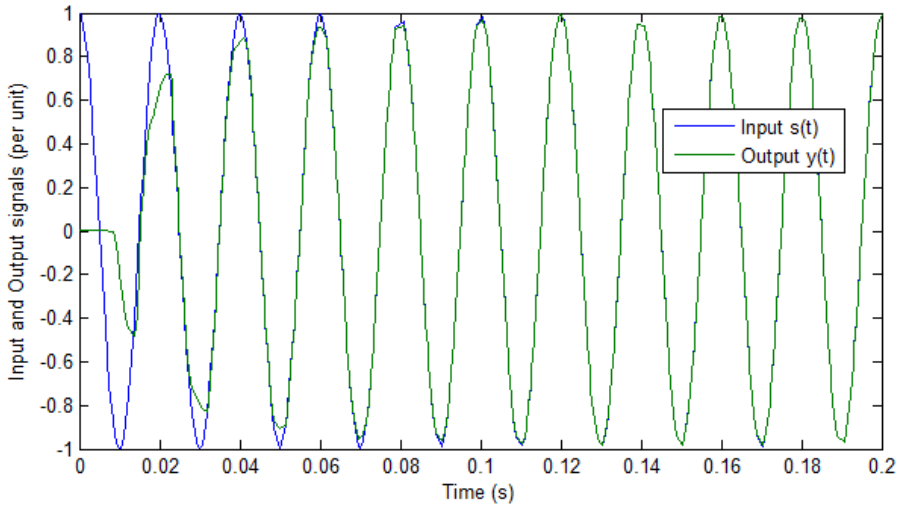

Figure 3-3. Initial convergence of the sinusoidal tracking algorithm.

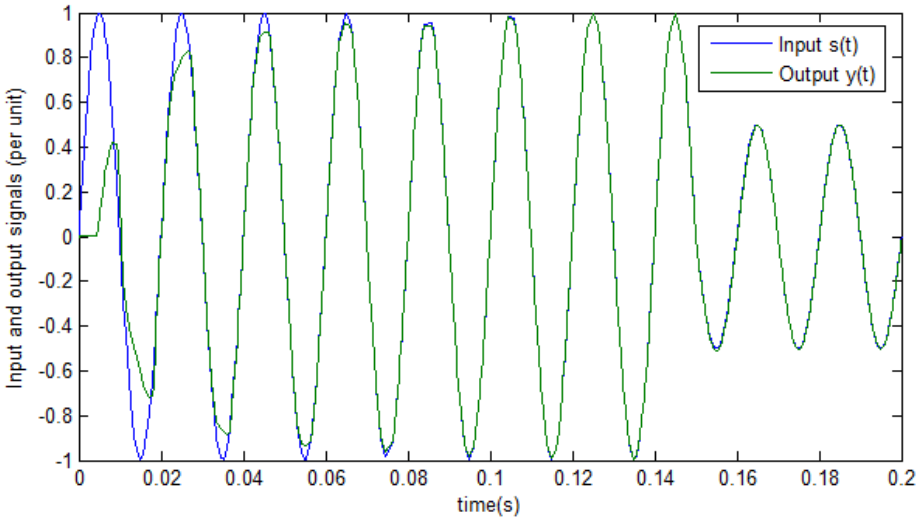

Figure 3-4. Filter response to a step change in amplitude.

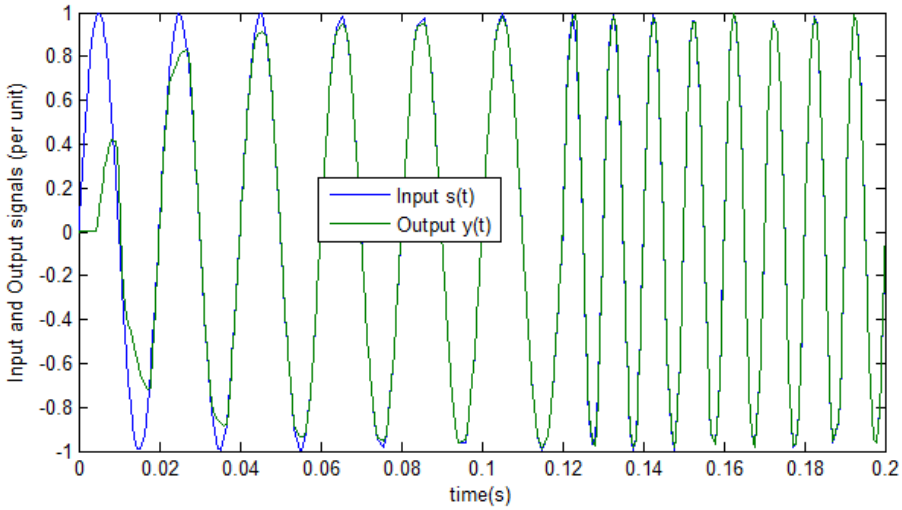

Figure 3-5. Filter response to a step change in frequency (increasing).

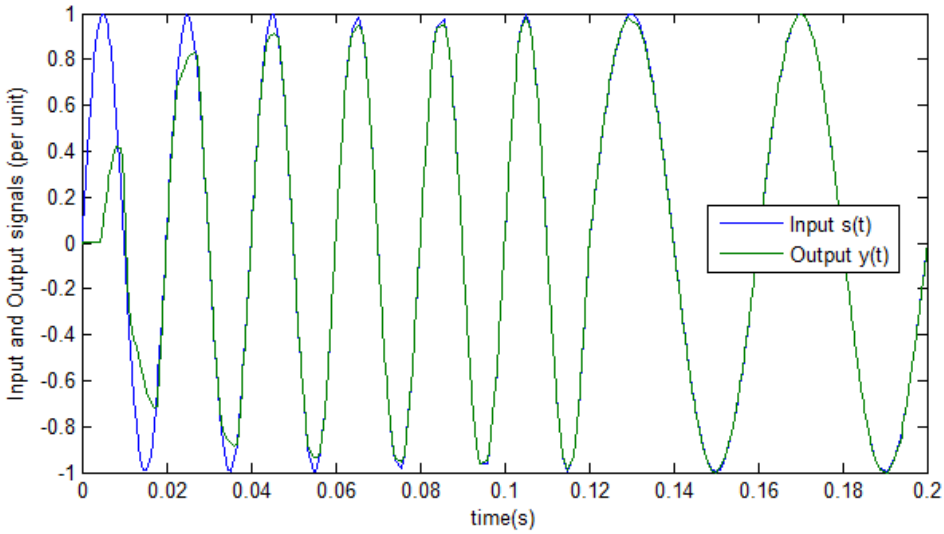

Figure 3-6. Filter response to a step change in frequency (decreasing).

The filter response to a step changes in amplitude, increasing frequency and decreasing frequency is shown in Figure 3-4, Figure 3-5 and Figure 3-6 respectively. In these cases, it is evident that the filter algorithm tracks the fundamental component during 50% changes in amplitude and frequency.

The adaptive sinusoid tracking algorithm can also perform noise cancellation as can be seen from Figure 3-7and Figure 3-8. The output signal $y(t)$ is shown to be cleaner than the input signal $s(t)$ which is corrupted by noise. This characteristic find application in signal processing techniques where measurement noise needs to be cancelled out.

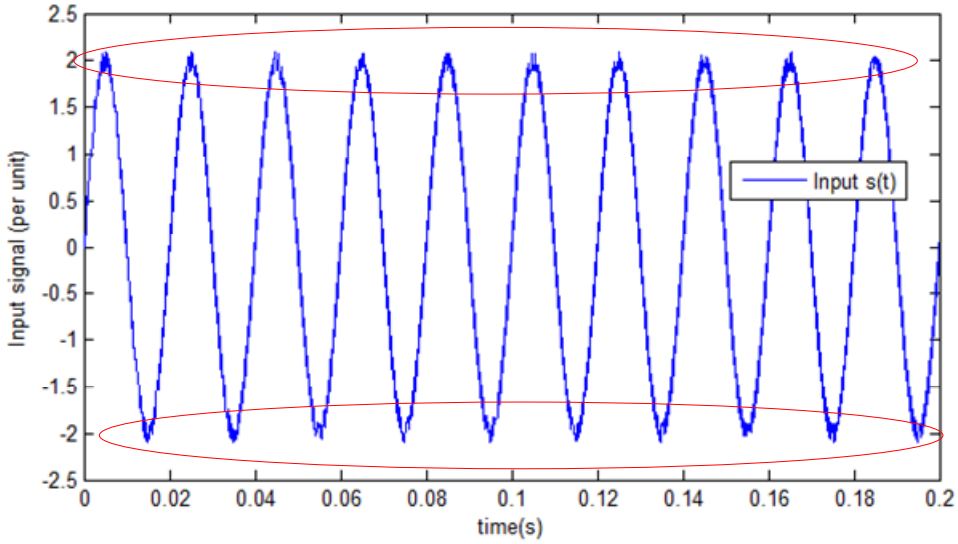

Figure 3-7. Input signal corrupted with noise.

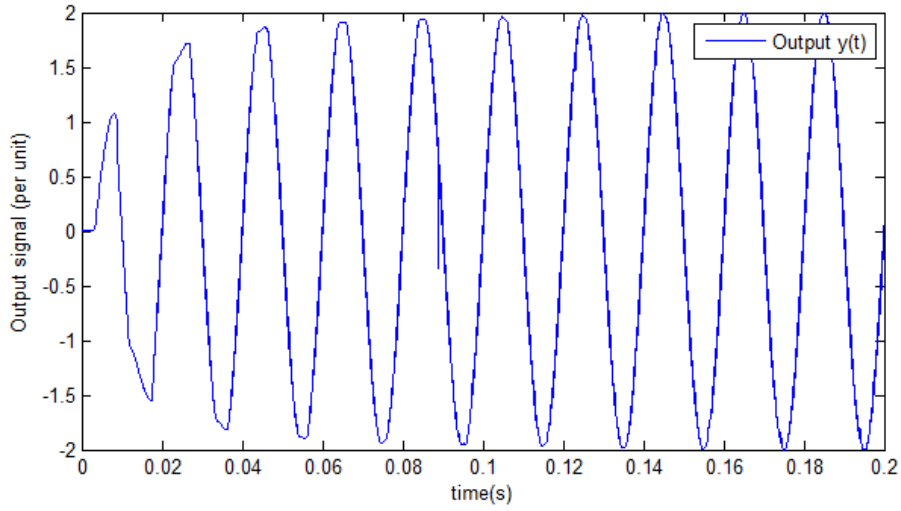

Figure 3-8. Filtered output signal.

3.4. Accuracy Comparison of Different Speed Estimation Techniques

An accuracy comparison of the different speed estimation results reported in literature is presented in Table 3-1.

Among the shaft-based techniques, the optical tachometer used in [70] present an error of <0.5% and has been used on an inverter-fed motor. Electrostatic based [72] and VBM

based [73] techniques are not declared for inverter-fed motors but present error of less than 3% with [73] reporting less than 0.5%.

These techniques can be adapted to inverter-fed driven motors without any additional hardware or software since they depend only on the rotating parts.

Almost all observed based references have been applied to inverter-fed machines. However, none of studied references reported numerical values of accuracy since the emphasis in these techniques is more of control strategies rather than purely speed estimation. The inherent drawbacks of the observer-based techniques were discussed in subsection 3.2.2.

The vibration analysis and all current spectrum-based techniques reported accuracies of grossly less than 1% with vibration analysis and rotor slot harmonic techniques reporting less than 0.5%. The experimental analysis of these claims and the issues with these techniques is presented in section 3.5 below.

Table 3-1. Reported accuracies (errors) for different speed estimation techniques.

Technique	Error	Inverter-fed?	References
Shaft Based	< 0.5%	Yes	[70]
		No	[73]
	0.5 to < 1%	Servo-drive	[74]
	1% to < 3%	No	[72]
Observer Based	0.5 to < 1%	Yes	Not declared numerically
Vibration	< 0.5%	No	[16], [19]
RSH	< 0.5%	Yes	[94], [95], [96]
		No	[99]
	0.5 to < 1%	Yes	[101], [103]
REH	< 0.5%	No	[111], [114]
		Yes	[116]
	0.5 to < 1%	Yes	[112]
	1% to < 3%	No	[115]
MCSA	< 0.5%	Yes	[91]
		No	[93]

3.5. Experimental Analysis of Vibration and Current Based Techniques

This section presents some experimental analysis of some vibration and current based techniques in order to compare with those reported in literature. The aim is to verify the practical application of these techniques and to highlight some of the shortcomings especially when applied to inverter-fed motors. The comparative analysis was conducted from data obtained from 250W, 37kW and 45kW IMs fed from inverter and grid supplies. The specification data of the three motors is shown in TABLE 3-2 below.

Vibration and current data were sampled at 25.6kS/s for 30 seconds in the case of the 250W motor using National Instruments' NI 9215 and NI 9234 modules. Current data was sampled at 1MS/s for 1 second using HBM Gen 7i high speed transient recorder and data acquisition system in the case of the 37kW and 45kW motors. The current data processing was based on adaptive frequency extraction (notch filtering), Hann windowing of the residual signal and a power spectral density FFT. The frequency of the component with highest amplitude (peak detection) was then detected from which the motor speed is estimated.

TABLE 3-2. Specification data of the test IMs.

Motor Rating	**250W**	**37 kW**	**45 kW**
Voltage (V)	190	400	400
Frequency (Hz)	50	50	50
Number of Poles	2	4	4
Full Load Current (A)	1.85	67.4	81.6
Full Load Speed (rpm)	2930	1475	1475
Number of Rotor Bars	34	58	58
Number of Stator Slots	24	72	72

The search frequency ranges for the different analysis methods in respect of the 250W, 37kW and 45kW inverter-fed motors are shown in TABLE 3-3.

The estimated motor speed values were compared with those obtained from a torque/speed sensor coupled on the motor shaft. The speed estimation errors using

different analysis techniques for three induction motors are shown in Figure 3-9 through to Figure 3-11.

TABLE 3-3. Search frequency ranges for different analysis methods.

Analysis Method	Search Frequency Range (Hz)		
	250W	**37kW**	**45kW**
Vibration	48.87 to 49.90	Not Installed	Not Installed
RSH	1712.19 to 1744.19	758.64 to 771.71	761.67 to 771.64
MCSA	47.00 to 49.85	24.48 to 24.84	24.58 to 24.84
REH	96.00 to 99.85	74.45 to 74.83	74.48 to 74.83

A comparative analysis (Figure 3-9) of the percent error when the motor is supplied from grid and from the inverter show better results when the motor is fed from grid supply than from inverter supply.

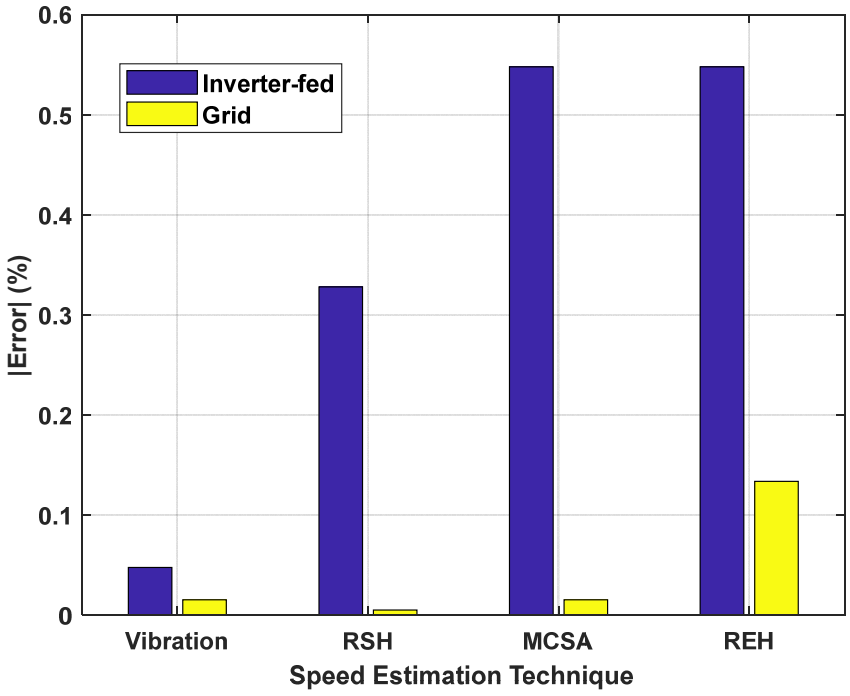

Figure 3-9. Comparative percent error when the motor (250W) is supplied from grid and from inverter using different analysis techniques at 50% load.

This is due to the difficulty in identifying the correct harmonic component when its amplitude is not large enough relative to nearby noise components when processing inverter current data. In this case, special treatment of the signal processing techniques may be necessary when the motor is fed by an inverter supply due to these random noises and supply harmonics. The percent error from the vibration signature analysis technique is much less compared to current spectrum-based techniques for inverter-fed applications due its immunity to the switching noises from the inverter supply.

The estimated speed percent errors for 37kW and 45kW motors at different load points using different current based analysis techniques when the motor is fed from inverter supply are shown in Figure 3-10 and Figure 3-11 respectively.

Considering both motors across the different loads, the rotor speed percent error using rotor slot harmonic, rotor eccentricity and MCSA analysis techniques was less than 0.07%, less than 0.3% and less than 0.4% respectively.

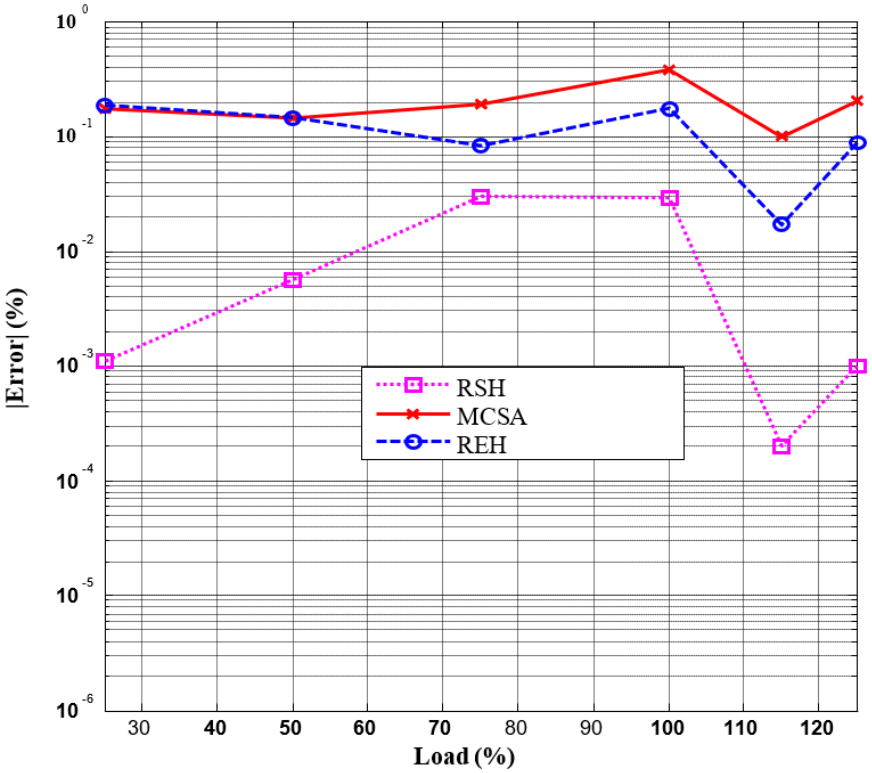

Figure 3-10. Speed estimate percent errors for the 37kW at different load points using different current based analysis techniques when the motor is fed from inverter supply.

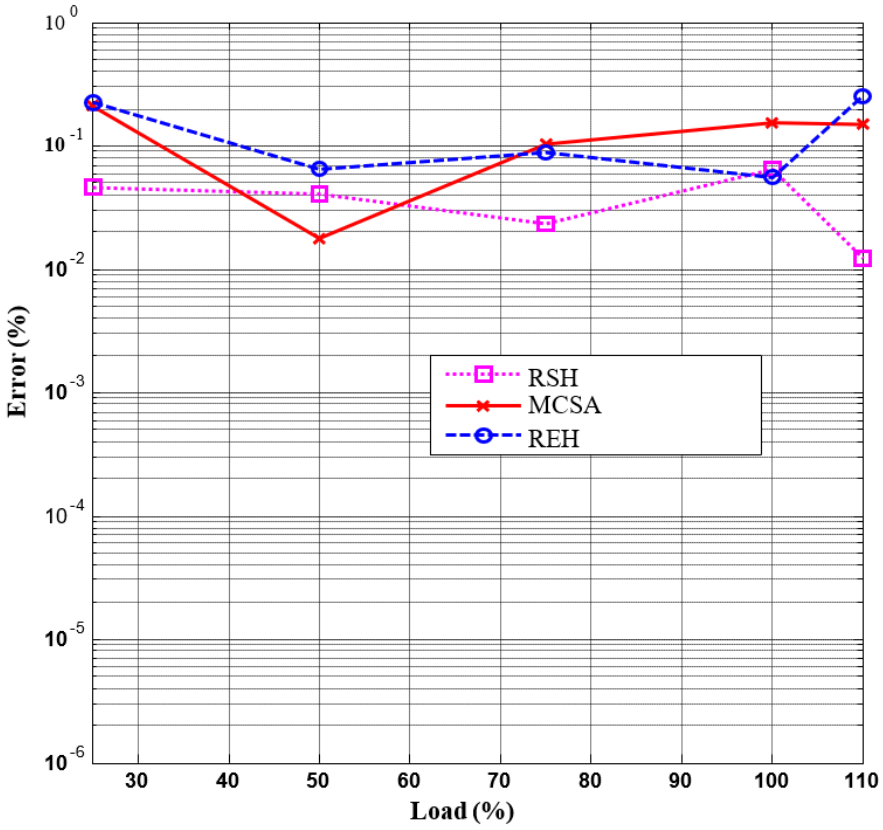

Figure 3-11. Speed estimate percent errors for the 45kW at different load points using different current based analysis techniques when the motor is fed from inverter supply.

It should be noted that, these results are in good agreement and are comparable to those reported in literature. Although the results were obtained under very narrow search frequency ranges as seen in TABLE 3-3, the use of advanced signal processing techniques such as MUSIC may widen the search frequency range due to the seperation of signal space and noise space. This means that the harmonic of interest may still be dominant over a wider signal space frequency range.

3.6. Sensitivity Analysis

The sensitivity analysis is carried out to investigate the impact of a small measurement error of the speed dependent harmonic frequency to the resultant estimated motor speed. A small change Δf equal to the frequency resolution used in this experimental test for the 250W motor was chosen. The frequency resolution, Δf was given by:

Δf = Sampling Frequency / Number of Samples

= 25600/768000

= 0.033 Hz

The impact of Δf to the resultant estimated speed for different analysis techniques is shown in TABLE 3-4, where Nr is the estimated speed at 50% load, Nr++ is the new estimated speed when a small frequency error is introduced. ΔNr is the resultant estimated speed error. It can be seen that the rotor slot harmonic analysis provides the least error in estimated speed when small variations in frequency estimation is encountered.

The rest of the techniques are fairly stable, providing resultant speed deviations within 1.5 rpm when the small frequency error is encountered. These sensitivity results instil confidence in the use of these non-intrusive motor speed estimation techniques due to their robustness.

TABLE 3-4. Sensitivity analysis for different speed estimation techniques using data obtained from 250W IM at 50% load.

Analysis Technique	Δf	Nr (rpm)	Nr++ (rpm)	ΔNr (rpm)
Vibration	0.033	2956.056	2957.5208	1.4648
RSH	0.033	2955.529	2955.5725	0.0431
MCSA	0.033	2956.056	2957.5208	1.4648
REH	0.033	2951.658	2953.1228	1.4648

3.7. Recommended Techniques for Non-intrusive Speed Estimation of Inverter-Fed Induction Motors

Based on the analysis of the speed estimation techniques and following the criteria of; non-intrusiveness, accuracy, applicability to inverter-fed motors and the current trend of research, it is recommended that current spectrum-based techniques, particularly RSH detection and REH, where applicable, be employed for non-intrusive speed estimation of inverter-fed induction motors. Fairly recent publications [101] (2015), [102] (2015), [103] (2016), [116] (2019) report good accuracies (within 5rpm) [96] even at very low

and zero speed. These techniques use advanced signal processing algorithms that fulfils the requirements of high frequency resolution, less computational time and applicable to non-stationary signals. Algorithms which are based on MUSIC typically separate the signal space and the noise space [101]. Their use is quite ideal in processing current data derived from inverter-fed IM which is normally infested with harmonic and inter-harmonic noise. Recent approaches [116] recommend the use of the supply side current of an inverter-fed IM which is practically unaffected by electromagnetic interference (EMI) effects. The current spectrum-based techniques are quite accurate and non-intrusive as seen from literature reports and experimental analysis. Their use for speed estimation in slip-based non-intrusive efficiency estimation is convenient since they are derived from current data which is also an input to machine parameter estimation algorithms [93], [117].

3.8. Concluding Remarks

Following the analysis of the rotor speed estimation techniques for inverter-fed induction motors reported in literature and from the experimental verification, it can be concluded that the current spectrum based speed estimation techniques coupled with advanced signal processing algorithms that fulfils the requirements of high frequency resolution, less computational time and applicable to non-stationary signals provide mature technology and are recommended for industrial use.

Although the accuracy of the vibration signature analysis technique is better than the current spectrum techniques, the current spectrum-based speed estimation is conveniently derived from the same data set that is used to estimate induction motor parameters in non-intrusive efficiency estimation, with sufficient accuracy.

The sensitivity analysis showed that the speed estimation techniques are robust and insensitive to small frequency fluctuations. In literature, interpolation techniques have been used to improve rotor frequency estimation.

Accuracies of less than 1% have been reported in literature and experimental verification when using vibration analysis, MCSA RSH and REH analysis techniques in inverter-fed IMs. Observer based techniques are only applicable as speed estimators in motor control systems and require specific parameters of the motor.

Chapter 4

EQUIVALENT CIRCUIT MODELLING, NON-INTRUSIVE PARAMETER ESTIMATION AND HARMONIC LOSS ANALYSIS OF INVERTER-FED INDUCTION MOTORS

4.1. Introduction

Recent research advances [56], [70], [123] have been focused on non-intrusive efficiency estimation of inverter-fed IMs based on equivalent circuit modelling and iterative optimization parameter estimation techniques.

Different equivalent circuit topologies have been used for efficiency estimation with various assumptions that govern their formulation. A better equivalent circuit is one that closely represents the electrical and magnetic characteristics of the IM when it is fed by a sinusoidal or non-sinusoidal supply. Most equivalent circuits for inverter-fed IMs are derived from the conventional (standard) IM equivalent circuit [93], [124], [125]. In some cases [124], [125], harmonic loss analysis is carried out using this equivalent circuit. However, in these cases, no-load and locked rotor tests are carried out to determine the equivalent circuit parameters. This operation is highly intrusive and is not suitable for non-intrusive loss analysis. Moreover, it may be necessary to consider parameter changes due to skin effect on the rotor losses at higher harmonic orders. Harmonic rotor parameters are not modelled in this conventional equivalent circuit.

The development of inverter-fed IM equivalent circuits has resulted in different harmonic equivalent circuit topologies. Most of these topologies differ in the way iron losses and stray load losses are treated and the assumptions taken when considering high frequency harmonic components. For the purpose of non-intrusive efficiency estimation of IMs, it is necessary to determine the parameters of the equivalent circuit in the least intrusive manner. In the last few decades, parameter estimation using iterative optimization techniques have been used [19], [20], [56], [70], [93], [123]. However, some approaches [19], [20] were based on IMs fed by sinusoidal supplies with no consideration for parameter changes due to harmonic frequencies.

This chapter presents the application of a non-intrusive PBIL and BFO algorithms to estimate parameters of two PWM inverter-fed motors using two different harmonic equivalent circuits. Two sets of parameters are obtained using PBIL from a single motor, that is, motor parameters when using rms PWM supply measurements and motor parameters when using fundamental components of the PWM supply (similar to

sinusoidal supply). The estimated parameters are compared to measured parameters according to IEC-60034-2-1 to validate the estimation technique. The estimated parameters due to fundamental components of the PWM supply are used as base parameters when harmonic rotor parameters (using BFO) and harmonic loss analysis are considered.

The chapter is organized as follows: Section 4.2 considers equivalent circuit topologies and parameter estimation. The aim is to identify the most suitable harmonic equivalent circuit and the best parameter estimation technique for non-intrusive efficiency estimation. Section 4.3 presents the proposed algorithm for non-intrusive efficiency estimation of inverter-fed IMs based on harmonic regression analysis, harmonic parameter estimation and harmonic loss analysis. Section 4.4 concludes the chapter.

4.2. Harmonic Equivalent Circuits and Parameter Estimation

This subsection explores the different inverter-fed induction motor equivalent circuit topologies in order to narrow into the most suitable equivalent circuit for the proposed efficiency estimation technique. The different equivalent circuit parameters are identified and described, and some equivalent circuit parameter estimation techniques are explored. A case study of parameter estimation using PBIL is described and some experimental results for two induction motors are presented.

4.2.1. Inverter-Fed IM Equivalent Circuit Topologies

Various harmonic equivalent circuit models have been developed for IMs fed by inverter supplies. The conventional equivalent circuit suitable for inverter supplies and from which other models are derived is shown in Figure 4-1 where:

R_s - is the stator resistance

X_s - is the stator leakage reactance

R_r - is the rotor resistance

X_r - is the rotor leakage reactance

R_m - is the core loss equivalent resistance

X_m - is the core leakage reactance

I_s, I_m, I_r - are the stator, magnetic core and rotor currents respectively

h - is the harmonic order

s - is the machine slip

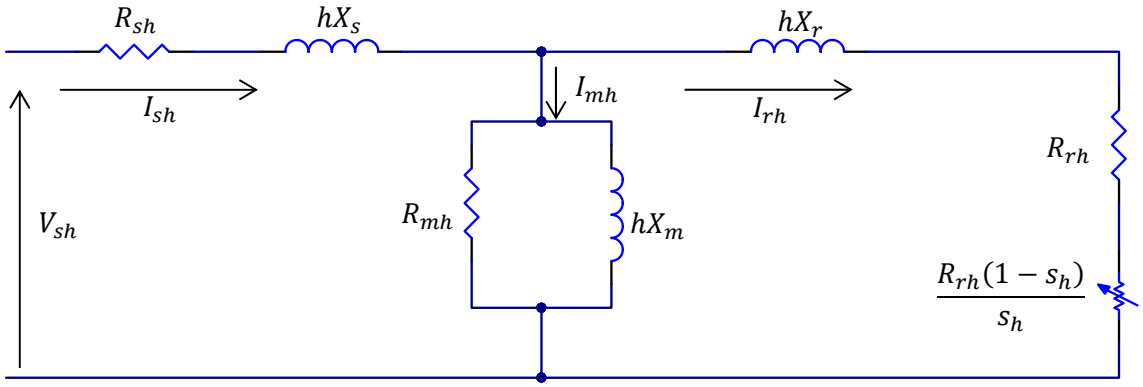

Figure 4-1. Harmonic equivalent circuit derived from conventional IM equivalent circuit.

It is quite evident in Figure 4-1 that the stray load component is not included in this circuit. In most cases [19], [20], [70], the stray load loss is determined using assumed values according to Table 2-1. In [126], an equivalent circuit with a stray load resistance in parallel with the rotor leakage reactance is proposed while [127] proposes a stray load resistance in series with the stator impedance. According to [128] these circuits do not consider the braking torques caused by slot harmonics and the losses caused by the inverter carrier frequency.

An improved equivalent circuit similar to Figure 4-1 with a stray load equivalent resistance, R_{sLL} in series with the rotor impedance and considers supply harmonics is presented in [128] and shown in Figure 4-2. Like Figure 4-1, this equivalent circuit is similar to the conventional equivalent circuit provided by the IEC 60034-2-1 Standard but provide additional analysis of the stray load loss. However, in [128] the circuit parameters were determined by FEM analysis and compared with those obtained by experiments. Although the difference between the results of the improved circuit and that obtained by experiments were relatively small, this method involved numerous off line calculations making it unsuitable for online parameter estimation for non-intrusive motor efficiency estimation. Moreover, it is reported that the qualification of this method is only verified particularly under high speed conditions.

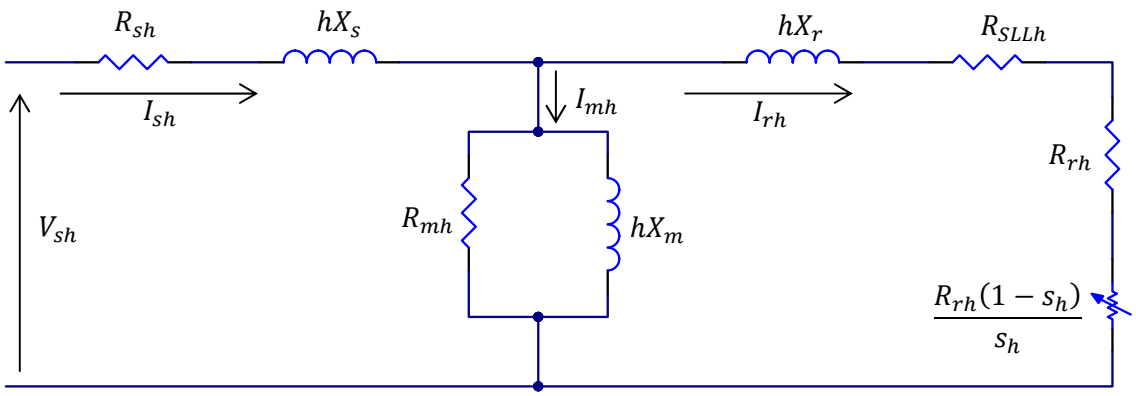

Figure 4-2. Equivalent circuit including stray load resistance.

A modified equivalent circuit of an inverter-fed, double cage IM that includes a load dependent stray load loss $R_{SLLh,r}$ and a constant stray harmonic loss $R_{SLLh,s}$ [129] is shown in Figure 4-3.

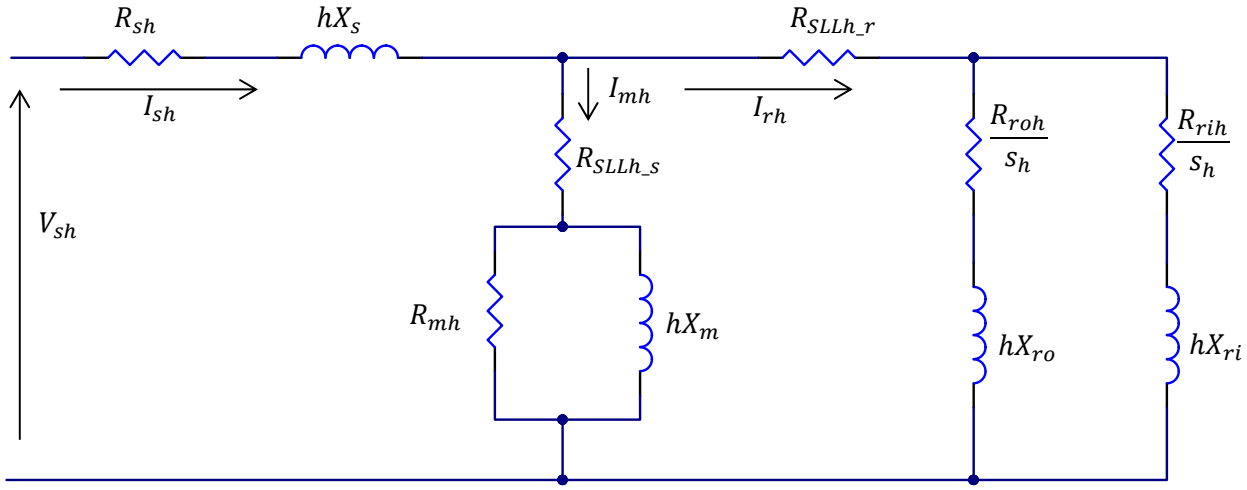

Figure 4-3. Modified equivalent circuit showing load dependent stray load loss and constant stray harmonic loss resistances.

Outer and inner rotor cage parameters are denoted by ro and ri respectively. It is observed in [129] that the harmonic stray load loss remains constant with motor loading in contrast to [6] which specifies a general increase with motor loading.

The harmonic equivalent circuit similar to that shown in Figure 4-4 was proposed in [56] and [125]. The equivalent circuit was developed based on the following assumptions.

1) The harmonic slip s_h is close to unity when the motor is running in its normal operating regions near the synchronous speed of the harmonic component.
2) Under this condition, the core loss resistance and magnetizing reactance are much larger than the stray load loss equivalent resistance R_{SLLh} and harmonic rotor resistance, R_{rh}.

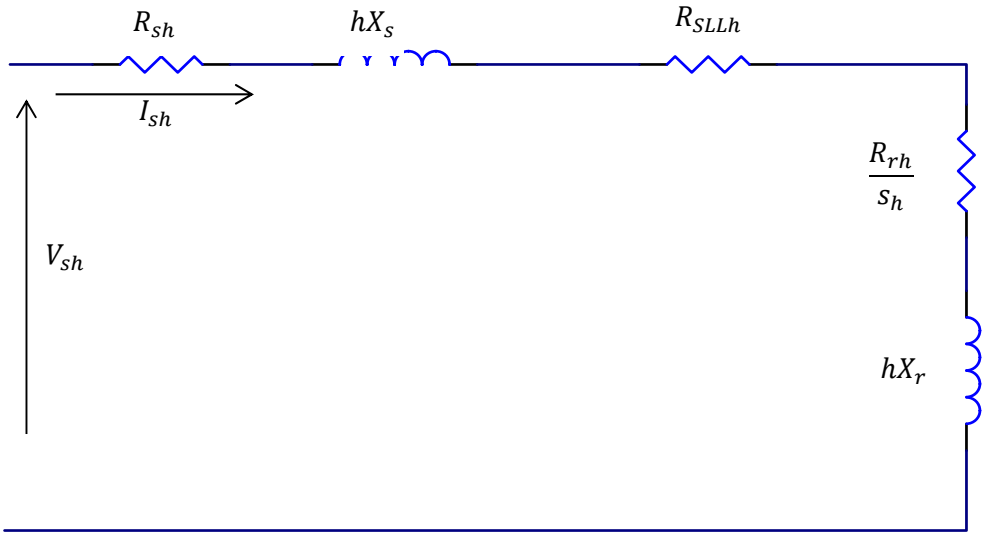

Figure 4-4. Harmonic equivalent circuit with no core loss.

The elimination of core losses due to assumption 2) raises some concerns since the core losses do not only depend on the magnetizing current (which decreases with the increase in harmonic frequency) but also depend on the square of the frequency (2-31).

Contrary to the aforementioned assumptions, Figure 4-5 shows a modified equivalent circuit that uses the phase sequence harmonic components of voltages and currents [56] that aim to consider the effect of harmonics on core losses. This equivalent circuit model can generally be used for both fundamental and harmonics and is applicable to all motor sizes fed by either sinusoidal or non-sinusoidal supplies [56].

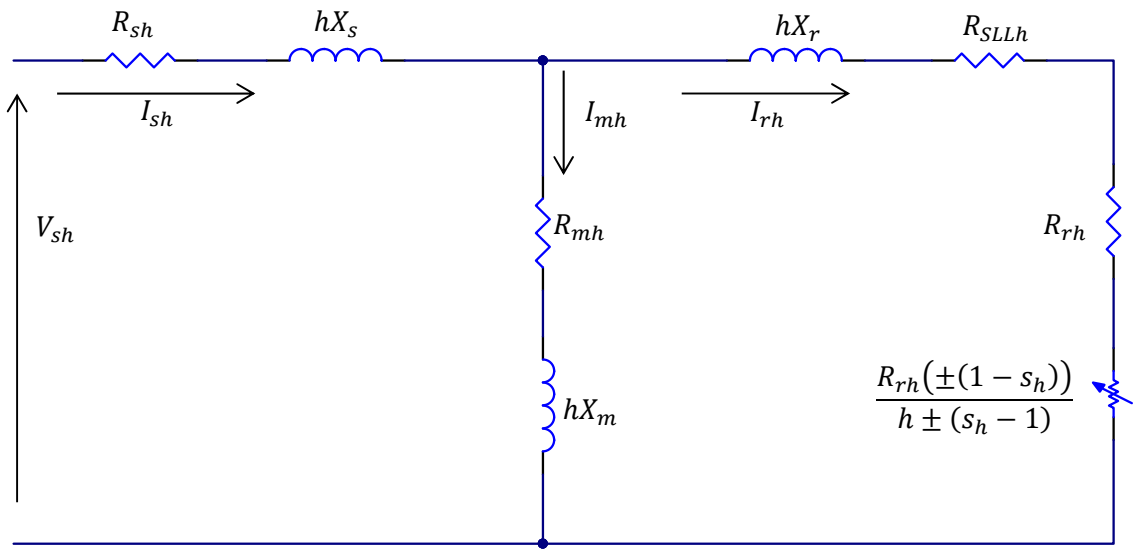

Figure 4-5. Modified harmonic equivalent circuit including core loss.

Despite the numerous equivalent circuits proposed for performance analysis of IM, [19] presents two versions for efficiency estimation, the standard equivalent circuit similar to Figure 4-2 and an iron loss equivalent circuit shown in Figure 4-6.

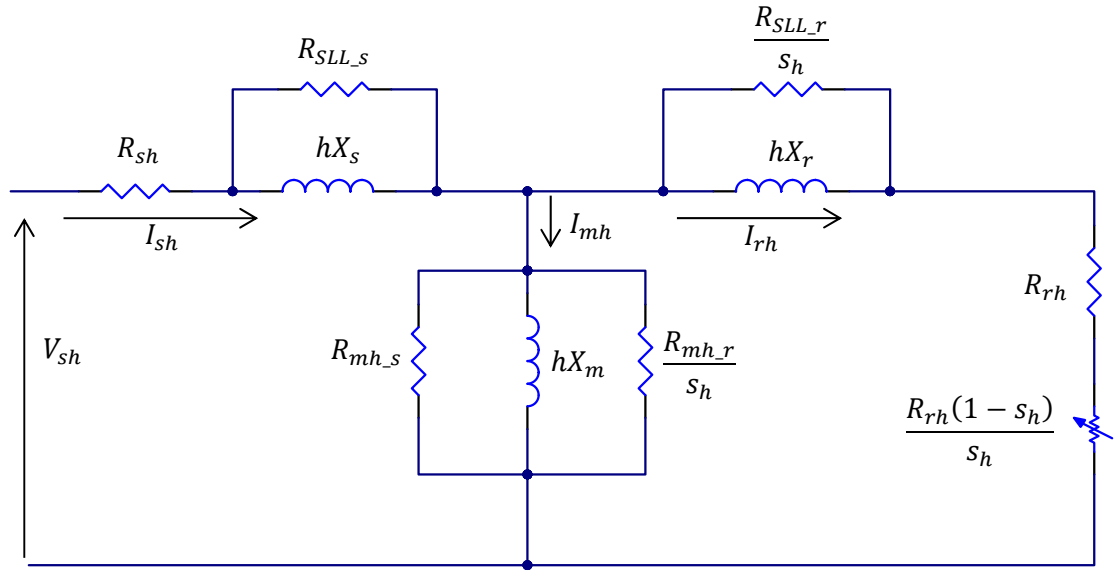

Figure 4-6. Iron-loss equivalent circuit.

These circuits have been presented in this thesis to analyse the machine parameters when fed from the inverter supply. The iron-loss equivalent circuit has stray-load and iron losses accounted for in the stator and rotor of an IM.

Another model presented in literature [130]-[133] is the motor inverse-Γ equivalent circuit shown in Figure 4-7. The circuit is claimed to have the same input impedance as the conventional equivalent circuit and the parameters of the two equivalent circuits are related by a set of equations presented in [133]. Clearly this circuit does not show the equivalent core resistance, therefore may not be used for core loss estimation.

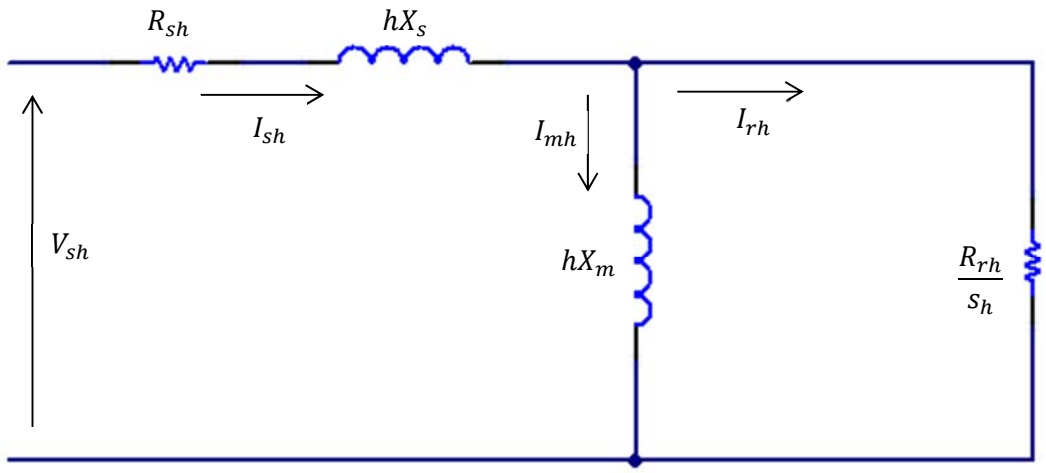

Figure 4-7. Induction motor inverse-Γ equivalent circuit.

From the discussion above, it is recommended that the equivalent circuit of Figure 4-2 be used for non-intrusive efficiency estimation because of the following criticisms of the other equivalent circuits:

1) Figure 4-1 does not include a stray load loss equivalent resistance. This means the non-intrusive efficiency estimation technique will only rely on assumed values of stray load loss which is a constant percentage of machine rated power at all load points. It is desirable to compute stray load loss at any load point.
2) Figure 4-3 is suitable for double cage induction motors and thus increases the number of parameters. The effect in optimization algorithms is to increase the search space resulting in huge computational overhead before convergence to a solution.

3) Figure 4-4 does not include the core loss and may cause substantial efficiency estimate errors.
4) Figure 4-5 considers the core impedance as a series combination of core loss resistance and magnetising reactance. This deviates from the standard equivalent circuits of IEEE 112 and IEC 60034-2-1 and may cause substantial errors when the estimated parameters are compared with the standard measurement of parameters. This notion is for convenience only where parameter estimation analysis is prioritized. Otherwise, this circuit has been used in optimization based efficiency estimation algorithms with good accuracy.

Therefore, the equivalent circuit of Figure 4-2 will be used for parameter estimation and the efficiency results will be compared to those obtained by IEC-TS 60034-2-3 standard and a direct method. Contrary to [128], the fundamental and harmonic parameters of Figure 4-2 will be estimated using evolutionary algorithms based on measured values across a wide speed range. The iron loss circuit of Figure 4-6 will only be used for fundamental parameter estimation to enhance the estimation technique.

4.2.2. Considerations about Parameters

Some considerations regarding the parameter determination and search interval constraints used in parameter estimation based on iterative algorithms including the assumptions made for harmonic parameters are considered in the following subsections

The cold stator resistance is normally measured directly and corrected to operating temperature according to temperature class [3]. The corrected stator resistance R'_s (in ohms) can be found from equation (2-22). The measurement of the cold stator resistance is usually an intrusive operation that entails the shutdown of the motor. The stator resistance is assumed to be the same at all harmonic frequencies due to negligible skin effect on the stator conductor. However, the stator loss due to harmonic currents will be investigated under this condition.

4.2.2.1. Stator Leakage Reactance

The stator fundamental leakage reactance X_s is considered to be within 7% and 15% of the base input impedance, Z_b given by (4-1) [132]. However, a constraint 0 -50 is used as the initial search interval in the iteration algorithm used to estimate the value of X_s.

$$Z_b = \frac{V_n}{\sqrt{3}.I_n} \tag{4-1}$$

where:

$$V_n = \sqrt{\left({V_{s1}}^2\right) + \sum_{h=2}^{\infty}\left({V_{sh}}^2\right)} \tag{4-2}$$

is the rms value of the input stator line voltage and

$$I_n = \sqrt{\left({I_{s1}}^2\right) + \sum_{h=2}^{\infty}\left({I_{sh}}^2\right)} \tag{4-3}$$

is the rms value of the stator line current.

The measurement methods used in IEC 60034-2-1 Standard depend on some values obtained through no-load tests which are too intrusive for in-service parameter estimation.

The harmonic stator leakage reactance X_{sh} is directly proportional to the fundamental stator leakage reactance as shown in (4-4).

$$X_{sh} = hX_s \tag{4-4}$$

4.2.2.2. Rotor Leakage Reactance

The rotor leakage reactance X_r is related to the stator leakage reactance by a constant factor, k that depends on NEMA machine design class.

$$X_r = \frac{X_s}{k} \tag{4-5}$$

where $k = 1.0$ for Design A, D and wound rotor motors, $k = 0.67$ for Design B motors and $k = 0.43$ for Design C motors (see Table 4-1). The effect of these assumptions on the

overall efficiency of the motor was investigated in [58] and it was concluded that the algorithm used was barely sensitive to k.

The harmonic rotor leakage reactance X_{rh} is directly proportional to the fundamental rotor leakage reactance as shown in (4-6).

$$X_{rh} = hX_r \tag{4-6}$$

At higher frequencies, the rotor bar current is concentrated toward the top of the bar, decreasing the effective conductive area of the bar, which increases the bar resistance and decreases the bar inductance [56].

4.2.2.3. Rotor Resistance

The determination of rotor resistance by the methods detailed in IEEE and IEC standards involves numerous locked rotor, variable frequency and variable voltage impedance tests. These methods are too invasive for in-service motor parameter estimation.

High-frequency harmonic rotor currents flowing in the rotor bars cause substantial changes to rotor resistance due to skin effect. The determination of rotor resistance at these harmonic frequencies is difficult to achieve because of variations in the shapes and sizes of the rotor bars. Some analysis of rotor resistance as a function of frequency and conductor height for a rectangular conductor with open slots is conducted in [45] and outlined in subsection 2.5.2 of this thesis. In this chapter, the base rotor resistance due to the fundamental component of the PWM supply and the rotor resistance due to the rms PWM supply are considered. Harmonic rotor resistance is considered in subsection 4.3.2.

4.2.2.4. Core Loss Equivalent Resistance

The IEEE and IEC standards determine core loss equivalent resistance by carrying out no-load tests which are intrusive for in-service motor parameter estimation.

The core loss equivalent base resistance R_m constraint is chosen in such a way that R_m is significantly larger than the magnetizing reactance. Both are much larger than the rotor leakage reactance and the rotor resistance at fundamental frequency. The harmonic core loss equivalent resistance is a function of harmonic voltage squared and harmonic core

loss as shown in (4-42) based on harmonic loss factor characteristic curves for a particular machine.

Magnetizing Reactance

The magnetizing reactance, X_m constraint is chosen in such a way that X_m is much larger than the rotor leakage reactance and the rotor resistance but much less than the core loss resistance at fundamental frequency.

The harmonic magnetizing reactance is directly proportional to frequency.

$$X_{mh} = hX_m \tag{4-7}$$

4.2.2.5. Stray Load Loss Equivalent Resistance

Stray load losses vary with the load conditions and are assumed to vary closely with the square of the applied load torque [3]. With reference to the equivalent-circuit-based parameter estimation approach, a stray load loss representative resistance is added in the rotor circuit (Figure 4-2 - Figure 4-6) to allow for the variation of stray load loss with load. The fundamental stray load loss resistance R_{SLL1} is given by (2-34) based on Figure 4-2 and assumed values of the stray load loss recommended by IEEE-112-2017 Standard [3] (see Table 2-1).

The variation of the harmonic stray load resistor R_{SLLh} with frequency is assumed to be proportional to $h^{0.8}$ with sufficient accuracy as shown in (2-35) [56].

4.2.2.6. Friction and Windage Losses

In most non-intrusive efficiency estimation cases [58]-[60], the friction and windage losses are assumed to be 1.2% of the rated input power. At the time of writing this thesis, there is no friction and windage representative resistance in any of the IM equivalent circuits. This is because the friction and windage losses are not directly related to input voltage or current but rather to the speed of the motor shaft in accordance with equation (5-7).

4.2.3. Parameter Estimation Methods

The following subsections explore some of the parameter estimation methods of IMs and assess their suitability for use in non-intrusive efficiency estimation of inverter-fed motors.

4.2.3.1. Standard Methods

International efficiency testing standards such as IEEE 112 Standard, IEC 600034-2-1 and JEC 37 employ methods that measure parameters of the IM. These methods are generally highly intrusive but will be discussed here for completeness of the entire parameter estimation study.

The IEEE 112 Standard measures IM parameters and efficiency using equivalent circuit-based Methods F and F1. These methods are discussed here because most of the non-intrusive efficiency estimation techniques [16], [19], [58] are developed based on some assumptions used in these methods. The difference between the two methods is simply the way stray-load loss is determined. The stray load loss is directly measured in Method F and an assumed value as a percentage of the output power is used in Method F1, in accordance with Table 2-1.

In Method F/F1, the parameters of the equivalent circuit are derived from test data during a no-load test and a locked rotor impedance test. Having obtained the stator resistance from direct resistance measurement of the stator windings, the no-load and the impedance test data are used to calculate X_m and X_s using an assumed initial value for X_s/X_m and an iterative scheme. The rotor leakage reactance, X_r is calculated based on the ratio of X_s/X_r for machine design class defined by NEMA MG-1-2003 as shown in Table 4-1.

Table 4-1. Assumed values for X_s/X_r according to motor design class.

Motor Design Class	X_s/X_r
A, D and wound rotor motors	1.0
B	0.67
C	0.43

R_m is calculated using the values for the above parameters and the total core losses as determined by the no-load test. R_r is calculated using the values for the above parameters and the values measured from locked rotor tests.

The IEC 60034-2-1 and JEC 37 standards essentially employ the same procedures for determining motor parameters as IEEE 112 Standard except that IEC 60034-2-1 assumes different values for stray-load losses as a fraction of the input power as shown in Table 4-2. The JEC 37 method sets stray-load losses equal to zero. The IEC 60034-2-1 and JEC 37 measured efficiencies are generally higher than those obtained by IEEE 112 Standard owing to the different assumed values of stray-load losses.

Table 4-2. IEC 60034-2-1 Assumed stray-load loss values.

Machine rating P_2 in kW	**Stray-load loss as a fraction of input power P_1**
$P_o \leq 1kW$	$P_i \times 0.025$
$1kW < P_o < 10000kW$	$P_i \times \left[0.005 - 0.005log10\left(\frac{P_o}{1kW}\right)\right]$
$P_o \geq 10000kW$	$P_i \times 0.005$

Although the standard methods are quite accurate for efficiency estimation based on the measured parameters, they are generally highly intrusive, and their use is only focused on sinusoidal supplies. The IEC-TS 60034-2-3 Technical Specification [6] provides methods and procedures for determining efficiency of inverter-fed motors. However, at the time of writing this thesis, the IEC-TS 60034-2-3 is still a draft awaiting qualification to a standard. The Technical Specification refers all its sinusoidal supply testing procedures to IEC-60034-2-1 Standard. This testing standard is adopted in this study to obtain parameters of the PWM inverter-fed motor(s) using PWM supply fundamental measurements and rms PWM supply measurements (Chapter 5).

4.2.3.2. Observer-Based Methods

The estimation of the instantaneous IM's rotor flux position requires the priori knowledge of IM parameters [135]. Changes in temperature and saturation levels of the machine vary the machine parameters and, hence, indirectly influence both the steady

state and the dynamic operation of the drive system. The process of parameter estimation can be performed offline or online. The online process is usually automated and can be one of two forms. The first is parameter identification during the first power up based on special designated test cycles of the motor. This form is termed auto-commissioning or self- commissioning. The second is online identification of motor parameters during normal operation of the drive.

Different observer-based methods for parameter estimation have been proposed [135]-[140]. In [132] an automatic procedure for the identification of the inverse-Γ equivalent circuit of inverter-fed IM is presented. The procedure operates at standstill and includes both magnetic non-linearity and compensation of inverter non-ideality. It is non-intrusive given that the procedure is performed at standstill without any changes in motor connections and is suitable for motors already installed in the plant. It is however an off-line procedure that is not ideal for real time parameter estimation for instantaneous control of the motor.

In [137] the results of an off-line parameter identification method based on minimum Mean Square Error (MSE) of the recorded time responses and mathematical models of the drive are presented. The numeric static optimization of Box's method was applied in parametric identification of the drive system parameters. The results were compared with catalogue data and with results obtained from no-load and short circuit tests. It is pointed out in this paper that identification errors could largely be caused by the identification method, plan and experimental techniques used.

A procedure to estimate the parameters of a five-phase induction machine is presented and implemented in [138]. The procedure is based on standstill time domain tests and Recursive Least Squares (RLS) algorithms. Correlation with corresponding parameters obtained from previous tests is established where electrical parameters of the same five-phase inverter motor drives were identified using various procedures based on sinusoidal excitation of the machine only.

Although observer-based methods for parameter estimation are ideally applicable for optimization control of induction machines, the estimated parameters can well be

adapted for use in efficiency determination using segregation of losses. However, the implementation of the observers and the requirement for linearizing nonlinear models of the IM in order to estimate the parameters at a specific operating point makes the whole process extremely complex. The detailed study of observer-based parameter estimation and induction motor control is beyond the scope of this research.

4.2.3.3. Optimization Methods

The parameters of IMs have been estimated using iterative methods or search algorithms based on measured values obtained from the IM's supply. These methods are non-intrusive since a shutdown of the machine is not required to determine its parameters. The estimation of parameters can be done off-line or on-line. Different optimization techniques for parameter estimation have been reported in literature as described in the following paragraphs.

The Particle Swarm Optimization (PSO) technique was used to estimate parameter values in [141]-[143]. The PSO is a population-based search algorithm based on the simulation of the social behaviour of birds, bees or a school of fishes. The particle swarm technique for optimization purpose was first proposed by Kennedy and Eberhart in the year of 1995. Experimental data was analyzed using PSO and H-G diagram (complex impedance plane) based resistance estimation techniques in [141]. In [143] a simple online parameter estimation scheme utilizing only online measured data is reported. The equivalent circuit parameters are estimated using the PSO technique based on Kirchoff's laws. In both cases, the results are compared with those obtained from IEEE 112 Standard procedures. However, the application of the PSO technique in this case was only validated for grid supplied machines. The application of the technique to inverter-fed machines is worthwhile.

Evolutionary search algorithms such as GAs have been used to estimate parameters of IMs [20], [58], [93], [123], [144]-[146]. A GA is a heuristic search algorithm that is inspired by Charles Darwin's theory of natural evolution. This algorithm reflects the process of natural selection where the fittest individuals are selected for reproduction in order to produce offspring of the next generation. In most cases [20], [93], [58], [123] the GA is used as a tool to estimate parameters for the purpose of efficiency estimation of IMs.

In [144] the GA is compared to Genetic Programming (GP) as tools for parameter estimation in an application developed for low accuracy system level studies. Among other merits, the GA has found strengths in automatically generating the initial guess for the algorithm solution and most probably converging to a global optimum. However, these merits are benefited at the expense of large processing overheads by the algorithm.

In [145] an off-line technique is proposed for the estimation of electrical parameters of an improved space vector dynamic model of an IM which takes into account the magnetic saturation and iron losses. The electrical parameters are estimated based on GA using input-output measurements. Nevertheless, this technique depends on the knowledge of magnetic conditions of the machine unlike other techniques which estimate parameters based entirely on measured electrical values.

A technique that uses GA and heuristic relationships for the determination of all parameters of the equivalent circuit of IM from manufacturer catalog data is reported in [146]. The parameter values along with slip values at partial loads and the mechanical losses are estimated through analytical process described in [146] and are used to define the search space for the GA. The GA is then used to refine the estimates based on catalogue data. However, manufacturer catalogue data is not always accurate. In addition, stray load loss parameter is totally neglected in [146].

Bacterial Foraging Optimization Algorithms (BFOA) have been used to estimate IM parameters. The BFOA is a swarm intelligence optimization algorithm which was proposed by Passino [149] in 2002. The algorithm was inspired by the social foraging behaviour of Escherichia coli bacteria. It has advantages, such as parallel distributed processing, insensitivity to initial value, and global optimization [148].

A procedure is presented in [70] that estimates the parameters of IM using BFOA based on an equivalent circuit under non-sinusoidal working conditions with the end goal of estimating the efficiency of the motor using a loss segregation method. Although the procedure takes into account the use of non-sinusoidal supplies, it is not suitable for practical implementation since some known harmonic voltages were injected in the

supply. This work [70] is a continuation of [56], but with a different treatment in stray load and core losses.

However, the classical BFOA is robust and not largely affected by the size and non-linearity of the problem further to it's the advantages mentioned earlier. To that effect and further justification, the algorithm will be used later to estimate some harmonic parameters of the inverter-fed IM in subsection 4.3.2.

The efficiency estimation method in [19] implements a PBIL algorithm, in order to ascertain key machine equivalent circuit parameters, and hence estimates a machine's efficiency over a range of loading conditions. Although the efficiency estimates using the proposed algorithm were correlated to those obtained by the IEEE 112B and IEC 60034-2-1 international efficiency testing standards, there was no low-level comparison of the estimated parameters against those obtained by the same testing standards. Moreover, this method is based on sinusoidal excitation of the IM, therefore does not account for harmonic influence on estimated parameters.

This chapter partly presents the application of a non-intrusive PBIL optimization algorithm to estimate base parameters of inverter-fed IMs using measured fundamental and rms values of the inverter supply. The estimated parameters of the PWM inverter-fed motor(s) are compared to those obtained from IEC 60034-2-1 procedures of no-load and locked rotor tests.

The PBIL algorithm will be used in this research because its simplicity, robustness, global optimization capability and superior performance compared to GA [150]-[151].

The following section provides the underlying principles of the PBIL algorithm followed by its application to estimate the parameters of two (Figure 4-2 and Figure 4-6) equivalent circuits of an IM based on experimental measurements.

4.2.4. Parameter Estimation Using PBIL

The PBIL optimization technique can be used to estimate some parameters of the equivalent circuit. It is a stochastic guided search algorithm that obtains its directional information from the previous best solutions. Initially a population of trial solutions is generated based on the random sampling of a probability vector. A trial solution or

individual is a set of binary coded real numbers with each member of the set representing an unknown parameter. Each individual is based on the newly computed random vector. A flowchart of the population based incremental learning algorithm is shown in Figure 4-8 [19].

4.2.4.1. Generating a Population Individual

A population of *individuals, I* representing a *trial solution* of the unknown parameters is generated based on random sampling of a probability vector, ρ. The generation of a population of individuals is illustrated in A and equation (4-8). For five unknown parameters, an *individual* consists of five sets of binary coded real numbers each of length 15 bits (in this example) making a total length of 15 x 5 = 75 bits. Initially each position in the probability vector is occupied by a value of 0.5 which corresponds to unbiased bit generation. A random vector, φ of the same length (75 bits) is produced by generating a uniformly distributed random number in the range [0,1] for each bit position. An *individual* is derived by comparing corresponding bits in the probability and random vectors. An *individual* bit is set to one if the random number is less than the corresponding probability vector element, or to zero otherwise:

$$\ddot{\mathrm{I}}(i)_{i=1}^{75} = \begin{cases} 1 & for\ \rho(i) > \varphi(i) \\ 0 & for\ \rho(i) \leq \varphi(i) \end{cases} \qquad (4\text{-}8)$$

The binary encoded parameters in an individual population are decoded using a binary to decimal inverter to real values in the range [0,1]. This is achieved by obtaining a dot product of the 15-bit parameter array and the decoder array $\ddot{D}$ defined by:

$$\ddot{D}_{i=1}^{15} = 2^{-i} \qquad (4\text{-}9)$$

After decoding the bit representation, the unknown parameters of the IM equivalent circuit are scaled according to boundary limits shown in Table 4-3.

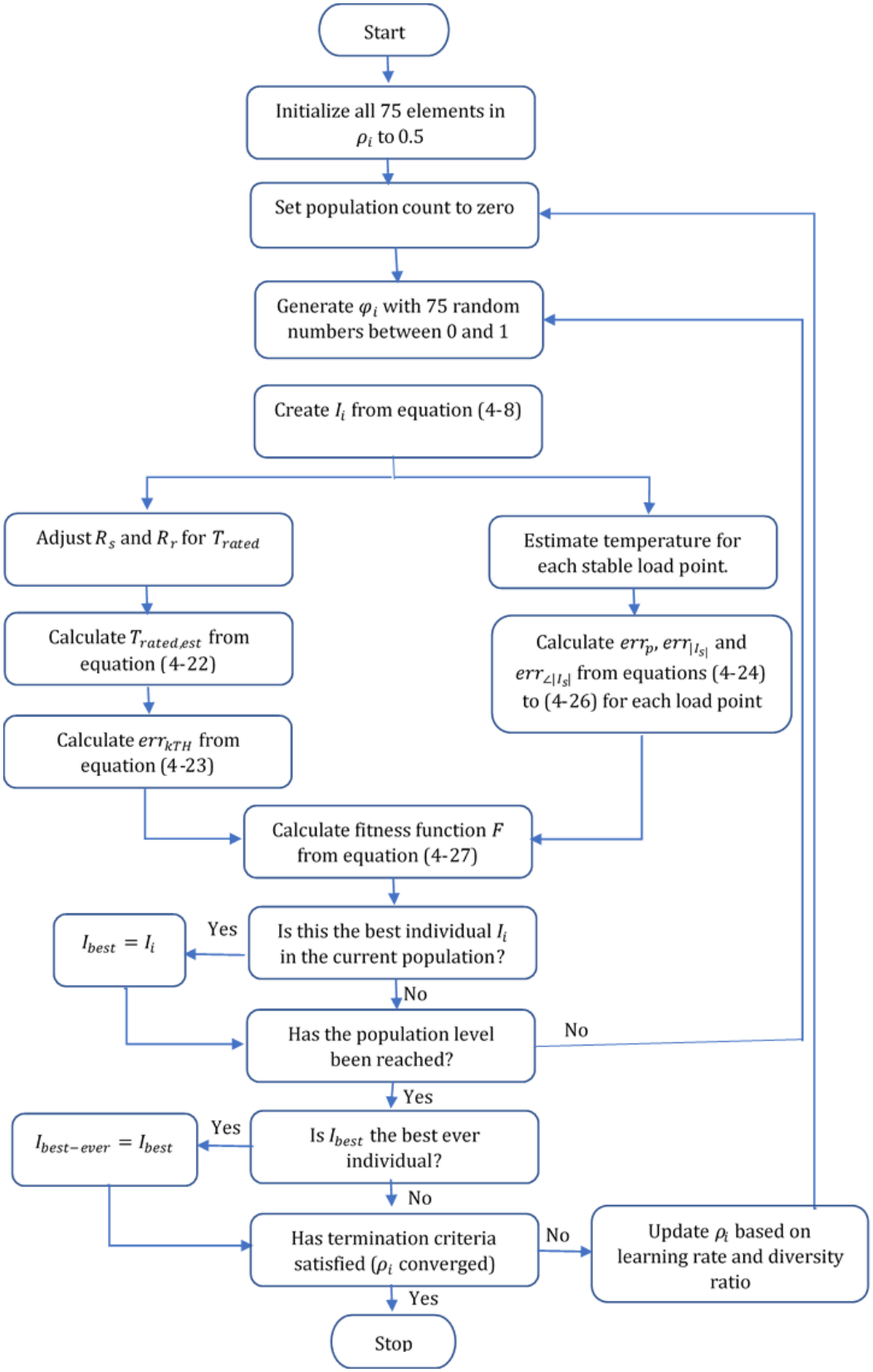

Figure 4-8. Flowchart of the population based incremental learning [19].

Table 4-3. Parameter real boundary limits defined.

Parameter	Binary Assignment	Real Boundary	Real Resolution
X_s (Ω)	Ï(1-15)	[0,50]	±0.0015
X_m (Ω)	Ï (16-30)	[0,500]	±0.015
R_m(Ω)	Ï (31-45)	[300,450]	±0.0045
R_r (Ω)	Ï (46-60)	[0,50]	±0.0015
K_{TH} (°C/W)	Ï (61-75)	[0,1]	±2^{-15}

4.2.4.2. Evaluating a Population Individual

To assess whether the parameter values derived from a population individual represent the actual parameters of the IM, these trial parameter values are used to estimate the measured values based on the equivalent circuit model. The measured values are the 3-phase line voltages and currents. The difference between the population-based estimate and the measured values determine the individual's *fitness*. Since there are five parameters to be solved, a set of equations for five load points operated within a certain thermal load point is required in order for the optimization algorithm to converge to a unique solution.

The trial parameters are used to obtain a trial estimate of the stator, rotor and magnetizing currents (4-13) to (4-15) using the measured stator voltages based on the equivalent circuits. The approximate input power (4-16) is also determined from the estimated currents and real values of the impedances. In the research related to this thesis, two equivalent circuits, Figure 4-2 and Figure 4-6 are considered for parameter estimation. The respective base impedances of the two equivalent circuits are summarized in Table 4-4.

From Table 4-4, the respective admittances are given by:

$$\vec{Y}_s = \frac{1}{\vec{Z}_s} \qquad (4\text{-}10)$$

$$\vec{Y}_r = \frac{1}{\vec{Z}_r} \qquad (4\text{-}11)$$

$$\vec{Y}_c = \frac{1}{\vec{Z}_c} \quad (4\text{-}12)$$

Table 4-4. Formulation of impedances for the two equivalent circuits.

Impedance	Figure 4-2	Figure 4-6
$\vec{Z}_s$	$= R'_s + jX_s$	$= R'_s + \frac{jX_s . R_{SLL,s}}{jX_s + R_{SLL,s}}$
$\vec{Z}_r$	$= R'_r + \frac{R'_r(1-s)}{s} + R_{SLL} + jX_s$	$= R'_r + \frac{R'_r(1-s)}{s} + \frac{jX_s . R_{SLL,r}}{jsX_s + R_{SLL,r}}$
$\vec{Z}_c$	$= \frac{R_m . jX_m}{R_m + jX_m}$	$= \frac{jX_m . R_{m,s} . R_{m,r}}{jX_m(R_{m,r} + R_{m,s} . R_{m,r} + R_{m,s})}$

The trial estimate of the stator, rotor and magnetizing currents using the measured stator voltage is given by:

$$\vec{I}_{s,est} = \frac{\vec{V}_s . \vec{Y}_s(\vec{Y}_r + \vec{Y}_c)}{\vec{Y}_s + \vec{Y}_r + \vec{Y}_c} \quad (4\text{-}13)$$

$$\vec{I}_{r,est} = \frac{\vec{V}_s . \vec{Y}_s(\vec{Y}_c)}{\vec{Y}_s + \vec{Y}_r + \vec{Y}_c} \quad (4\text{-}14)$$

$$\vec{I}_{m,est} = \frac{\vec{V}_s . \vec{Y}_s(\vec{Y}_r)}{\vec{Y}_s + \vec{Y}_r + \vec{Y}_c} \quad (4\text{-}15)$$

The approximated input power is given by:

$$P_{i,est} = 3\left(\left(\mathbb{R}(\vec{Z}_s)\left|\vec{I}_{s,est}\right|^2 + \mathbb{R}(\vec{Z}_r)\left|\vec{I}_{r,est}\right|^2 + \mathbb{R}(\vec{Z}_c)\left|\vec{I}_{m,est}\right|^2\right)\right) \quad (4\text{-}16)$$

The determination of all the parameters in the equivalent circuits of Figure 4-2 and Figure 4-6 are summarized in Table 4-5.

If the stator resistance at ambient temperature, the rotor resistance from PBIL optimization and the operating temperature are known, it is possible to correct the stator

and rotor resistances to the operating temperature in accordance with (2-22) and (2-27) respectively.

Table 4-5. Determination of equivalent circuits parameters.

Parameter	Derived from:
X_s	PBIL optimization
X_m	PBIL optimization
R_m *or* R_{m_s}	PBIL optimization
R'_r	PBIL optimization and equation 2-27
R'_s	Equation 2-22
X_r	Table 4-1
R_{m_r}	Equation 4-19
R_{SLL_s}	Table 4-2 and equation 4-17
R_{SLL_r}	Equation 4-18
s	Slip from speed estimate based on RSH, Chapter 3

Considering the iron loss equivalent circuit of Figure 4-6 and treating the stator and rotor stray load losses separately, it is assumed that the stator stray load resistance $R_{SLL,s}$ at base frequency is related to rated full-load stray load loss power $P_{SLL,rated}$ at stator phase current $I_{s,rated}$ by equation (4-17) [48]:

$$\frac{{I_{s,rated}}^2 . R_{SLL,s} . {X_s}^2}{{R_{SLL,s}}^2 + {X_s}^2} = \frac{P_{SLL,rated}}{3} \qquad (4\text{-}17)$$

where $\frac{P_{SLL,rated}}{3}$ is the rated stray load loss per phase and X_S is obtained from the PBIL algorithm as shown in Table 4-5.

The solution of the quadratic equation (4-17) yields two values for $R_{SLL,s}$. The larger value is chosen to keep the voltage drop across the stator inductance unchanged [48].

Since it was proved from experimental results in [58] that the overall efficiency of a machine is not dependent on the leakage reactance ratio, the difference between the stator reactance and the rotor leakage reactance at base frequency can be ignored. Therefore, the standstill values of the rotor stray load loss resistor

$R_{SLL,r}$ and core loss resistor $R_{m,r}$ can be assumed to be equal to their stator counterparts as follows [48]:

$$\frac{R_{SLL,r}}{s_{rated}} = R_{SLL,s} \quad (4\text{-}18)$$

$$\frac{R_{m,r}}{s_{rated}} = R_{m,s} \quad (4\text{-}19)$$

When the optimization algorithm converges to a solution of parameters, the IM losses are computed in order to estimate efficiency as discussed in Chapter 5.

4.2.4.3. Temperature Estimation

Given that the stator and rotor resistances of the machine need to be corrected at the load temperature in accordance with equations (2-22) and (2-27), the load temperature at any operating point must be determined. In most cases, the load temperature is read off from a measurement obtained by thermocouples that are embedded in the stator windings. In this situation, the measurement operation is intrusive since the machine has to be stopped in order to install the thermocouples.

In [19] a temperature estimation technique is proposed that is based on the total losses dissipated by a machine. The temperature of the machine, T_{load} and the losses, P_{losses} incurred is assumed to be linearly proportional as shown in (4-20).

$$T_{load} = K_{TH} * P_{losses} + T_{amb} \quad (4\text{-}20)$$

where:

T_{amb} - is the ambient temperature and

K_{TH} - is machine thermal coefficient.

However, to obtain P_{losses} an initial machine temperature must be assumed or estimated. In this work the initial temperature is estimated from rated current, I_{rated}, measured current, I_{load} and temperature difference, ΔT (rated temperature minus ambient temperature) as follows [20]:

$$T_{load,est} = \frac{I_{load}}{I_{rated}} * \Delta T + T_{amb} \quad (4\text{-}21)$$

The final load temperature T_{load} is obtained by an iterative process shown in Figure 4-9 and detailed in [19], [20]. The iterative algorithm in Figure 4-9 is part of the PBIL algorithm that determines the equivalent circuit parameters and the machine temperature coefficient, Kth. For each trial solution of the PBIL algorithm at a particular load point, the operating temperature is estimated based on the current value of K_{TH}. K_{TH} is improved after every population iteration by aiming for the smallest error between the estimated full load temperature $T_{rated,est}$ and the actual full load temperature T_{rated} where:

$$T_{rated,est} = P_{rated,loss}.K_{TH} + T_{amb} \quad (4\text{-}22)$$

where $P_{rated,loss}$ is the power loss at rated load.

$$err_{kTH} = \frac{T_{rated} - T_{rated,est}}{T_{rated}} \times 100\% \quad (4\text{-}23)$$

This process is repeated until the difference between the current temperature and the preceding temperature is less than 0.01. Once the estimated loading temperature has converged to a value, the errors between the measured and estimated values shown in (4-24) to (4-26) are used to redefine the probability vector used to generate future trial populations in order to improve the estimated values over all the load points as shown in (4-27).

$$err_P = \frac{P_i - P_{i.est}}{P_i} \times 100\% \quad (4\text{-}24)$$

$$err_{|I_s|} = \frac{I_s - I_{s,est}}{I_s} \times 100\% \quad (4\text{-}25)$$

$$err_{\angle|I_s|} = \frac{\angle I_s - \angle I_{s,est}}{\angle I_s} \times 100\% \quad (4\text{-}26)$$

$$F = \frac{1}{1 + err_{k-TH}{}^2 + \sum_{i=1}^{5}\left(err_{P,i}{}^2 + err_{|I_s|,i}{}^2 + err_{\angle|I_s|}{}^2\right)} \quad (4\text{-}27)$$

To make it clear, there are 5 operating points but the least square errors for err_P, $err_{|I_s|}$ and $err_{\angle|I_s|}$ are determined separately for each load point. However, to improve the estimated parameters over all the load points, equation (4-27) combines all the load points.

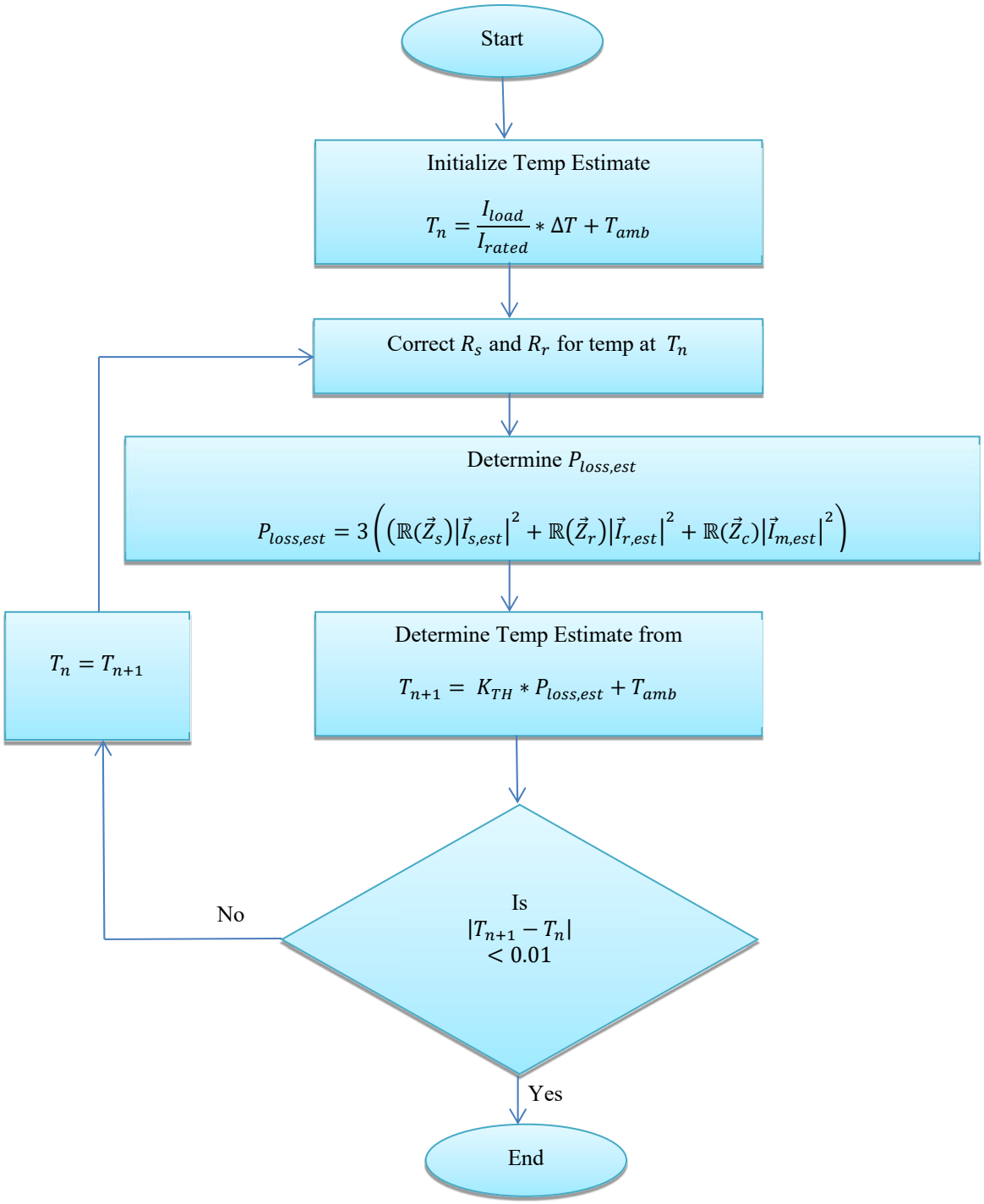

Figure 4-9. Non-intrusive temperature estimation process [19], [20].

4.2.4.4. Equivalent Circuit Parameters Experimental Results

The motor parameter estimation was carried out using the PBIL iterative algorithm based on experimental data acquired from 37kW and 45kW IMs fed by PWM inverter supply. The estimation of parameters was performed on the modified IEEE and IEC standard circuit (Figure 4-2) and the iron loss circuit (Figure 4-6). The PBIL algorithm parameters were setup as follows:

- Number of variables (parameters to be estimated) - 5
- Precision of variables (resolution in bits) - 15
- Number of trial solutions per population - 10
- Number of generations before migration - 20
- Number of parallel populations - 10
- Number of migration cycles - 30

The binary encoded parameters were converted and scaled to real number parameters in accordance with boundary limits shown in Table 4-3.

The experimental setup of the 110kW flexible test rig including the data acquisition thereof is described in section 5.4.

The actual parameter values were determined according to IEC 60034-2-1 procedures which are based on no-load and impedance (locked rotor) tests.

The experimental results are analyzed in terms of accuracy and repeatability. Table 4-6 and Table 4-7 show accuracy (in terms of % error) and repeatability (in terms of standard deviation – σ) for estimated parameters of the 37kW and 45kW motors respectively and for the two different equivalent circuits. In both cases, tests are performed on the fundamental component of the PWM supply because of the following reasons:

1) The use of fundamental components of the PWM supply should lead to estimated base parameters of the IMs with no influence of the harmonics. Harmonic rotor parameters will be determined based on these base parameters as discussed in subsection 4.3.2.

2) The parameters obtained from the fundamental components can be fairly comparable to actual parameters obtained from IEC 60034-2-1 which is based on pure sinusoidal supply.
3) The fundamental voltages and currents were derived from the PWM power supply using the proposed harmonic regression analysis technique in section 4.3.1.1. The values of these components were verified to agree with those obtained from measurements using a high performance HBM's Gen 7i high speed transient recorder and data acquisition system mentioned in section 5.4.

Table 4-6. Repeatability and accuracy test results for estimated parameters of a 37kW motor using PWM fundamental values.

	Modified Standard Circuit					Iron Loss Circuit				
	X_s	X_m	R_r	R_m	K_{TH}	X_s	X_m	R_r	R_m	K_{TH}
Run 1	0.972	26.123	0.148	560.000	0.033	1.001	26.001	0.154	560.000	0.027
Run 2	0.981	26.108	0.148	560.000	0.033	1.001	26.001	0.154	560.000	0.027
Run 3	0.903	26.016	0.150	559.999	0.033	1.001	26.001	0.154	560.000	0.027
Run 4	1.007	26.123	0.148	558.307	0.033	1.001	26.001	0.154	560.000	0.027
Run 5	0.975	26.123	0.148	560.000	0.033	1.001	26.001	0.154	560.000	0.027
$\bar{x}$	0.968	26.099	0.148	559.661	0.033	1.001	26.001	0.154	560.000	0.027
IEC 34	0.970	26.539	0.153	560.114	N/A	0.970	26.539	0.153	560.114	N/A
% Error	0.247	1.659	3.007	0.081	N/A	3.196	2.027	0.654	0.020	N/A
σ	0.034	0.042	0.001	0.677	0.000	0.000	0.000	0.000	0.000	0.000

Table 4-7. Repeatability and accuracy test results for estimated parameters of a 45kW motor using PWM fundamental values.

	Modified Standard Circuit					Iron Loss Circuit				
	X_s	X_m	R_r	R_m	K_{TH}	X_s	X_m	R_r	R_m	K_{TH}
Run 1	0.763	20.752	0.113	550.000	0.027	0.772	20.599	0.118	549.994	0.022
Run 2	0.763	20.752	0.113	550.000	0.027	0.772	20.615	0.118	550.000	0.022
Run 3	0.761	20.737	0.113	550.000	0.027	0.772	20.615	0.118	550.000	0.022
Run 4	0.763	20.752	0.113	550.000	0.027	0.772	20.615	0.118	550.000	0.022
Run 5	0.763	20.752	0.113	550.000	0.027	0.774	20.599	0.118	549.961	0.022
$\bar{x}$	0.763	20.749	0.113	550.000	0.027	0.772	20.609	0.118	549.991	0.022
IEC 34	0.784	21.133	0.114	549.415	N/A	0.784	21.133	0.114	549.415	N/A
% Error	2.692	1.816	0.616	0.106	N/A	1.442	2.481	3.433	0.105	N/A
σ	0.001	0.006	0.000	0.000	0.000	0.001	0.007	0.000	0.015	0.000

From both Table 4-6 and Table 4-7, the accuracy of the estimated parameters is within 3.5% for the modified standard and the iron loss circuits. The repeatability of the estimated parameters for five consecutive runs shows convergence (low value of standard deviation).

In general, it is evident from the test results that both equivalent circuits can accurately estimate the parameters of the IMs tested. The performance is measured on the analysis of both accuracy and repeatability. Low values of accuracy (% error) and repeatability (standard deviation) represent better performance.

Table 4-8 and Table 4-9 show accuracy and repeatability test results for estimated parameters of a 37kW and 45kW motors using PWM rms values. It is observed that these parameters are almost similar but in general slightly lower than those obtained when only fundamental components were used.

Table 4-8. Repeatability test results for estimated parameters of a 37kW motor using measured PWM rms values.

	Modified Standard Circuit					**Iron Loss Circuit**				
	X_s	X_m	R_r	R_m	K_{TH}	X_s	X_m	R_r	R_m	K_{TH}
Run 1	0.946	26.291	0.147	350.000	0.029	1.000	26.169	0.156	350.000	0.022
Run 2	0.946	26.291	0.147	350.000	0.029	1.000	26.169	0.156	350.000	0.022
Run 3	0.946	26.291	0.147	350.000	0.029	1.000	26.169	0.156	350.000	0.022
Run 4	1.018	26.398	0.145	350.000	0.029	1.000	26.169	0.156	350.000	0.022
Run 5	0.949	26.367	0.147	350.000	0.029	1.000	26.169	0.156	350.000	0.022
$\bar{x}$	0.961	26.328	0.146	350.000	0.029	1.000	26.169	0.156	350.000	0.022
IEC 34	0.960	26.473	0.149	349.158	N/A	0.960	26.473	0.149	349.158	N/A
% Error	0.133	0.548	1.615	0.241	N/A	4.210	1.147	4.711	0.241	N/A
σ	0.028	0.046	0.001	0.000	0.000	0.000	0.000	0.000	0.000	0.000

Table 4-9. Repeatability test results for estimated parameters of a 45kW motor using measured PWM rms values.

	Modified Standard Circuit					**Iron Loss Circuit**				
	X_s	X_m	R_r	R_m	K_{TH}	X_s	X_m	R_r	R_m	K_{TH}
Run 1	0.662	20.798	0.122	350.000	0.024	0.665	20.752	0.118	350.000	0.019
Run 2	0.661	20.783	0.122	350.000	0.024	0.665	20.752	0.118	350.000	0.019
Run 3	0.661	20.783	0.122	350.000	0.024	0.665	20.752	0.118	350.000	0.019
Run 4	0.661	20.783	0.122	350.000	0.024	0.663	20.737	0.118	350.000	0.019
Run 5	0.661	20.783	0.122	350.000	0.024	0.681	20.783	0.118	350.000	0.019

$\bar{x}$	0.661	20.786	0.122	350.000	0.024	0.668	20.755	0.118	350.000	0.019
IEC 34	0.675	21.069	0.123	349.813	N/A	0.675	21.069	0.123	349.813	N/A
% Error	2.045	1.344	0.730	0.053	N/A	1.076	1.489	4.704	0.053	N/A
σ	0.001	0.006	0.000	0.000	0.000	0.007	0.015	0.000	0.000	0.000

This is because of the slightly different measured values fed to the PBIL algorithm which are caused by supply harmonic distortions in the PWM inverter supply. The estimated parameter values agree with those obtained using IEC 60034-2-1 when the PWM rms values were used in no-load and locked rotor tests. The repeatability of the estimated parameters for five consecutive runs shows convergence.

4.3. Harmonic Analysis, Harmonic Parameter Estimation and Harmonic Loss Analysis

In this section, the efficiency estimation technique of the inverter-fed IM is described. The flowchart of the basic algorithm is shown Figure 4-10. It is based on harmonic regression analysis of the voltage and current waveforms, harmonic parameter estimation and harmonic loss analysis. The measured voltage and current waveforms are analyzed using a harmonic regression technique to determine the amplitudes, frequency and phases of finite number of harmonics. The harmonic parameters are estimated from harmonic data and some fundamental parameters using a BFO algorithm. The fitness function for this algorithm is based on least square error between the computed motor input impedance and the estimated input impedance. The harmonic loss analysis is computed from the harmonic parameters and the harmonic currents.

On the other hand, the fundamental parameters are estimated using the PBIL algorithm based on the fundamental values from the harmonic regression analysis. The fundamental losses are computed using these parameters and the fundamental voltages and currents.

Finally, the total losses (fundamental and harmonic losses) are obtained and the efficiency is calculated, while the input power is known. The details of the measured data are given in section 5.4. The same experimental data used in that section was used in this proposed algorithm. Data was recorded after thermal stabilization at each load point.

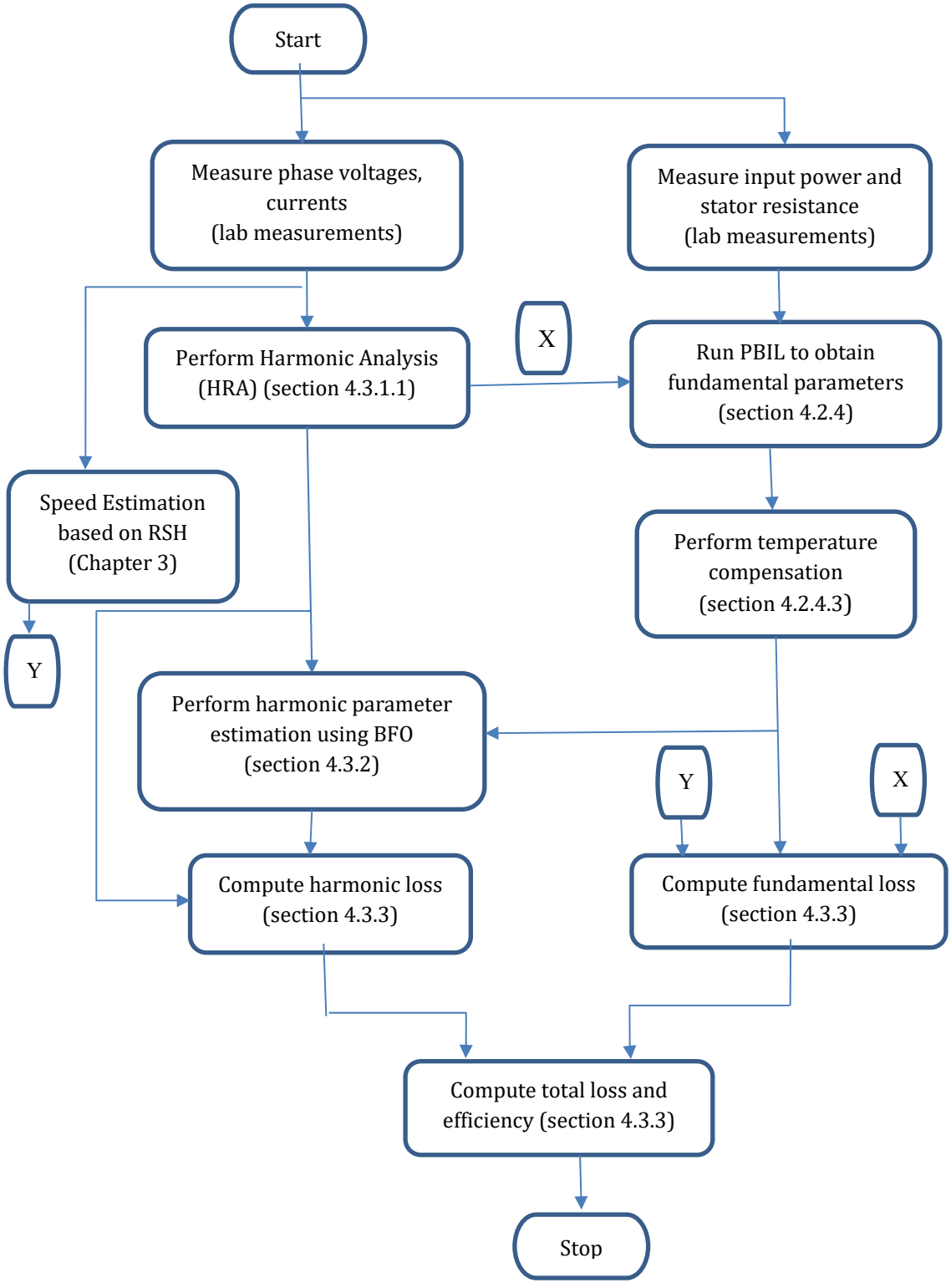

Figure 4-10. Flowchart of the efficiency estimation of inverter-fed IM based on harmonic loss analysis.

4.3.1. Harmonic Analysis of PWM Waveform Data

Power systems, particularly PWM supplies for induction motors are infested with harmonics which have a negative impact on the overall efficiency of the motor. Harmonics caused by power supply quality are termed time harmonics as opposed to space harmonics which exist in the induction machine due to its design or construction constraints. Space harmonics are analyzed by Finite Element Methods (FEM) and are not the focus of this research. Time harmonic analysis is performed in order to determine the attributes (amplitude, frequency, phase) of the harmonic components present in the power supplies. This information is vital if the harmonic frequency response of the machine and the harmonic losses incurred are to be determined.

In the time domain the instantaneous rms voltage of a supply waveform is the sum of the fundamental and individual harmonic components as seen in (4-28) assuming that the voltage waveform is known and its Fourier analysis have been obtained [36].

$$v(t) = \sqrt{2}[V_1 \sin(\omega t + \theta_1) + V_5 \sin(5\omega t + \theta_5) + V_7 \sin(7\omega t + \theta_7) \dots \dots . V_h \sin(h\omega t + \theta_h)] \quad (4\text{-}28)$$

where:

V - is the peak voltage

ω - is 2π times the fundamental frequency

h - is the harmonic order

θ - is the phase angle

t - is the time

Harmonic analysis has traditionally been performed using FFT analysis and its variants. The FFT may be inaccurate in determining the phase angles because it fits harmonics of a wave whose period is equal to the length of the time series, and the harmonic of interest may not lie at exactly one of those frequencies. In this subsection, a Harmonic Regression Analysis (HRA) technique is used to perform harmonic analysis. This technique omits the FFT process, especially that the harmonic frequencies of interest are known. The underlying theory of the harmonic regression technique is described in subsection 2.

4.3.1.1. Harmonic Regression Analysis

This harmonic analysis technique calculates the harmonic regression of a time series data by fitting designated harmonics of different frequencies using non-linear regression algorithms [153]-[155]. The input to the harmonic regression model can be a vector of sample times, or a scalar of the time step between equally spaced sample times, T, a vector of data samples, X and a vector of frequencies, F of interest. The output of the model are vectors A and B (of lengths equal to the length of frequencies vector) containing amplitudes of cosine and sine components of the model with the best least squares fit to the data [154]. A and B are chosen to minimize the error, E according to:

$$E = \sum_{n=1}^{N}\{X(n) - \sum_{m=1}^{M}[A(m)cos\ (2\pi.F(m).T(n) + B(m)sin\ (2\pi.F(m).T(n)]\}^2 \quad (4\text{-}29)$$

where:

N - is the number of data samples and

M - is the number of harmonic frequency points of interest.

The estimated voltage amplitude, $V(m), est$ of the mth harmonic frequency is found from:

$$V(m), est = \sqrt{A(m)^2 + B(m)^2} \quad (4\text{-}30)$$

The phase angle $\theta_v(m), est$ of the mth harmonic frequency component is given by a four quadrant inverse tangent according to:

$$\theta_v(m), est = atan2(A, B) \quad (4\text{-}31)$$

The motor phase angle is the difference between the voltage and current phase angles, $\theta_v(m) - \theta_i(m)$.

To verify the effectiveness of the harmonic regression analysis technique, the estimated voltage and current amplitudes and the corresponding power factors of the fundamental components are compared with the measured values at different load points for two different motors. The estimated values refer to the fundamental voltage, current and

power factor values obtained using the Harmonic Regression Analysis. The measured values refer to actual fundamental voltage, current and power factor obtained during experimental measurements. It can be seen from Table 4-10 and Table 4-11 that percent error due to the technique is within 2.5%.

Table 4-10. Estimated fundamental voltage, current and power factor of the 37kW motor at different loading points.

% Load	V,est	V,meas	% Error	I,est	I,meas	% Error	CosØ, est	CosØ, meas	% Error
25	402.338	402.386	0.012	30.607	30.595	0.039	0.521	0.524	0.57
50	401.554	401.609	0.015	40.796	40.797	0.002	0.732	0.741	1.21
75	401.108	401.154	0.011	53.401	53.383	0.033	0.819	0.826	0.85
100	400.626	400.683	0.014	67.863	67.752	0.164	0.858	0.864	0.69
115	400.288	400.337	0.012	77.569	77.478	0.117	0.870	0.875	0.57
125	400.185	400.230	0.011	84.251	84.048	0.242	0.875	0.879	0.46

Table 4-11. Estimated fundamental voltage, current and power factor of the 45kW motor at different loading points.

% Load	V,est	V,meas	% Error	I,est	I,meas	% Error	CosØ, est	CosØ, meas	% Error
25	402.895	402.952	0.0143	38.3266	38.3411	0.0376	0.5052	0.518	2.45
50	402.026	402.081	0.0139	50.0691	50.1446	0.1507	0.7207	0.730	1.30
75	401.555	401.568	0.0032	64.6866	64.9774	0.4475	0.8132	0.821	0.96
100	400.929	400.996	0.0166	82.1382	82.3181	0.2184	0.8576	0.863	0.66
110	400.795	400.818	0.0056	89.3906	89.6199	0.2558	0.8673	0.873	0.61
115	400.723	400.7634	0.0101	93.2438	93.3086	0.0694	0.8711	0.8761	0.57

It can be seen in Table 4-12 that the amplitudes obtained using the HRA are comparable to those obtained using FFT. The HRA harmonic phase angles cannot be reliably compared to those obtained from FFT because of the shortcomings of the FFT described in subsection 0. However, Table 4-10 and Table 4-11 show good correlation between HRA estimated power factors and measured power factors at different loading conditions.

Table 4-12. Estimated harmonic amplitudes of voltage and current data from the 37kW motor.

h	FFT, V	HRA, V	ΔV	FFT, I	HRA, I	ΔI
5	0.59540	0.59533	0.00007	0.57603	0.57600	0.00003
7	0.54800	0.54800	0.00000	0.68063	0.68060	0.00003
11	0.53470	0.53490	0.00020	0.06517	0.06510	0.00007
13	0.51640	0.51650	0.00010	0.03257	0.03260	0.00003
17	0.47030	0.47047	0.00017	0.04277	0.04280	0.00003
19	0.45420	0.45453	0.00033	0.02303	0.02300	0.00003
23	0.38010	0.38043	0.00033	0.02130	0.02130	0.00000
25	0.35910	0.35940	0.00030	0.02093	0.02090	0.00003
29	0.33940	0.33993	0.00053	0.01720	0.01720	0.00000
31	0.31550	0.31603	0.00053	0.01637	0.01640	0.00003

Parseval's theorem states that if $V[k]$ is the Fourier transform of $v[n]$, then the energy stored in $v[n]$ is the same as the energy contained in $V[k]$ [156] according to:

$$\sum_{n=0}^{N-1}|v[n]|^2 = \frac{1}{N}\sum_{k=0}^{N-1}|V[k]|^2 \qquad (4\text{-}32)$$

This phenomenon can be reliably applied to the HRA concept. This implies that the sum of the powers of the individual harmonics obtained by HRA is equal to the measured input power.

In the case of a three-phase inverter-fed induction motor, the measured input power is derived from:

$$P_{in,meas} = 3.\left(V_{A,rms}.I_{A,rms}.cos(\theta_v - \theta_i)\right) \qquad (4\text{-}33)$$

where $V_{A,rms}$ and $I_{A,rms}$ are measured rms phase voltage and rms phase current respectively.

The estimated input power is obtained from:

$$P_{in,est} = \sum_{h=1}^{N}\left(3.\left|V_{A,h}\right|.\left|I_{A,h}\right|.cos\,(\theta_{v,h} - \theta_{i,h})\right) \qquad (4\text{-}34)$$

assuming a balanced three phase input power, where

$$h = 3k \pm 1 \qquad (4\text{-}35)$$

and k is an integer from $1, 2, 3, \ldots \ldots . N$. N determines the highest harmonic of interest.

$V_{A,h}$ and $I_{A,h}$ are the harmonic amplitudes of voltage and current obtained from the HRA or FFT. The term $\cos(\theta_{v,h} - \theta_{i,h})$ is the power factor as discussed further in subsection 4.3.1.2. The harmonic orders $h = 2, 4, 5, 7, 8, 10, 11, 13, 14 \ldots \ldots$, according to (4-35) have been chosen because they alternately contribute to negative and positive torques as seen in subsection 2.6.2. Figure 4-11 shows the normalized power spectrum of the input power of the 45kW motor at 100% load point considering the above harmonics of interest.

To guard against the inevitable unbalanced conditions in practical power system usages, the averages of the three computed voltages and currents are taken according to:

$$\left.\begin{aligned} V_{phase,h} &= \frac{V_{A,h}+V_{B,h}+V_{C,h}}{3} \\ I_{phase,h} &= \frac{I_{A,h}+I_{B,h}+I_{C,h}}{3} \end{aligned}\right\} h = 1, 5, 7, 11, 13 \ldots \ldots \ldots \qquad (4\text{-}36)$$

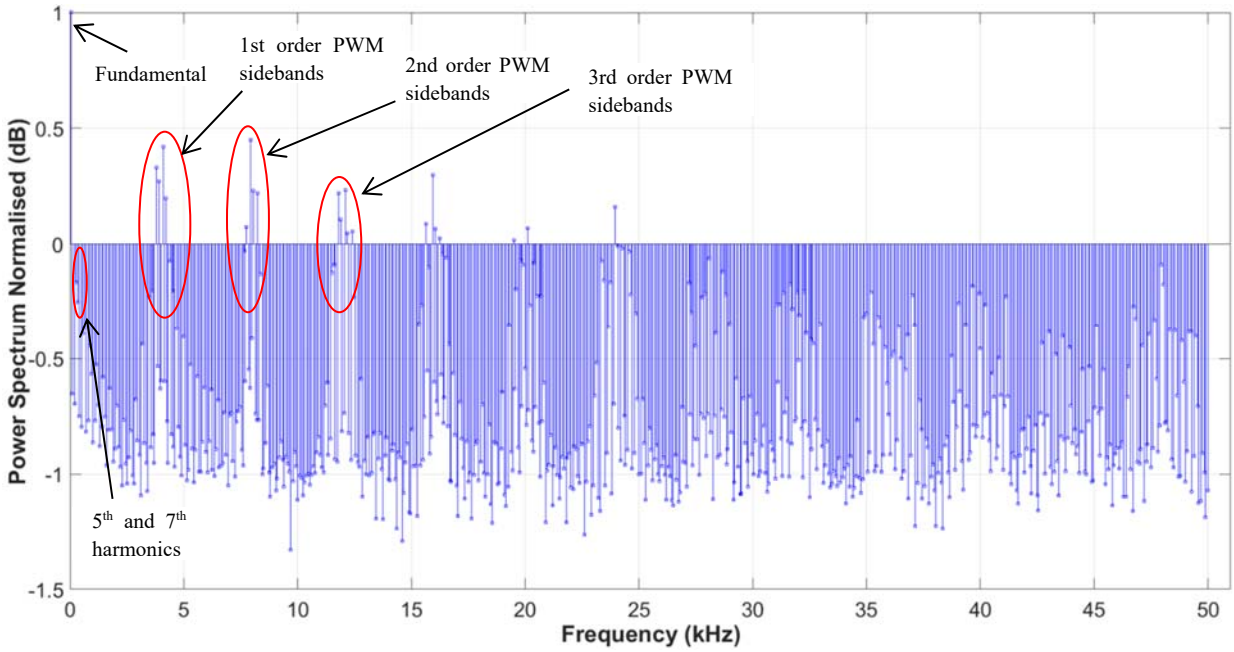

Figure 4-11. Harmonic input power spectrum of the 45kW motor at 100% load point.

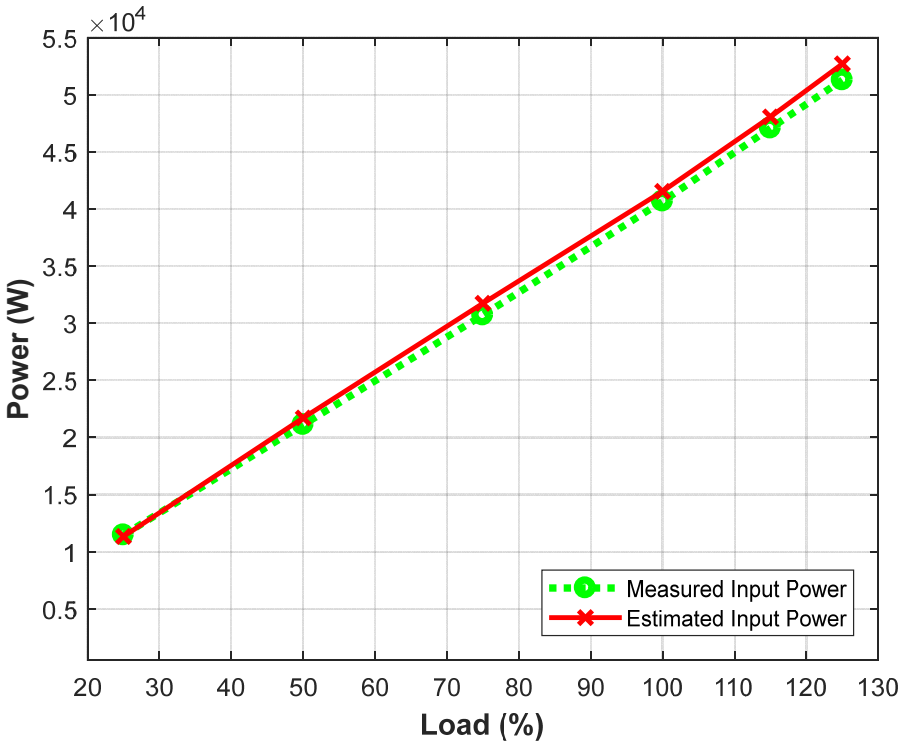

Figure 4-12. Estimated versus measured input power for a 37kW motor at different load points.

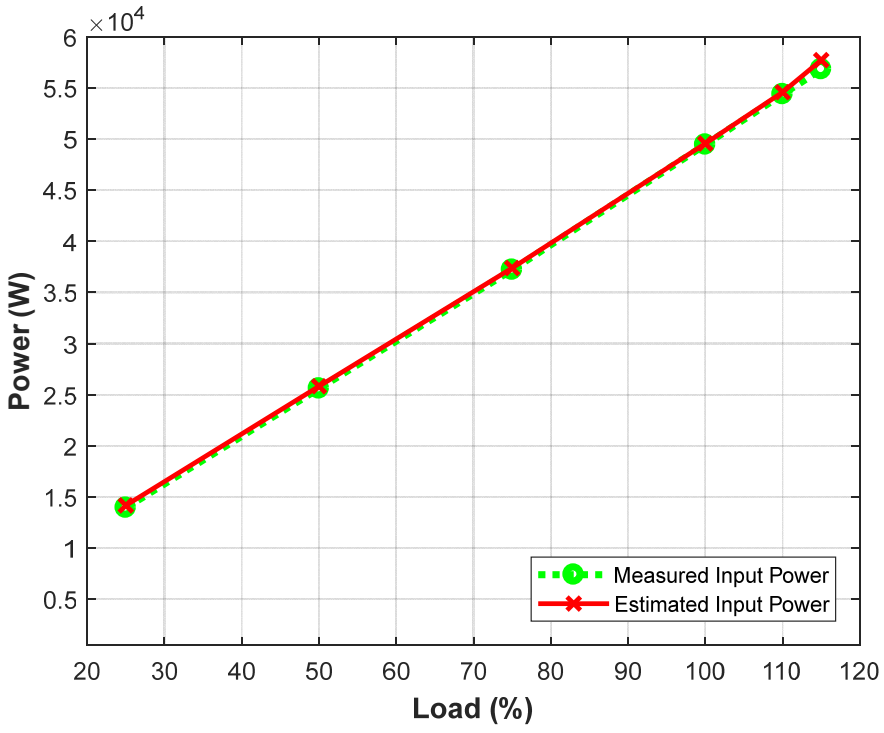

Figure 4-13. Estimated versus measured input power for a 45kW motor at different load points.

To ascertain the effectiveness of the harmonic analysis technique, the estimated input power is compared with the measured input power at different load points.

The correlation between the estimated input power and the measured input power for the 37kW motor and the 45kW motor is shown in Figure 4-12 and Figure 4-13 respectively. Both graphs show good agreement between the estimated input power and the measured input power within 3.5% error for the 37kW motor and within 2% error for the 45kW motor.

4.3.1.2. Power Factor under Non-Sinusoidal Conditions

The power factor of an induction motor is expressed in terms of the phase relationship of its supply voltage and current. The phase relationship is in turn influenced by the values of the motor's resistive and reactive parameters at specified frequency and loading point. In general, the power factor, pf is given by:

$$pf = \frac{P}{S} \qquad (4\text{-}37)$$

$$= \cos(\theta_v - \theta_i)$$

where:

P - is the real power and

S - is the apparent power.

In a non-sinusoidal supply, the real power and the apparent power per phase are given by:

$$P = \sum_{h=1}^{N} V_{h,rms} I_{h,rms} cos(\theta_v - \theta_i) \qquad (4\text{-}38)$$

$$S = V_{rms} I_{rms} \qquad (4\text{-}39)$$

In the presence of non-sinusoidal waveforms, the true power factor can be defined as a product of the displacement power factor (based on the fundamental) and the distortion power factor (based on the harmonic components) [156]. The distortion power factor pf_{dist} is inversely proportional to THD as follows [158]

$$pf_{dist} = \frac{1}{\sqrt{1+THD_v}\cdot\sqrt{1+THD_i}} \qquad (4\text{-}40)$$

The true power pf_{true} is given by:

$$pf_{true} = \frac{P_1}{S} \cdot \frac{1}{\sqrt{1+THD_v} \cdot \sqrt{1+THD_i}} \qquad (4\text{-}41)$$

$$= pf_{disp} \cdot pf_{dist}$$

where:

P_1 - is the real power based on the fundamental.

pf_{disp} - is the displacement power factor

while THD_v and THD_i are in accordance with (2-19) and (2-21) respectively.

Figure 4-14 and Figure 4-15 show the vvariations of the three power factors with load, considering first 10 harmonics of interest, on a 37kW motor and a 45kW motor respectively.

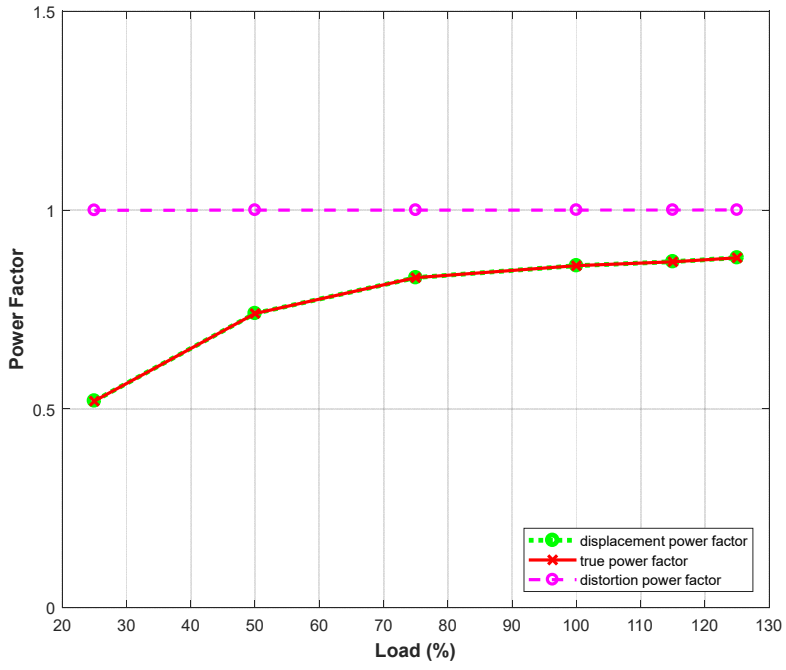

Figure 4-14. Variation of power factors with load, considering first 10 harmonics of interest, on a 37kW motor.

In these cases, the true power factor agrees with the displacement power factor owing to negligible distortions caused by the first 10 harmonics. It is worthwhile to recall that if the amplitude modulation ratio $m_a \leq 1$, where

$$m_a = \frac{Amplitude\ of\ the\ modulating\ signal\ voltage}{Amplitude\ of\ the\ switching\ signal\ voltage},$$

the PWM pushes the harmonics into a higher frequency range around the switching frequency and its multiples [163] as seen in Figure 4-11. In this case, the lower order harmonics has negligible effect on the harmonic distortion of the voltage signal. The distortion power factor is approaching unity across all loading points.

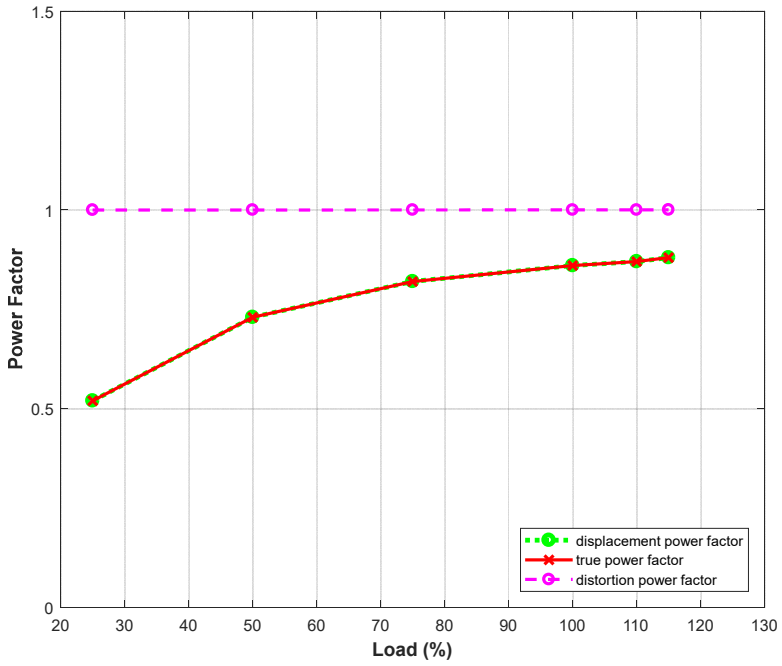

Figure 4-15. Variation of power factors with load, considering first 10 harmonics of interest, on a 45kW motor.

Figure 4-16 and Figure 4-17 show the variations of the three power factors with load, considering first 3300 harmonics of interest, on a 37kW motor and a 45kW motor respectively.

In these cases, the true power factor is well less than the displacement power factor owing to substantial distortions caused by the abundant harmonics, that includes sidebands of the PWM switching frequency and its multiples considered. The distortion power factor falls to around 0.8 across all loading points.

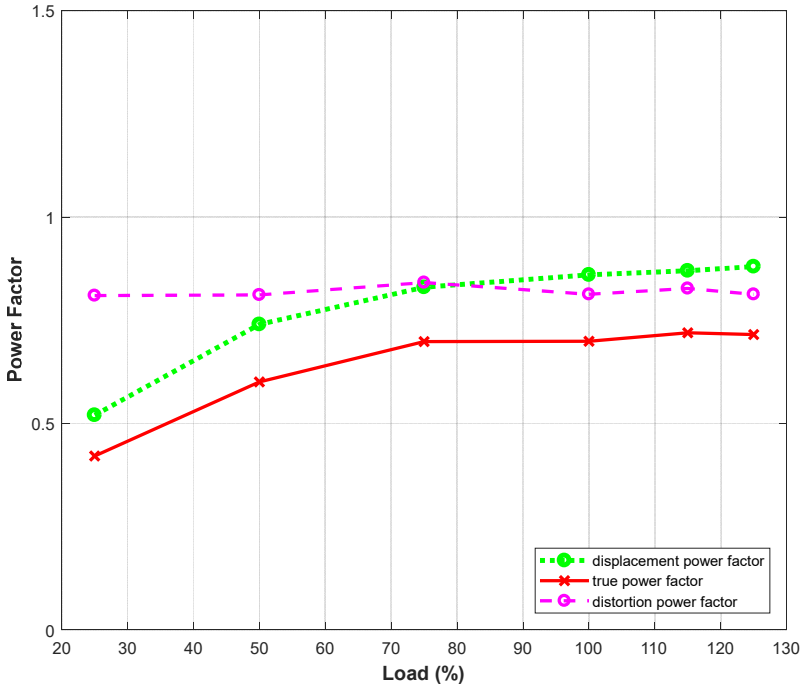

Figure 4-16. Variation of power factors with load, considering first 3300 harmonics of interest, on a 37kW motor.

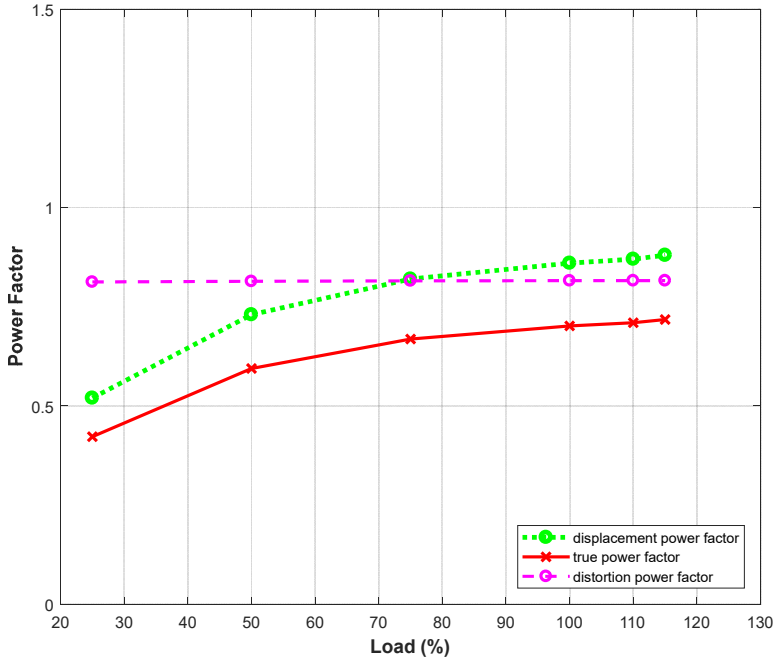

Figure 4-17. Variation of power factors with load, considering first 3300 harmonics of interest, on a 45kW motor.

It can be observed that the true power factor can result in underestimated motor efficiency (compared to direct method) when considered for inverter-fed motors. However, it should be noted that true power factor emanates from negative and positive torques which in most cases cancel out. The effective torque is measured in the direct method and is mainly due to the fundamental component. Therefore, the displacement power factor is the best choice for efficiency estimation even in non-sinusoidal supply cases.

4.3.2. Harmonic Parameter Estimation

The harmonic parameter estimation of an induction machine due to inverter supplies have not been provided by any standard methods. The usual method for induction motor parameter estimation is based on no-load and locked rotor tests [3], [4] as discussed in subsection 4.2.3.1. However, these methods are only valid for induction motors fed by sinusoidal supplies in addition to their intrusive nature. Observer based and optimization techniques discussed in subsections 0 and 4.2.3.3 respectively were mainly developed for machine base parameters. In literature different methods for harmonic parameter estimation and harmonic loss estimation have been proposed [159], [160]. Most of these methods use FEM analyses which require knowledge of some magnetic properties of the machine, while others are based on the standstill frequency response of the machine at varying values of voltage and frequency. In this non-intrusive application the harmonic parameters are estimated based on the knowledge of previously estimated PBIL base parameters and the harmonic impedance at each harmonic order. The following assumptions will be considered when estimating harmonic parameters:

1) The stator resistance R_s remains constant across harmonic frequencies due to negligible skin effects on its small conductor size [7]. In this case the stator leakage reactance X_s is linearly proportional to the harmonic order according to (4-4).
2) The harmonic core loss equivalent resistance $R_{m,h}$ due to eddy current and hysteresis harmonic losses combined [161] varies with harmonic frequency and is given by [162]:

   $$R_{m,h} = {V_h}^2/\left(P_{core,h}/3\right) \quad (4\text{-}42)$$

   where:

$P_{core,h}$ - is the total harmonic core loss in a three-phase induction machine

V_h - is hth harmonic voltage, all based on harmonic loss factor characteristics as will be discussed in section 4.3.3.

3) The variation of the harmonic stray load resistor R_{SLLh} with frequency is assumed to be proportional to $h^{0.8}$ with sufficient accuracy as shown in (2-35) [56].
4) The hth harmonic slip, s_h is given by (2-39) and close to unity at harmonic frequencies [56].

Based on these assumptions, the only parameters that vary in non-deterministic manner with harmonic frequency are the rotor resistance R_{rh} and the rotor leakage reactance X_{rh} mainly due to skin effect in the rotor bars. The estimation of these harmonic parameters is based on the input impedance of the motor at each harmonic frequency which is derived from computed harmonic voltage, current and phase angle as discussed in subsection 2. This technique allows the estimation of harmonic rotor parameters without prior knowledge of the rotor shape and its physical dimensions. The harmonic parameters are estimated using Bacterial Foraging Optimization (BFO) technique in contrast to the PBIL used earlier because of the following reasons:

1) The PBIL technique's main area of application is for problems that are too multi-modal in nature [151]. In this case, only two parameters need to be estimated at each harmonic order. BFO is not largely affected by the size and non-linearity of the problem.
2) The BFO also has advantages such as less computational burden, global convergence, due to its elimination dispersion process [70]. The estimation of harmonic rotor parameters for different harmonic orders demands intense processing requirements to cover the entire harmonic spectrum. The BFO can take a finite time to complete the estimation process due to its relatively faster convergence.

4.3.2.1. Bacterial Foraging Optimization

The Bacterial Foraging Optimization (BFO) algorithm was proposed by Passino [149] in 2002 who was inspired by the social foraging of the *Escherichia coli (E.coli)* bacteria [148]. Bacteria with less developed foraging strategies tend to be eliminated while those with

successful foraging strategies are retained [60]. This algorithm was applied to optimal search of induction motor parameter values [148]. It has advantages, such as parallel distributed processing, insensitivity to initial value, and global optimization [148].

The BFO is governed by four processes namely; chemotaxis, reproduction, elimination and dispersal, and swarming which are described below.

a) Chemotaxis

This process simulates the movement of an *E.coli* cell through swimming and tumbling. When a bacterium meets a favourable condition, it continues to swim in the same direction. When it meets an unfavourable condition it tumbles, i.e., changes direction. If $\theta^i(j,k,l)$ represents the *i*-th bacterium at the *j*-th chemotactic, *k*-th reproductive, and

l-th elimination and dispersal step, then the movement of the bacteria may be represented by [148]:

$$\theta^i(j+1,k,l) = \theta^i(j,k,l) + C(i)\varphi(j) \qquad (4\text{-}43)$$

where: $C(i)$ - is the size of the step taken in the random direction specified by the tumble within a unit length run, and

$\varphi(j)$ - is in the random direction specified by the tumble

b) Reproduction

After the completion of the chemotaxis process, the fitness of each bacterium is evaluated. The sum of the fitness function J_{health} is given by:

$$J^i_{health} = \sum_{j=1}^{Nc} P^{i,j,k,l} \qquad (4\text{-}44)$$

where Nc, is the total number of chemotaxis steps and P is the dimension of the optimization problem or the number of variables to be optimized.

Half of the healthier (with minimum fitness function) bacteria are allowed to survive while the other half die. Each healthier bacterium splits into two bacteria and they are placed at the same location. This ensures that the size of bacteria population remains the same.

c) Elimination and Dispersal

The chemotaxis process forms the basis for local search while the reproduction process speeds up the convergence. These two processes may lead to the bacteria being stuck in local optima. It is possible to globalize the BFO by introducing gradual or sudden changes to eliminate the problem of local optima. Therefore, some bacteria are chosen to be killed (elimination) based on small probability or moved to another position (dispersion) within the environment.

d) Swarming

The swarming behavior of the *E-coli* bacteria is derived from their specific sensing, actuation and decision-making mechanism. As each bacterium moves, it releases attractant to signal other bacteria to swarm towards it. At the same time, each bacterium a repellent to keep other bacteria at a safe distance among each other. This social behavior is simulated by the BFO as follows:

$$J_{cc}\big(\theta, P(j,k,l)\big) = \sum_{i-1}^{S} J_{cc}\big(\theta, \theta(j,k,l)\big) = \sum_{i=1}^{S}\left[-d_{attractant} exp\left(-\omega_{attractant}\sum_{m=1}^{D}\big(\theta_m - \theta_m^i\big)^2\right)\right] + \sum_{i=1}^{S}\left[h_{repellant} exp\left(-\omega_{repellant}\sum_{m=1}^{D}\big(\theta_m - \theta_m^i\big)^2\right)\right] \quad (4\text{-}45)$$

where $J_{cc}\big(\theta, P(j,k,l)\big)$ is now a time varying the fitness function value to be added to (4-51), S is the total number of bacteria, $d_{attractant}$, $\omega_{attractant}$, $h_{repellant}$, $\omega_{repellant}$ are the different coefficients that that should be chosen properly according to [148], [164].

e) Objective Function

The objective (fitness) function of the above algorithm was formulated based on the input impedance, $z_{in,h}$ of the motor at each harmonic order. From the obtained values of harmonic voltage $V_{s,h}$, harmonic current $I_{s,h}$ and harmonic phase angle $\big(\theta_{v,h} - \theta_{i,h}\big)$, it is possible to calculate the input impedance $\vec{z}_{in\_cal,h}$ of the motor using (4-46).

$$\vec{z}_{in\_cal,h} = \frac{V_{s,h}}{I_{s,h}} \angle\big(\theta_{v,h} - \theta_{i,h}\big) \quad (4\text{-}46)$$

The harmonic stator impedance $Z_{s,h}$ and the harmonic core impedance $Z_{c,h}$ are determined from (4-47) and (4-48) respectively using the base parameters obtained from the PBIL and following the assumptions declared in subsection 4.3.2. The impedances are applicable to the equivalent circuit in Figure 4-2.

$$\vec{Z}_{s,h} = R'_s + jhX_s \qquad (4\text{-}47)$$

$$\vec{Z}_{c,h} = \frac{jR_{m,h}.hX_m}{R_{m,h}+jhX_m} \qquad (4\text{-}48)$$

where $R_{m,h}$ is the equivalent core loss resistance from equation (4-42).

The harmonic rotor impedance $Z_{r,h}$ is determined from:

$$\vec{Z}_{r,h} = R_{r,h} + \frac{R_{r,h}(1-s_h)}{s_h} + R_{SLL,h} + jX_{r,h}, \qquad (4\text{-}49)$$

where:

s_h - is the harmonic slip given by (2-39)

$R_{SLL,h}$ - is the harmonic stray load loss given by (2-35)

$R_{r,h}$ and $X_{r,h}$ are the harmonic rotor resistance and the harmonic rotor leakage reactance which are not linearly related to harmonic order due to skin effect.

The estimated harmonic input impedance $\vec{Z}_{in\_est,h}$ is now obtained using the above impedances as shown in (4-48)

$$\vec{Z}_{in\_est,h} = \vec{Z}_{s,h} + \frac{\vec{Z}_{c,h}.\vec{Z}_{r,h}}{\vec{Z}_{c,h}+\vec{Z}_{r,h}} \qquad (4\text{-}50)$$

The fitness function is obtained by a minimum, J according to:

$$\min J = \left|\frac{\vec{Z}_{in\_est,h}}{\vec{z}_{in\_cal,h}} - 1\right|^2 \qquad (4\text{-}51)$$

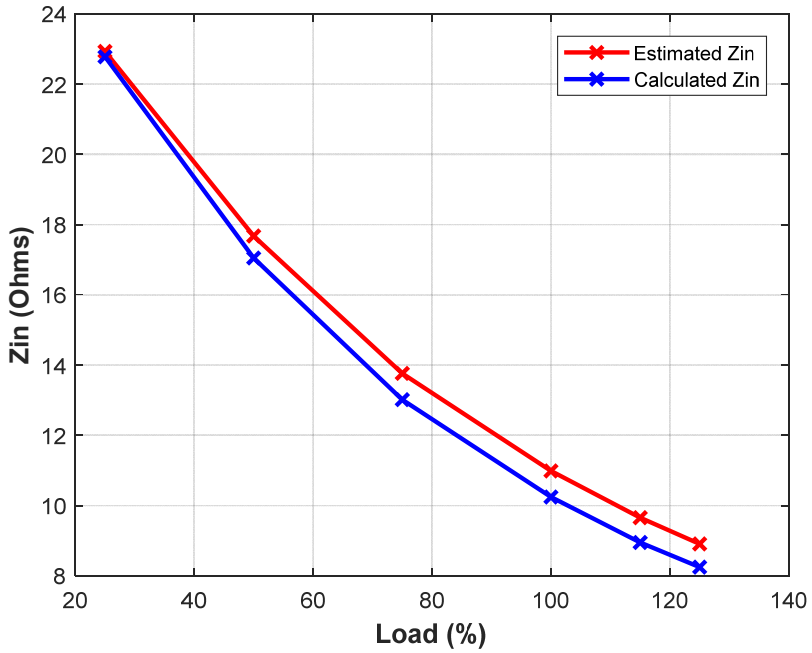

Figure 4-18. Estimated versus calculated input impedance for the 37kW motor at different load points.

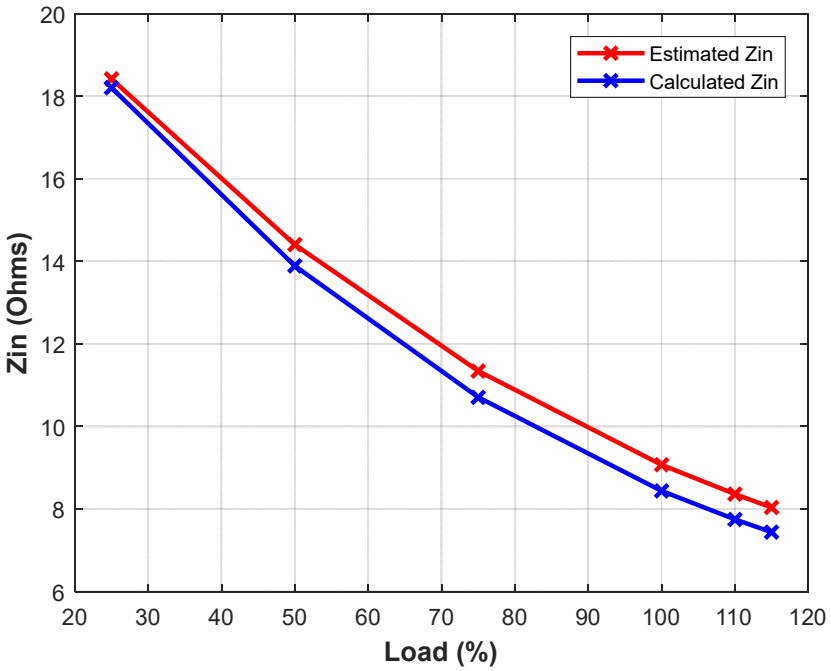

Figure 4-19. Estimated versus calculated input impedance for the 45kW motor at different load points.

To prove the relationship between the calculated input impedance from (4-46) and the estimated input impedance from (4-50), the following are considered.

- Measured fundamental voltage, current and power factor are used to calculate the input impedances at different load points.
- Parameters from the PBIL algorithm are used to estimate the input impedance at different load points.

It is seen from Figure 4-18 and Figure 4-19 that estimated and calculated input impedance are in good agreement (within 0.6%-8% error) across the entire loading range. The amount of error increases with increase in load due to saturation effects which might affect the estimated parameters.

f) Procedure Summary for the BFO

The procedure for the development of the BFO is summarized according to the following steps [70]:

Step 1: Input BFO parameters

$p = 2$: dimension of the optimization problem equal to the number of unknown parameters, where n_h is the number of harmonics to be analysed. The harmonic parameters to be optimised are r_r and x_r.

$S = 60$ is the population of the E. coli bacteria.

$N_c = 25$ is the maximum number of chemotaxis steps.

$N_s = 4$ is the maximum number of swims.

$N_{re} = 4$ is the maximum number of reproduction steps.

$N_{ed} = 2$ is the maximum number of elimination-dispersal events.

$S_r = \frac{S}{2}$ is the maximum number of elimination-dispersal events.

$P_{ed} = 0.5$ The probability that each bacteria will be eliminated/dispersed.

Step 2: Generate the positions of the equivalent circuit parameters randomly for a population of bacteria.

Step 3: Evaluate the objective value of each bacterium in the population, according to the performing of the objective function.

Step 4: Modify the positions of the equivalent circuit parameters for all the bacteria using the tumbling/swimming process.

Step 5: Perform the reproduction and elimination-dispersal operations.

Step 6: If the maximum number of chemotactic, reproduction and elimination-dispersal steps are reached, then go to Step 7. Otherwise, go to Step 3.

Step 7: Output the equivalent circuit parameters corresponding to the overall best bacterium.

Step 8: Calculate the total losses, the output power, and the efficiency of the motor with the parameters obtained.

4.3.2.2. Harmonic Parameters Estimation Results

The analysis of rotor harmonic parameters with increase in harmonic frequency can be complicated especially that the input impedance at harmonic frequencies may not follow a specific rule due to non-deterministic harmonic phase angles [163]. However, the input impedance can be fixed for analysis at any reasonable value, for instance at the 5^{th} harmonic input impedance so that the harmonic rotor parameters can only follow the changes in harmonic order.

Figure 4-20 and Figure 4-21 show the trends in the harmonic rotor resistance and harmonic rotor leakage reactance as the harmonic order increases. It is shown that the harmonic rotor resistance gradually increases with increase in harmonic frequency due to the decreasing conducting surface caused by skin effect. The harmonic rotor leakage reactance increases steeply with increase in harmonic frequency up to about 2.25 kHz and becomes constant due to magnetic saturation in the case of the 45kW motor.

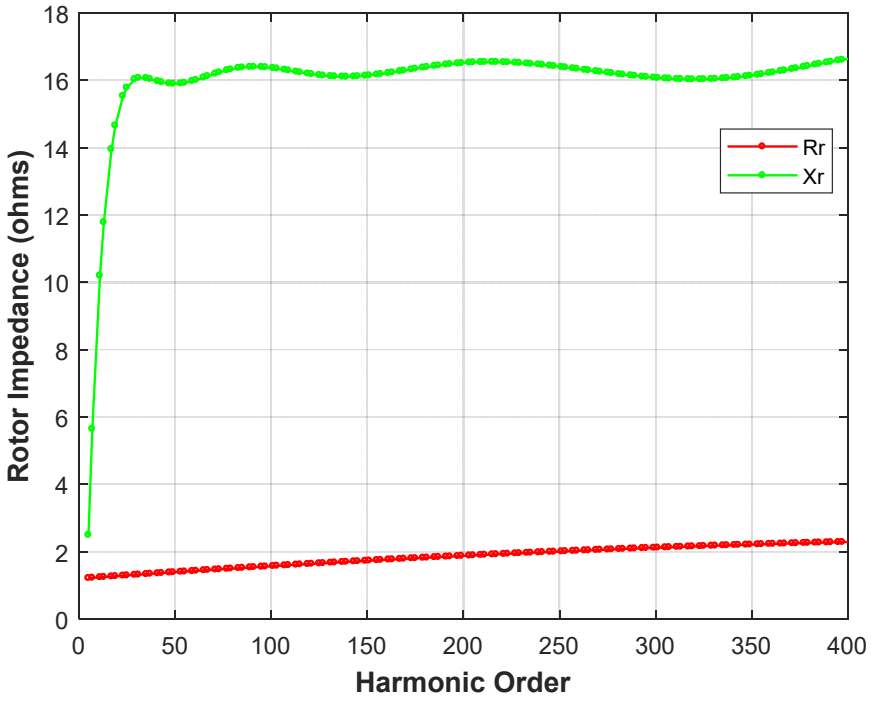

Figure 4-20 Variation of rotor impedance with increase harmonic order for the 37kW motor.

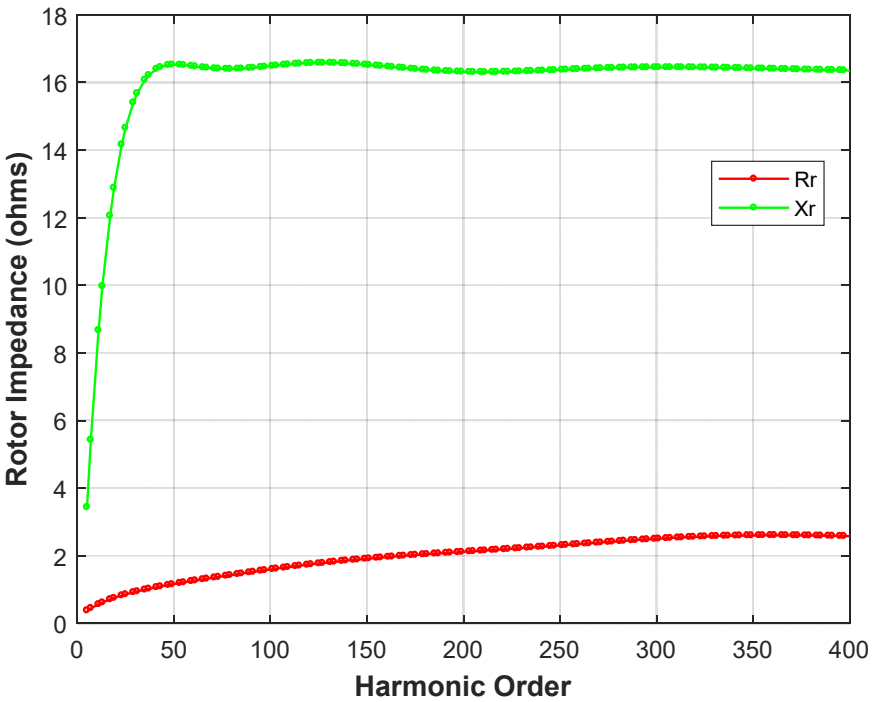

Figure 4-21 Variation of rotor impedance with increase harmonic order for the 45kW motor.

4.3.3. Harmonic Loss Analysis

In this subsection, the harmonic loss analysis of two different induction motors is presented. The theoretical references to the respective harmonic losses are cited where applicable and the experimental results are discussed.

The measured voltages and currents were sampled at 1MS/s. This means that harmonics with frequencies up to 500 kHz can be reliably analyzed according to Nyquist theorem. At a fundamental frequency of 50 Hz, 10 000 (500000/50) harmonics can be extracted. The extraction of these harmonics requires a huge amount of memory in the computing device. Since PWM pushes the significant harmonics into a higher frequency range around the switching frequency and its multiples (for $m_a \leq 1$) [163], only harmonics around the switching frequency (4kHz, in this case) and its multiples up to 50kHz are considered. This consideration will also ease the computational burden of the algorithms in determining the harmonic amplitudes and harmonic parameters. The 5th and 7th lower order harmonics are also considered though, since their power levels may be significant as observed from the power spectrum of Figure 4-11.

Theoretically, the frequencies f_h at which the significant harmonics occur can be indicated as [163]:

$$f_h = (jm_f \pm k)f_1 \tag{4-52}$$

where f_1 is the fundamental frequency and the harmonic order, h corresponds to the kth sideband of the j times the frequency modulation ratio, m_f given by:

$$m_f = \frac{switching\ frequency}{fundamental\ frequency} \tag{4-53}$$

Essentially h is given by:

$$h = (jm_f \pm k)f_1 \tag{4-54}$$

For odd values of j, the harmonics only exist for even values of k. For even values of j, the harmonics only exist for odd values of k. In this instance 10 significant sidebands around the switching frequency and its multiples are considered for loss estimation.
A total of 163 harmonics of interest (up to 50 000 kHz) are analyzed with the assumption that higher order harmonics beyond 50 000 kHz (even sidebands around multiples of switching frequency) contribute negligible losses. For example at 49 550 kHz ($991th$ harmonic), the amplitudes of line voltage and line current are already at 1.68V and 4.18 mA respectively.

The harmonic losses are mainly due to harmonic currents flowing in the respective ohmic resistances of the motor. The estimated harmonic stator currents, $I_{s,h}$ are derived from measured motor current as seen in Table 4-12. The harmonic magnetizing currents, $I_{m,h}$ and the harmonic rotor currents, $I_{r,h}$ are determined from the current divider rule as shown below:

$$I_{m,h} = \frac{Z_{r,h}}{Z_{c,h}+Z_{r,h}} . I_{s,h} \qquad (4\text{-}55)$$

$$I_{r,h} = \frac{Z_{c,h}}{Z_{c,h}+Z_{r,h}} . I_{s,h} \qquad (4\text{-}56)$$

where $Z_{c,h}$ and $Z_{r,h}$ in equations (4-55) and (4-56) are obtained from (4-48) and (4-49) respectively.

The harmonic stator loss is derived from (2-23) where the second part of the equation represents the harmonic loss. It is assumed that the corrected stator resistance R'_s has negligible change in value (due to skin effect) at harmonic frequencies owing to its small conductor diameter size as discussed in subsection 4.3.2.

The harmonic rotor loss is derived from (2-28) where the second part of the equation represents the harmonic loss. It is assumed that the corrected rotor resistance R'_r changes at harmonic frequencies due to skin effect as discussed in subsection 4.3.2. The harmonic slip is found from (2-39).

The harmonic core loss is derived from the harmonic loss characteristic curve for a particular motor [165] based on measured (or calculated) harmonic loss factors and curve fitting.

The total harmonic loss, P_m in mW is given by [161], [166]-[168]:

$$P_m = \sum_{h=2}^{N-1} \left(\frac{A}{{f_h}^{1.5}} + \frac{B}{{f_h}^{\beta}} \right) . {V_h}^2 \qquad (4\text{-}57)$$

where A, B and β are constant values in loss characteristic curves. Basically β varies between 0.3-0.5. V_h and f_h are the hth harmonic voltage and frequency respectively. N is the total number of harmonics to be considered. From the loss characteristics of the 37kW motor at 100% load, $B = 26.98$. From the loss characteristics of the 45kW motor at 100% load, $B = 38.51$. β was kept at 0.32 in both instances.

Initially, P_m can be derived from computed harmonic voltages and currents during harmonic regression analysis. Using curve fitting with a customized polynomial based on computed values of V_h and f_h, the values of A and B can be found.

The total harmonic loss in equation (4-57) is the sum of copper harmonic losses and core harmonic losses. After obtaining the value of B, the total core losses can be determined from:

$$P_{c\_harm} = \sum_{h=2}^{N-1} \left(\frac{B}{{f_h}^{\beta}} \right) . {V_h}^2 \qquad (4\text{-}58)$$

The equivalent core loss resistance $R_{m,h}$ in equation (4-42) is derived from (4-58).

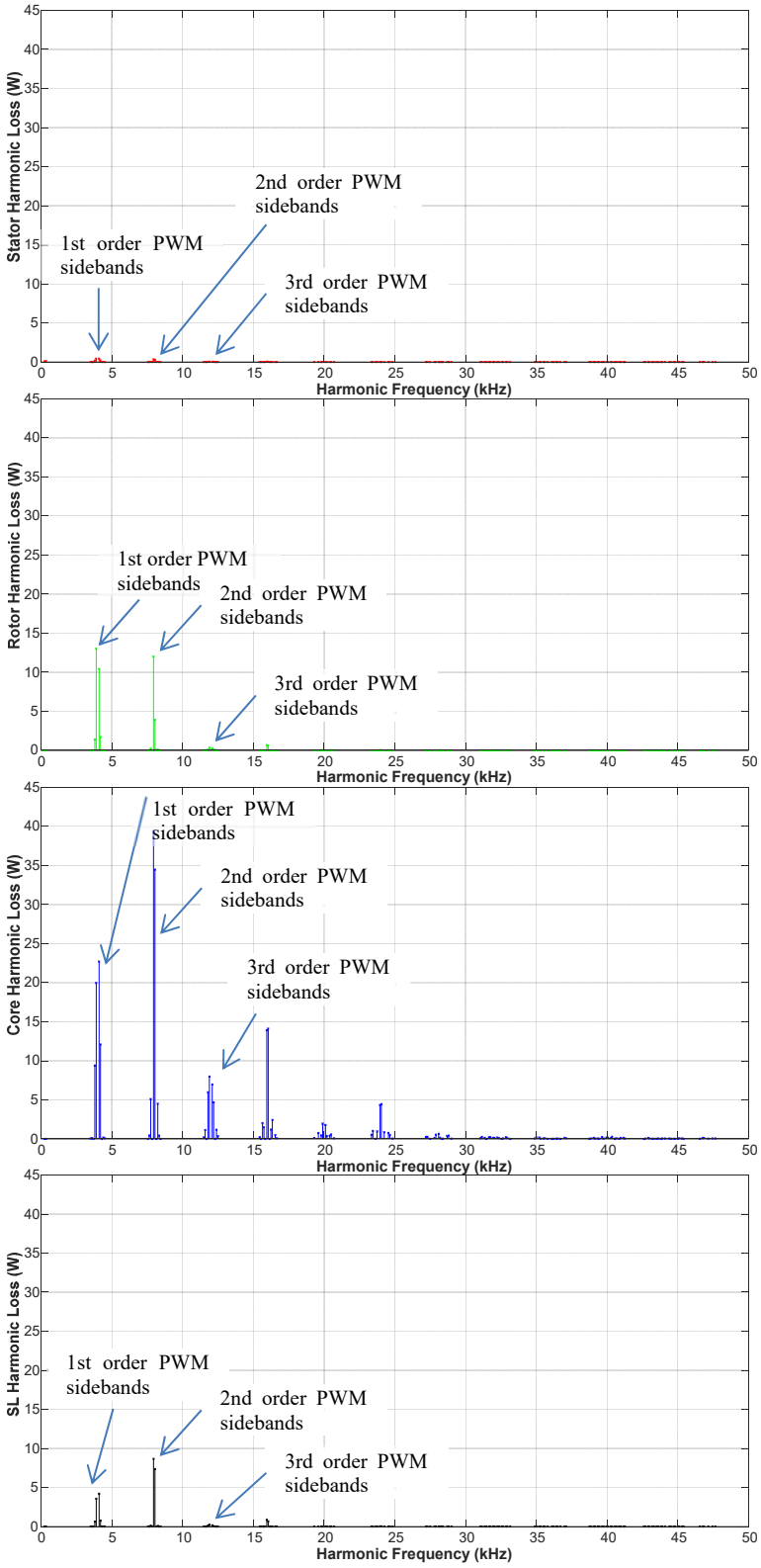

Figure 4-22. Variation of harmonic losses with frequency for the 37kW motor at 100% load.

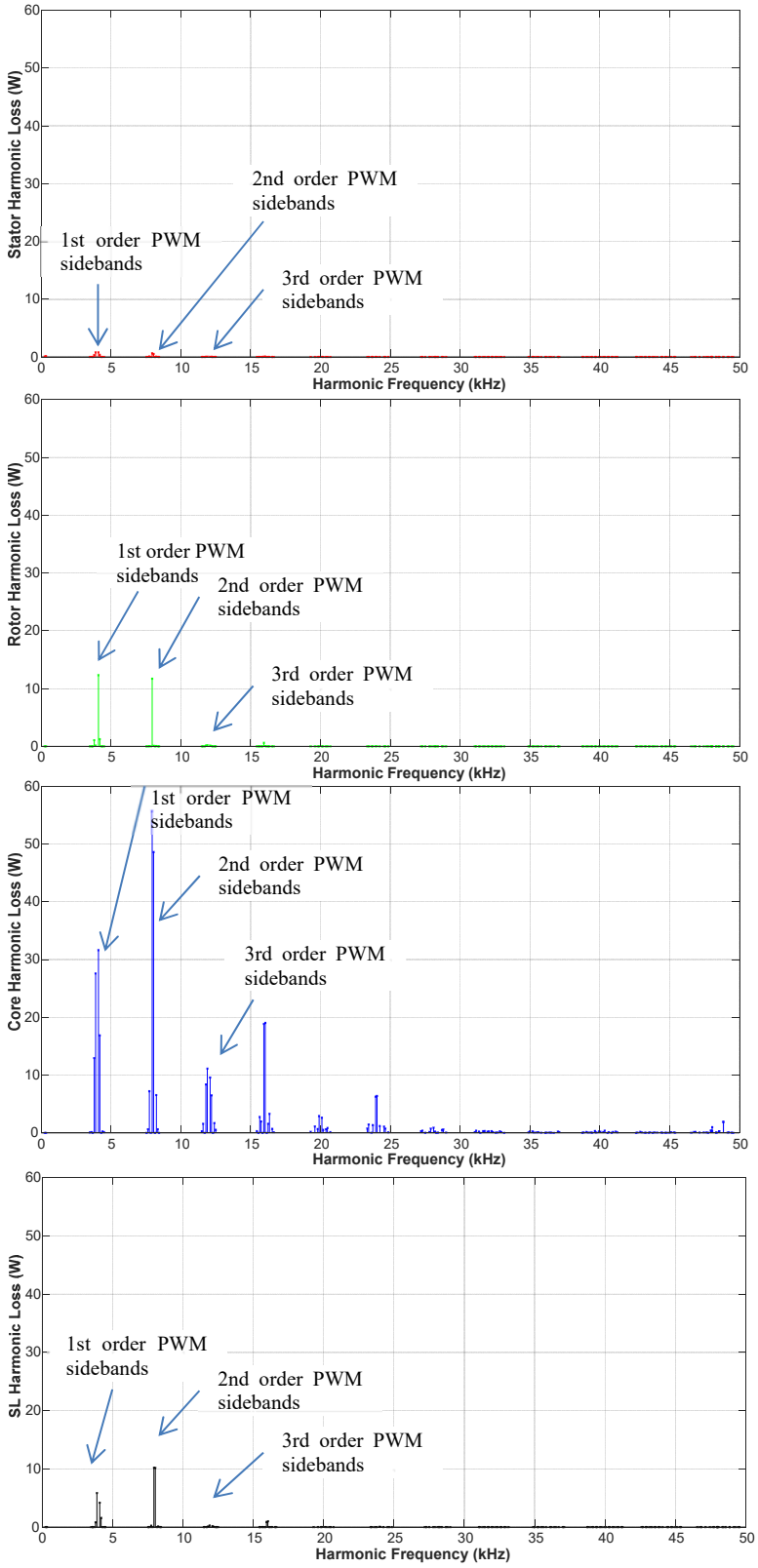

Figure 4-23. Variation of harmonic losses with frequency for the 45kW motor at 100% load.

The harmonic stray load loss is derived from (2-36) where the second part of the equation represents the harmonic loss.

The friction and windage losses are not directly related to harmonic currents [7]. However, the value of these losses is adjusted according to the square of motor operating speed as given by (5-7).

The variation of the harmonic losses outlined above (except friction and windage losses) with increase in harmonic order (or harmonic frequency) is shown in Figure 4-22 and Figure 4-23 for the 37kW and the 45kW motors respectively. In both cases, it is clear that appreciable harmonic losses mainly occur at harmonic frequencies around multiples of the PWM switching frequencies (4 kHz, 8 kHz, 12 kHz, 16 kHz, etc).

The variation of the harmonic loss components at different loading conditions (% of rated torque) is shown in Figure 4-24 and Figure 4-25 for the 37kW and the 45kW motors respectively. It is evident in both cases that the total harmonic core loss is substantial and almost constant across the entire loading range considered. The harmonic rotor and stray load losses seem to very marginally increase with increase in load. The harmonic stator loss remains marginally low based on earlier assumption declared in subsection 4.3.2.

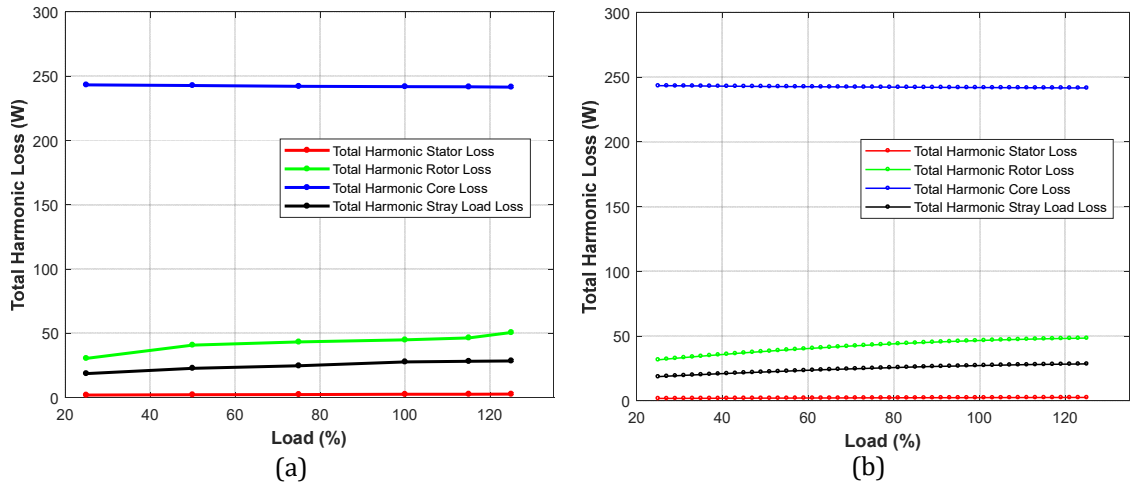

Figure 4-24. Total harmonic loss segregation at different load points of the 37kW motor (a) Point plot (b) Extrapolated plot.

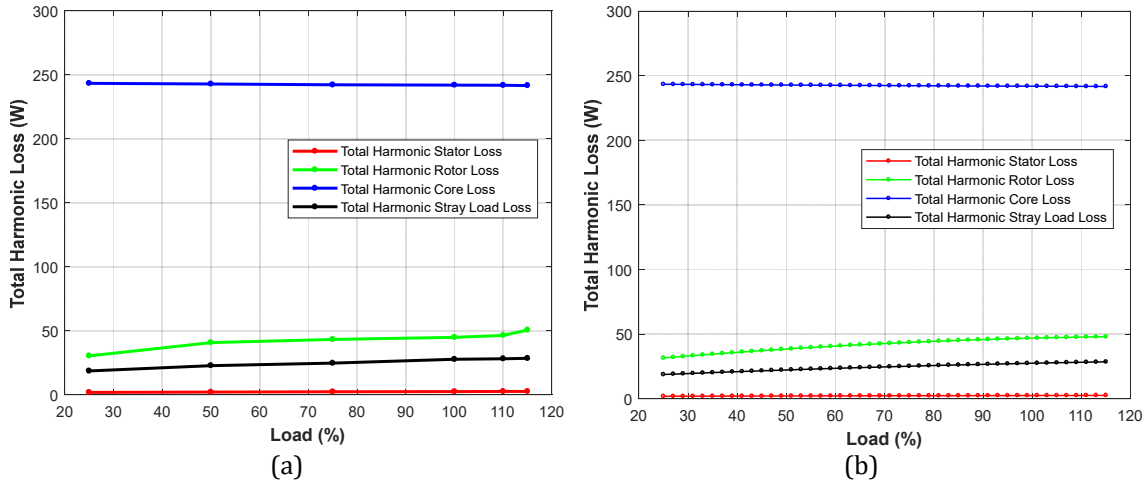

Figure 4-25. Total harmonic loss segregation at different load points of the 45kW motor (a) Point plot (b) Extrapolated plot.

Figure 4-26 and Figure 4-27 show a comparison of the total harmonic losses against the total fundamental loss at different load points. It can be seen that, the total additional harmonic losses contribute an appreciable amount to the total motor losses but remains small compared to the fundamental loss. The total additional harmonic losses very marginally increase with motor loading with reference to the motors tested.

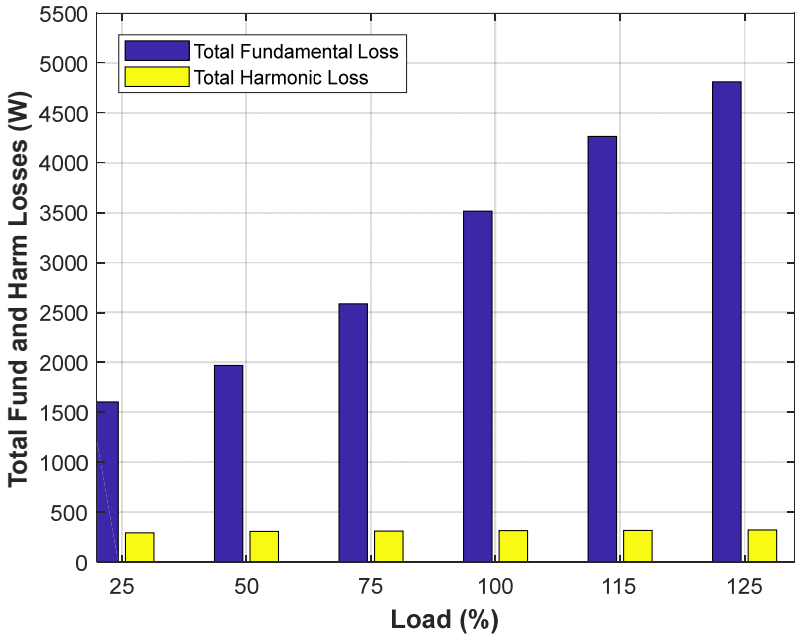

Figure 4-26. Comparison of the total harmonic loss to the fundamental loss at different load points of the 37kW motor.

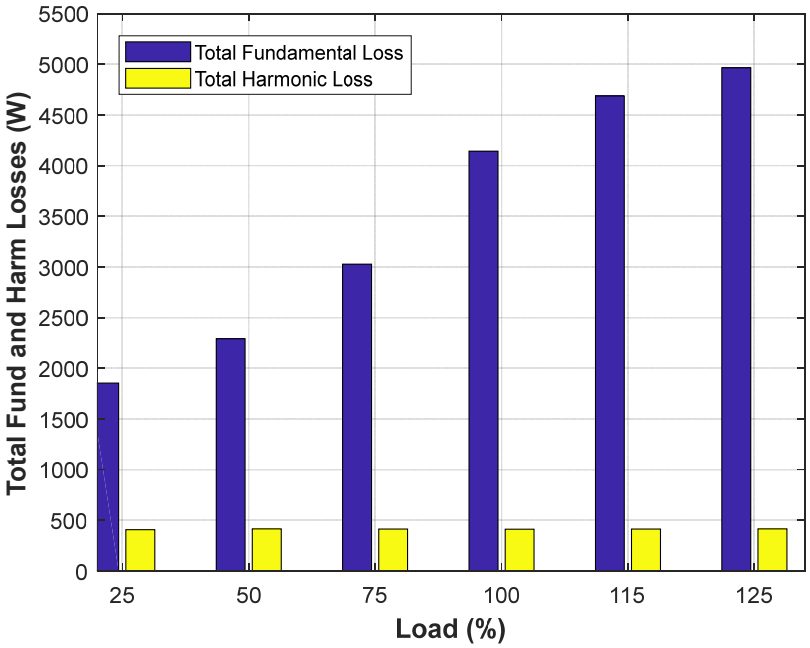

Figure 4-27. Comparison of the total harmonic loss to the fundamental loss at different load points of the 45kW motor.

To prove the effectiveness of the proposed harmonic analysis, harmonic parameter estimation and harmonic loss analysis techniques, the efficiencies of the motors are computed using (4-59) and shown in Table 4-13 and Table 4-14 for the 37kW and 45kW motors respectively and compared to actual values obtained from the direct measurement method.

Table 4-13. Efficiency determination of the 37kW motor at different load points.

Load (%)	Pin	Fund Loss	Harm Loss	Tot Loss	Est Eff	Actual Eff	% Error
25	11462.14	1605.10	294.10	1899.20	83.43	82.97	0.55
50	21115.53	1970.30	308.41	2278.71	89.03	89.12	0.11
75	30708.80	2587.40	312.29	2899.69	90.45	90.68	0.25
100	40667.77	3516.40	316.84	3833.24	90.51	90.75	0.26
115	47067.75	4264.70	318.78	4583.48	90.21	90.40	0.21
125	51276.86	4811.00	323.17	5134.17	89.95	90.12	0.18

Table 4-14. Efficiency determination of the 45kW motor at different load points.

Load (%)	Pin	Fund Loss	Harm Loss	Tot Loss	Est Eff	Actual Eff	% Error
25	13947.31	1854.30	407.39	2261.69	83.78	82.57	1.47
50	25608.92	2292.40	415.23	2707.63	89.43	89.06	0.41
75	37212.03	3028.20	413.48	3441.68	90.75	90.98	0.26
100	49455.23	4142.40	412.74	4555.14	90.79	91.03	0.27
110	54380.41	4687.30	414.35	5101.65	90.62	90.85	0.25
115	56828.04	4965.30	416.35	5381.65	90.53	90.93	0.44

The efficiency η, is given by:

$$\eta(\%) = \left((P_{in} - Tot\ Loss)/P_{in}\right) \times 100 \qquad (4\text{-}59)$$

where $Tot\ Loss$ is the total motor loss equal to the sum of fundamental loss, $Fund\ Loss$ and the harmonic loss, $Harm\ Loss$.

The efficiency of the inverter-fed motor using proposed approach is non-intrusive and involves the quantification of harmonic losses due to the PWM supply. This approach will be referred as the Non-Intrusive Efficiency Estimation using PWM Harmonics (NIEE PWM-HARM) quantification. It will also be referenced from Chapter 5 for comparison.

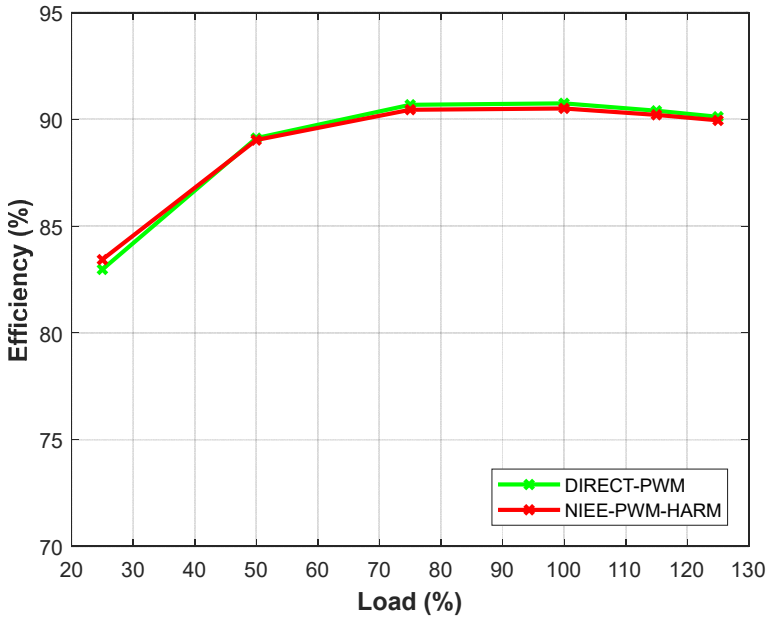

Figure 4-28. Estimated efficiency results compared to the direct method measurement for the 37kW motor at different load points.

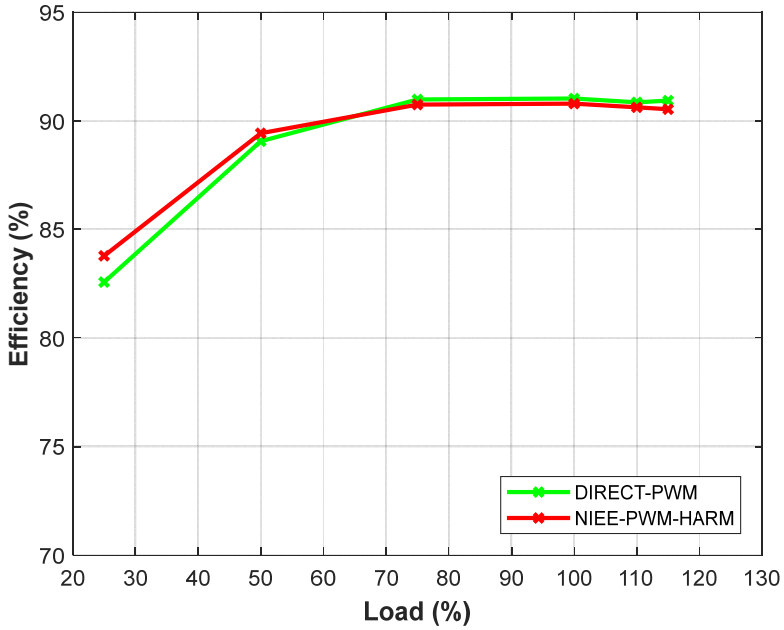

Figure 4-29. Estimated efficiency results compared to the direct method measurement for the 45kW motor at different load points.

It is evident from Figure 4-28 and Figure 4-29 that the efficiency results from the proposed NIEE PWM-HARM technique are comparable to the actual efficiency values from the direct measurement method within 1.5% error across the loading range for the two motors. However, at lower loading the proposed technique overestimates the efficiency of the 45kW motor slightly more than the 37kW motor This may be due to notable differences in the motor power factors at lower loads. Power factors are due to inherent winding inductances incurred during machine design. The power factors can be found in Table 4-10 and Table 4-11 for the 37kW motor and the 45kW motor respectively.

4.4. Concluding Remarks

A review of the equivalent circuit models suitable for non-intrusive parameter estimation of induction machines was presented and the selection of one equivalent circuit (Figure 4-2) for analysis is justified.

A PBIL algorithm was used to estimate the fundamental parameters of the induction motor equivalent circuit because of its recommended application to multi-modal problems and its ability to outperform other evolutionary algorithms in terms of computational overhead and convergence to global optimum solutions [151]. The estimated parameters were compared to those obtained from IEC-60034-2-1 Standard and the results showed good agreement within 3.5% error using the equivalent circuit of Figure 4-2.

Harmonic rotor parameter estimation was performed using the BFO algorithm using harmonic magnitudes and phases because it not affected by the size and non-linearity of the problem. A Harmonic Regression Analysis (HRA) technique was used to extract the harmonic magnitude and phase from the supply voltage and current data. It is shown that the harmonic rotor resistance gradually increases with increase in harmonic frequency due to the decreasing conducting surface caused by skin effect. The harmonic rotor leakage reactance increases steeply with increase in harmonic frequency and becomes constant due to magnetic saturation.

A harmonic loss analysis is conducted using the harmonic parameters and the harmonic voltage and current data. The following observations could be found:

- It is observed that appreciable harmonic losses mainly occur at the *nth* order PWM sidebands.
- The total harmonic loss is dominated by the harmonic core losses which are almost constant across the entire loading range. The harmonic rotor and stray load losses seem to very marginally increase with increase in load. The harmonic stator loss remains marginally low.

- The additional harmonic losses contribute an appreciable amount to the total motor losses but remain small compared to the fundamental loss. The total additional harmonic losses slightly increase with increase in the motor load.
- The proposed techniques and harmonic loss analysis provide accurate efficiency estimates of within 1.5% error when compared to the direct method.

Chapter 5

NON-INTRUSIVE EFFICIENCY ESTIMATION FOR INVERTER-FED INDUCTION MOTORS: COMPARED TO IEC-TS 60034-2-3

5.1. Introduction

Chapter 4 proposed a non-intrusive efficiency estimation technique based on harmonic regression analysis, harmonic parameter estimation and harmonic loss analysis of PWM inverter-fed induction motors and shall be referred to as NIEE-PWM-HARM. An alternative technique that caters for a holistic loss contribution by all harmonics and based on motor parameter estimation using measured rms values of the PWM inverter supply is proposed in this chapter and shall be referred to as NIEE-PWM-RMS. Both techniques are compared to IEC-TS 600-2-3 and direct method for estimating the efficiency of inverter-fed induction motors.

The presentation of NIEE-PWM-RMS in this chapter is not meant to supercede the NIEE-PWM-HARM presented in Chapter 4 but to provide an alternate state-of-the-art solution to the research problem.

The motivation of the proposed technique in this chapter is summarised below to adequately present the contribution of the chapter.

Many recent efforts have attempted to estimate the efficiency of induction motors. However, most of these efforts [71], [124], [125], [169]-[172] are not suitable for efficiency estimation of in-service motors due to their intrusive test procedures which involve no load tests, variable voltage and variable load tests. More attractive in-situ efficiency estimation techniques are presented in [20], [19], [172] which use optimization techniques such as GA and PBIL to estimate machine parameters based on measured voltage and current values. These parameters are used to compute losses at stable machine temperatures and hence efficiency. However, these techniques focus only on sinusoidal supplies even though a considerable number of motors in industry are driven by inverter supplies that contain harmonics that are detrimental to the efficiency of the motors.

The efficiency estimation of induction machines operating on unbalanced and distorted voltages is presented in [38], [56], [70],[172]. A GA is used in [172] to identify the parameters of the induction machine, which is suitable for an in-situ situation. However,

the method utilizes a database of a large number of induction motors tested for efficiency in the Laboratoire des Technologies de l'Énergie, Institut de Recherche, Hydro-Québec, Shawinigan, Québec, Canada, to specify the stray-load loss and the friction and windage loss for induction motors that have similarities with the tested motors within the data set. This limits the method to only those who have easy access to the database to find matching motors. Moreover, the new stray load loss formula is validated for small and medium sized in the range of 1-50 hp and may not perform satisfactorily for larger motors. The method uses different combinations of voltage unbalance and total harmonic distortion.

A BFA is used in [56], [70] to estimate the parameters of the induction motors supplied with unbalanced and distorted voltages. The methods used are quite ideal for in situ efficiency estimation. However, the determination of motor speed in this work involved the use of optical tachometers which pose a number of drawbacks in terms of intrusiveness, cost, and reliability.

Reference [38] specifically focuses on non-intrusive efficiency estimation of inverter-fed induction motors at various frequencies and loads using measured data. The motor equivalent circuit parameters at any load were evaluated by the use of measured values in conjunction with the GA. This method appears very promising for non-intrusive efficiency estimation of inverter-fed induction motors, but it is not suitable for practical implementation since some known harmonic voltages were injected in the supply.

The analysis of the harmonic content of the inverter supplies requires thorough treatment if the loss calculation is to be reasonably accurate. In most cases [38], [56], [70], sinusoidal supplies are deliberately corrupted by certain harmonic voltages for loss analysis. This approach is only for laboratory work and not suitable for online efficiency estimation process.

At the moment, there is no European standard for determining the efficiency of inverter-fed induction machines. The IEC-TS 60034-2-3 [6] is still in draft form awaiting qualification to a standard at the time of writing this thesis. According to this Technical Specification, the total additional loss caused by inverter supply can be determined from

no-load and load tests with a sinusoidal supply and with an inverter supply. The additional harmonic loss is the difference of the measured losses due to inverter supply and those due to sinusoidal supply. The existence of IEC 61800-9-2:2017 [5] is well known by the author. It mainly allows evaluation of power losses of CDMs and PDSs which is beyond the scope of this research.

This chapter presents an online non-intrusive efficiency estimation technique of inverter-fed machines that does not depend on injected harmonic voltages but caters for a holistic loss contribution by all harmonics in a non-intrusive manner. The proposed technique can be used for both sinusoidal and inverter-fed machine efficiency estimation and does not require any prior knowledge of previously tested similar machines. The sinusoidal loss contribution is obtained from the same inverter supply by extracting the fundamental voltage, current and input power values, thus eliminating set-up errors. The equivalent circuit parameters are estimated from a PBIL iteration algorithm based on the rms and the extracted/derived fundamental voltage, current and input power values. The efficiency results from the proposed technique are compared with those obtained from IEC-TS 60034-2-3 Technical Specification. The efficiency results derived from the extracted fundamental values are compared with those obtained from IEC 60034-2-1 Standard as supplementary analysis. A sensorless motor speed estimation technique using RSH is adopted from Chapter 3.

This chapter is organized as follows. Section 5.2 outlines the development of the proposed efficiency estimation technique that includes the machine slip, parameter identification, thermal compensation, losses determination, efficiency calculation and total harmonic loss estimation. Section 5.3 reviews IEC-TS 60034-2-3 Technical Specification and discusses the problems associated with its implementation. Section 5.4 and section 5.5 present the experimental setup and experimental results respectively including the discussion thereof. Section 0 and section 5.7 present the error analysis and repeatability test of the proposed technique respectively. Section 5.8 shows some sensitivity analysis. Section 5.9 provides concluding remarks of the chapter.

5.2. Development of the Proposed Technique

The efficiency estimation in this work is based on the equivalent circuit shown in Figure 5-1. This equivalent circuit is similar to that shown Figure 4-2 with additional illustration of fundamental and harmonic sources. The descriptions of variables R_s, X_s, R_m, X_m, R_r, X_r and h are as per subsection 4.2.1. This equivalent circuit model can generally be used for both fundamental and harmonics and is applicable to all motor sizes fed by either sinusoidal or non-sinusoidal supplies.

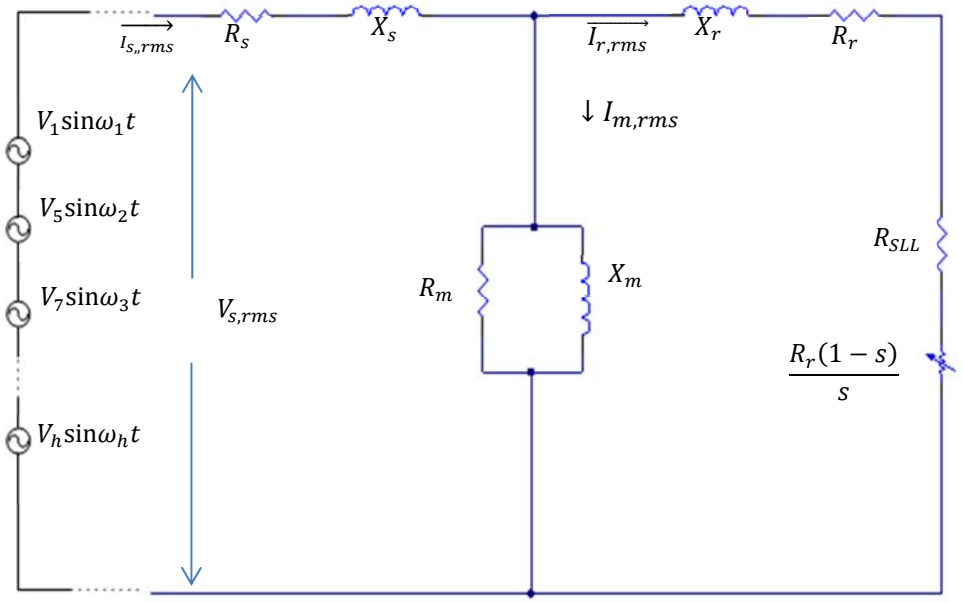

Figure 5-1. Harmonic equivalent circuit of a PWM inverter-fed induction motor.

The measured rms input phase voltage $V_{s,rms}$ and rms input phase current $I_{s,rms}$ of the PWM supply are given by (5-1) and (5-2) respectively.

$$V_{s,rms} = \sqrt{\sum_{h=1}^{\infty} {V_h}^2} \qquad (5\text{-}1)$$

$$I_{s,rms} = \sqrt{\sum_{h=1}^{\infty} {I_h}^2} \qquad (5\text{-}2)$$

The measured input power is given by:

$$P_{in,meas} = 3\left(V_{s,rms}.I_{s,rms}cos(\theta_v - \theta_i)\right) \qquad (5\text{-}3)$$

where $cos(\theta_v - \theta_i)$ is the displacement power factor. Equation (5-3) is similar to equation (4-33). It has been placed here for convenience and context.

The individual harmonic voltages and currents are considered as separate sources on the harmonic equivalent circuit and suitably combined using superposition.

The measured rms input voltage, rms input current and input power are applied to a PBIL algorithm to obtain the motor equivalent circuit parameters. A block diagram of the proposed efficiency estimation methodology is shown in Figure 5-2.

The fundamental ($h = 1$) loss component will be considered separately for analysis purposes only while the fundamental plus harmonics ($h = 1\ to\ \infty$) will be considered for the holistic motor loss, typical of a practical PWM inverter supply.

The measured values are obtained in the least intrusive manner and include PWM supply line voltages, line currents and input power, plus ambient temperature, T_a. The fundamental voltages and currents values can be easily extracted from the PWM supply using an adaptive extraction of nonstationary sinusoids algorithm [174] in an online application. This algorithm is specifically suitable for use in a PWM supply since it is capable of tracking the changing supply frequency and provides the corresponding signal amplitude and phase. Alternatively, a HRA presented in subsection 2 of Chapter 4 can be used to extract the fundamental components. The measured fundamental frequency only needs to be accurate when the latter is used. The motor speed is estimated using a sensorless technique based on rotor slot harmonic in the motor current in order to obtain the machine slip, s as discussed in subsection 5.2.1. The cold stator resistance is premeasured from the motor terminals at ambient temperature. The input power and stator current will be used as objective functions in the parameter estimation iterative algorithm as described in subsection 5.2.2. Once the parameters are obtained and temperature compensation performed on the resistive parameters, the losses are calculated, and the efficiency estimation presented. The proposed in-situ efficiency estimation methodology allows estimation of additional harmonic losses from the difference between PWM losses and fundamental losses of an induction motor fed from a single PWM supply.

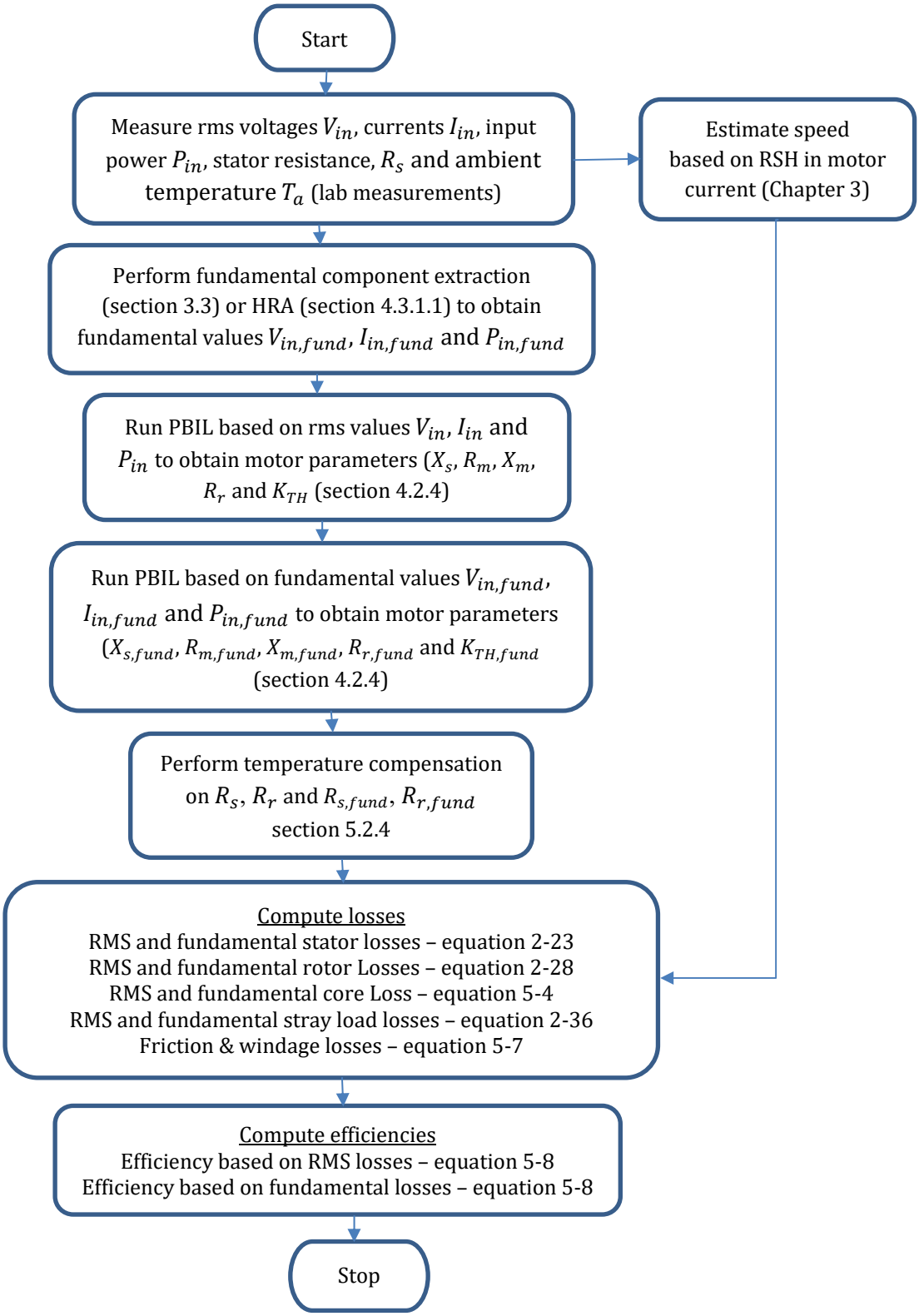

Figure 5-2.Flowchart of the proposed algorithm.

5.2.1. Machine Slip

The machine slip is derived from the measured/estimated rotor speed. The rotor speed in this work is obtained from the motor current by extracting the RSH whose frequency depends on the rotor speed. This technique is very accurate and requires only the number of rotor slots and the number of poles of the motor as input parameters for its computation. These parameters can easily be found from the motor's nameplate and/or datasheet. The details of this rotor speed estimation technique can be found in Chapter 3, section 3.2.4.2 of this thesis.

5.2.2. Parameter Identification

The PBIL optimisation technique is used to estimate some parameters of the equivalent circuit shown in Figure 5-1 because of its simplicity, robustness, global optimization capability [151]. The underlying principle of the PBIL algorithm is detailed in section 4.2.4. There are two sets of parameters as can be seen in Figure 5-2. One set of parameters consists of $X_{s,fund}$, $X_{m,fund}$, $R_{m,fund}$, $R_{r,fund}$ and $k_{TH,fund}$ which are estimated based on the fundamental values of voltage, current and input power. These parameters are used to compute the motor losses due to the fundamental component of the PWM supply. Another set of parameters consist of X_s, X_m, R_m, R_r and k_{TH} which are estimated based on the PWM rms supply voltage, current and input power. These parameters are used to compute the motor losses due to the PWM supply. K_{TH} and $k_{TH,fund}$ are the machine's thermal coefficients measured in °C/W, in the case of PWM supply and fundamental supply respectively. The machine's thermal coefficient, machine's total losses and the ambient temperature are used to estimate the operating temperature of the machine as in (4-20). X_r is estimated based on the ratio of X_s to X_r according to NEMA [24] and which depend on the machine design class as shown in Table 4-1. The fundamental stray load loss resistance R_{SLL} is given by (2-34) and assumed values of the stray load loss recommended by IEEE-112-2004 Standard shown in Table 2-1. The premeasured stator resistance R_s is corrected to R'_s and $R'_{s,fund}$ when the machine is fed from PWM supply and sinusoidal supply respectively owing to the machine's different operating

temperatures under these conditions. R'_r and $R'_{r,fund}$ are the corrected rotor resistance for temperature under the same conditions.

A set of unknown parameters (trial solutions) are used to estimate the stator, magnetising and rotor currents of the equivalent circuit based on measured stator voltages as shown in equations (4-13) to (4-15). The estimated currents also lead to the estimation of the input power as in (4-16). The fitness of the trial solutions is evaluated by the magnitude of error between the estimated currents (and input power) and the measured values as in (4-24) and (4-27). The base admittances of the stator - Y_s, core -Y_r and rotor - Y_c are derived from their respective base impedances (Z_s, Z_r and Z_c) which are derived from the equivalent circuit and are given by equations (4-10) – (4-12).

The PBIL search algorithm converges to a solution of the unknown parameters when the magnitude of the errors between the estimated and measured values approaches zero.

5.2.3. Losses Determination

Following the parameter identification in the previous subsection, the losses due to the resistive parameters in accordance to the equivalent circuit model, together with the friction and windage losses and stray load losses are described in this subsection. The assumptions made with respect to any loss calculation will be justified in line with well-known standards and procedures.

5.2.3.1. Stator Loss

As discussed in subsection 2.5.1 the total stator loss, P_s due to the fundamental and harmonic currents according to Figure 5-1 is given by (2-23).

5.2.3.2. Rotor Loss

As discussed in subsection 2.5.2 the total rotor loss, P_r due to the fundamental and harmonic currents according to Figure 5-1 is given by (2-28).

5.2.3.3. Core Loss

The core loss, P_c with reference to Figure 5-1 is given by:

$$P_c = mR_m\left[{I_m}^2 + \sum_{h=2}^{\infty} {I_{mh}}^2\right] \qquad (5\text{-}4)$$

This is a classical eddy current loss which is a result of current flow in the ferromagnetic core material and is used in non-intrusive core loss estimation.

5.2.3.4. Stray Load Loss

With reference to the equivalent circuit based loss estimation approach, a stray load loss representative resistance is added in the rotor circuit as shown in Figure 5-1 to allow for the variation of stray load loss with load. As discussed in section 2.5.4, the total stray load loss, P_{SLL} due to the fundamental and harmonic currents with reference to Figure 5-1 is given by (2-36).

5.2.3.5. Friction and Windage Losses

In the case of non-intrusive machine loss estimation, the friction and windage losses are assumed to be 1.2% of the rated input power as discussed in section 2.5.5. However, the load dependent friction and windage losses vary according to square of operating speed as shown in (5-6) where k_{FW} is the friction and windage constant based on *Coulomb plus viscous friction* model [175].

$$P_{FW(rated)} = 1.2\% \times P_{i,rated} \tag{5-5}$$

$$k_{FW} = \frac{P_{FW,rated}}{{\omega_{r,rated}}^2} \tag{5-6}$$

The friction and windage losses for each machine load point $P_{FW,load}$ can then be determined by the product of k_{FW} and the square of the machine speed ${\omega_{r,load}}^2$ as follows:

$$P_{FW,load} = k_{FW} \times {\omega_{r,load}}^2 \tag{5-7}$$

5.2.4. Thermal Compensation

A non-intrusive machine temperature estimation technique based on the machine's dissipated power and an iterative algorithm discussed in subsection 4.2.4.3 is used to estimate the load temperature in order to correct the stator and rotor resistances at the loading points according to equations (2-22) and (2-27) respectively.

5.2.5. Efficiency Calculation

The efficiency η(%) of the IM follows the loss segregation approach of subtracting the total losses from the input power and dividing by the input power times 100 as follows:

$$\eta(\%) = \frac{P_i - (P_s + P_c + P_r + P_{sll} + P_{FW})}{P_i} \times 100 \qquad (5\text{-}8)$$

5.2.6. Total Harmonic Loss Estimation

As mentioned earlier, the proposed in-situ efficiency estimation methodology determines the total additional harmonic losses, $P_{T,harm}$ from the difference between the total PWM-fed motor loss, $P_{T,PWM}$ and the total fundamental loss $P_{T,fund}$ as shown in (5-9).

$$P_{T,harm} = P_{T,PWM} - P_{T,fund} \qquad (5\text{-}9)$$

5.3. IEC-TS 60034-2-3

The IEC-TS 60034-2-3 [6] is still a draft awaiting qualification to a standard at the time of writing this thesis. According to this Technical Specification, the total additional loss caused by inverter supply can be determined from load-curve tests plus a no load test at sinusoidal supply and at inverter supply. The additional harmonic loss is the difference of the measured losses due to inverter supply and those due to sinusoidal supply. However, most of the details are still under consideration, since it is not easy to consider a series of tests of general applicability. Such details include, inverter switching frequency which is still limited to a few kHz to tens of kHz with no over-modulation, inverter topology or DC bus voltage value which is still limited to 2-level inverter supplies as well as application to squirrel cage IMs only [169],[170].

Reference [169] reviews existing international standards related to motor and variable frequency drives (VFD). Most of these standards provide guidance in loss and efficiency estimation of motor-VFD systems rather that motor efficiency alone.

5.3.1. Test Methods

The IEC-TS 60034-2-3 provides four test methods for the determination of the efficiency of inverter-fed motors. The test methods are described as follows:

1) Method 2-3A: Summation of losses with test inverter supply

This method provides harmonic loss determination with a test inverter whose output voltage definition is in accordance with Annex A of the Technical Specification and requires a sinusoidal supply and test inverter supply for full-load operation.

2) Method 2-3B: Summation of losses with specific inverter supply

This method provides harmonic loss determination with a specific inverter for final application and requires a sinusoidal supply and specific inverter supply for full-load operation.

3) Method 2-3C: Input-output method

This method provides efficiency of the motor supplied by a specific inverter using direct torque and speed measurement and requires a dynamometer for full-load operation. The efficiency of the motor is found using equation (2-11).

4) Method 2-3D: Calorimetric method

This method provides loss determination from coolant temperature rise with measurements taken in accordance with IEC 60034-2-2 and requires a specific inverter supply.

This section describes the test procedures for Method 2-3A since it does not require a specific inverter supply and can be comparable to the developed technique because of its inherent loss segregation approach.

5.3.2. Method 2-3A Test Procedure

The test procedure for this method is detailed in IEC-TS 60034-2-3. For simplicity and convenience, given that the Technical Specification refers most of the details to IEC 60034-2-1 Standard, the procedure is reiterated here as follows:

1) The stator winding R_s at a temperature reading provided by a temperature-sensing device, for instance, thermocouple installed on the winding is measured. Resistances

for each load point may then be determined from the temperature of the winding at that point in relation to the resistance and temperature measured before the start of the test according to equation (2-22).

R_s is the phase stator resistance equal to 0.5 times line-to-line resistance for Y-connected three-phase machines and equal to 1.5 times line-to-line resistance for Δ-connected machines.

2) A rated temperature test of the loaded machine is performed at rated voltage and current until thermal equilibrium is achieved (gradient of 2 K per hour).
3) A load curve test is performed with sinusoidal power supply of rated frequency and rated voltage according to IEC 60034-2-1:2007 and the total losses determined accordingly at each load for six load points. Four load points should be chosen to be approximately equally spaced between not less than 25 % and up to and including 100 % load. The remaining two approximately equally-spaced load points should be suitably chosen above 100 % load, but not exceeding 150 % load. The machine must be loaded, starting at the highest load value and proceeding in descending order to the lowest. These tests shall be performed as quickly as possible to minimize temperature changes in the machine during testing. The frequency variation between all points shall be less than 0.1 %.

   For each load point, the following must be recorded: V_{meas}, I_{meas}, P_i, n_r, f, T, T_{load}

   The total loss shall be calculated from:

$$P_{losses,fund} = P_i - P_o \qquad (5\text{-}10)$$

   where:

$$P_o = \left(\frac{2\pi \times n_r \times T}{60}\right) \qquad (5\text{-}11)$$

4) A no-load test is performed immediately after a load test with sinusoidal power supply of rated frequency and rated voltage according to IEC 60034-2-1:2007 to determine the constant losses.

A minimum number of seven values of voltage, including rated voltage shall be tested so that four or more values are read approximately equally spaced between 125% and 60% of rated voltage and three or more values are read approximately equally spaced between 50% and approximately 20% of rated voltage, or (for an uncoupled running machine) to a point where the current no longer decreases.

The following shall be recorded at each of the voltage values: $V_{no-load}$, $I_{no-load}$, $P_{i,no-load}$, $T_{no-load}$

Subtracting the no-load winding losses, $P_{s,no-load}$ (at the temperature during the no-load test) from the no-load input power $P_{i,no-load}$ gives the constant losses P_k that are the sum of the friction, windage loss, $P_{FW,no-load}$ and iron, P_c losses.

The constant losses for each value of voltage recorded shall be determined from:

$$P_k = P_{i,no-load} - P_{s,no-load} = P_{FW,no-load} + P_c \qquad (5\text{-}12)$$

where:

$$P_{s,no-load} = 1.5 \times {I_o}^2 \times R'_s \qquad (5\text{-}13)$$

- Friction and Windage Losses

  From the no-load loss points determined above and using all those that show no significant saturation effect, a curve of constant losses P_k against the voltage squared, ${V_{no-load}}^2$ is developed.

  The friction and windage loss is read off from the intercept with zero voltage axis when a straight line is extrapolated to zero voltage.

- Iron Losses

  A curve of $P_c = P_k - P_{FW}$ against voltage $V_{no-load}$ is plotted from the values of voltage between 60% and 125% of rated voltage. The iron losses of the desired load point are taken from the curve at voltage, V_r given by:

$$V_r = \sqrt{\left(V_{meas} - \frac{\sqrt{3}}{2} \times I_{meas} \times R'_s cos\vartheta\right)^2 + \left(\frac{\sqrt{3}}{2} \times I_{meas} \times R'_s sin\vartheta\right)^2} \qquad (5\text{-}14)$$

where:

$$cos\vartheta = \frac{P_i}{\sqrt{3}\times V_{meas}\times I_{meas}} \qquad \text{and} \qquad sin\vartheta = \sqrt{1 - cos^2\vartheta} \tag{5-15}$$

5) A load curve test shall be performed with inverter power supply of rated frequency and rated voltage according to IEC 60034-2-1:2007 and the total losses determined according to step 3).
6) A no-load test shall be performed immediately after a load test with inverter power supply of rated frequency and rated voltage according to IEC 60034-2-1:2007 to determine the constant losses according to step 4).

5.3.3. Load Dependent Additional Harmonic Losses – Residual Loss

The residual loss is determined for each load point by subtracting from the input power: the output power, the uncorrected stator winding losses at the resistance of the test, the iron losses, the windage and friction losses, and the uncorrected rotor winding losses corresponding to the determined value of slip.

For the sinusoidal supply, the residual loss P_{SLL} is given by:

$$P_{SLL} = P_i - P_o - P_s - P_r - P_c - P_{FW} \tag{5-16}$$

For the inverter supply, the residual loss $P_{SLL,PWM}$ is given by:

$$P_{SLL,PWM} = P_{i,PWM} - P_{o,PWM} - P_s - P_r - P_c - P_{FW} \tag{5-17}$$

where P_{FW} is the corrected friction and windage loss at the load points according to:

$$P_{FW} = P_{FW,no-load} \times (1 - s)^{2.5} \text{ with } s = \frac{2\times P\times n_r}{f} \tag{5-18}$$

where P is the number of poles and n_r is the motor speed in rev/sec.

For both cases the residual loss data is smoothed by using the linear regression analysis in accordance to IEC 60034-2-1, based on expressing the losses as a function of the square

of the load torque to obtain values of additional load losses, P_{SLL} and $P_{SLL,PWM}$ for sinusoidal and inverter supplies respectively.

The difference between the additional load losses for operation with the test inverter and with a sinusoidal power supply gives the load-dependent part of the additional harmonic motor losses, $P_{SLL,harm}$ given by:

$$P_{SLL,harm} = P_{SLL,PWM} - P_{SLL} \quad (5\text{-}19)$$

5.3.4. Constant Additional Harmonic Losses

The difference between the no-load losses $P_{k,harm}$ for operation with the test inverter $P_{k,PWM}$ and with a sinusoidal power supply P_k is the constant part of the additional harmonic motor losses:

$$P_{k,harm} = P_{k,PWM} - P_k \quad (5\text{-}20)$$

5.3.5. Efficiency

The total additional harmonic motor loss P_{HL} is the sum of the constant additional harmonic losses and the load dependant additional harmonic losses:

$$P_{HL} = P_{k,harm} + P_{SLL,harm} \quad (5\text{-}21)$$

The additional harmonic motor losses shall be added to the fundamental motor losses, $P_{losses,fund}$ as determined with a sinusoidal power supply according to IEC 60034-2-1:2007, in order to obtain the total motor losses, $P_{losses,PWM}$ under frequency inverter operation:

$$P_{losses,PWM} = P_{losses,fund} + P_{HL} \quad (5\text{-}22)$$

The efficiency at test inverter supply is determined from:

$$\eta(\%) = \frac{Po}{Po + P_{losses,PWM}} \times 100 \quad (5\text{-}23)$$

The harmonic loss ratio r_{HL} is given by:

$$r_{HL} = \frac{P_{HL}}{P_{losses,fund}} \quad (5\text{-}24)$$

It should be rounded to a full (integer) number.

5.4. Experimental Setup

Motor efficiency estimation procedures were conducted based on data obtained from 37kW and 45kW IMs fed from a 2-level inverter (bidirectional) and grid supplies. The inverter was operated as open loop speed control, with switching frequency of 4 kHz, DC bus voltage of 700V and slip compensation switched off. The nameplate data of the 37kW and 45kW motors is presented in Table 5-1 below. The number of rotor bars and stator slots were obtained from the motor manufacturer's datasheets. An image of the laboratory test rig from which experimental measurements were taken is shown in Figure 5-3.

Table 5-1. Nameplate data of the test IMs.

Motor Rating	**37 kW**	**45 kW**
Voltage (V)	400	400
Frequency (Hz)	50	50
Number of Poles	4	4
Full Load Current (A)	67.4	81.6
Full Load Speed (rpm)	1475	1475
Number of Rotor Bars	58	58
Number of Stator Slots	72	72

Experimental data was sampled at 1MS/s for 1 second using HBM Gen 7i high speed transient recorder and data acquisition system as shown in Figure 5-3. The current was measured with MCTS-400 current transducers which have a high primary current range of up to 400A RMS and DC (f = 0 Hz). They also have a low phase error, wide bandwidth of up to 500 kHz, low offset of 0.004%, as well as high linearity. The output current ratio is 200mA at 400A [121]. An inline Magtrol TM 314 torque/speed transducer, which has an error of 0.1% at a rated torque of 1000Nm. The effective torque was found by averaging the torque samples to filter the torque ripples. It has a speed range of up to 7000rpm.

Algorithms were developed in Matlab/Simulink to extract speed dependent RSH from current data (Chapter 3) and to perform motor parameter estimation based on measured voltage, current and input power values (Chapter 4).

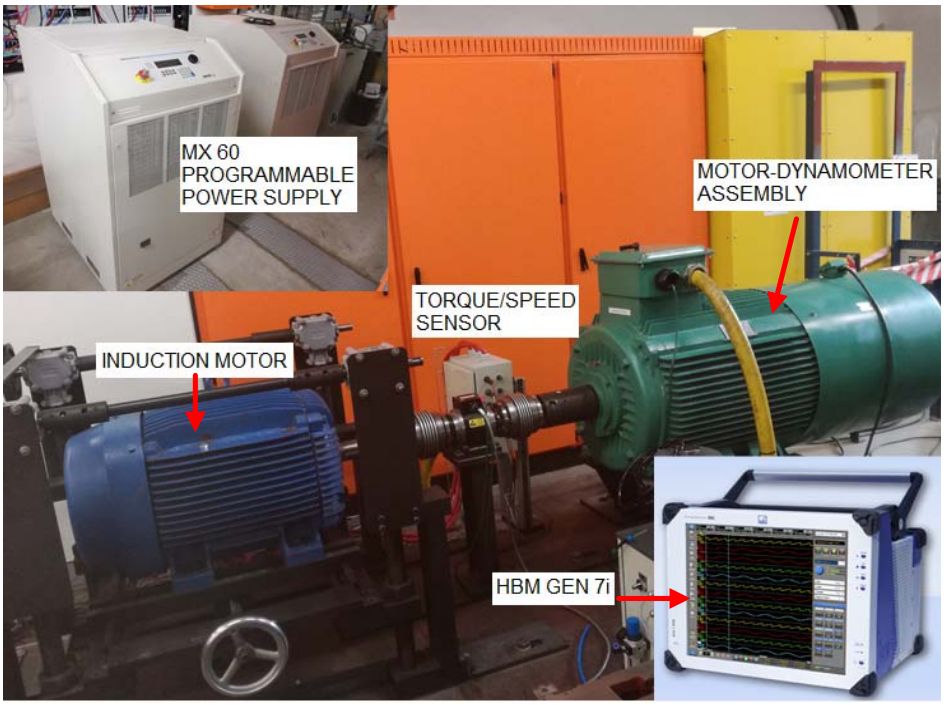

Figure 5-3 . Image of a flexible 110kW test rig highlighting the major equipment.

5.5. Experimental Results

The efficiency estimation results obtained from the proposed NIEE-PWM-RMS, NIEE-PWM-HARM techniques, the IEC-TS 60034-2-3 Technical Specification and a direct method are shown in Figure 5-4 (a) and (b) for the 37kW and the 45kW PWM inverter-fed motors respectively. The percentage errors for the results obtained using NIEE-PWM technique, NIEE-PWM-HARM and the IEC-TS 60034-2-3 Technical Specification when compared to the direct method are shown Table 5-2 and Table 5-3 for the 37kW and 45kW PWM inverter-fed motors respectively.

It can be deduced from these results that the proposed NIEE-PWM-RMS technique, the NIEE-PWM-HARM and the IEC-TS 60034-2-3 Technical Specification can estimate the efficiency of the inverter-fed motors accurately within 1.5%, 0.6% and 1.3% respectively

for the 37kW motor and within 1.4%, 1.5% and 1.4% respectively for the 45kW motor across the loading range (% of rated torque). Although the IEC-TS 60034-2-3 Technical Specification is not qualified into a standard yet, its efficiency estimation procedures generally produce accurate efficiency estimates of inverter-fed machines.

Table 5-2. Efficiency estimation results using the proposed NIEE-PWM-RMS, NIEE-PWM-HARM, IEC-TS 60034-2-3 and a direct method for the 37kW PWM inverter-fed motor.

Load (%)	DIRECT-PWM	NIEE-PWM-HARM	% Error	NIEE-PWM-RMS	% Error	IEC-TS 60034-2-3	% Error
25	82.97	83.43	0.56	81.77	1.45	81.95	1.23
50	89.12	89.03	0.10	88.15	1.09	88.53	0.66
75	90.68	90.45	0.25	89.60	1.19	90.19	0.54
100	90.75	90.51	0.26	89.61	1.26	90.38	0.41
115	90.4	90.21	0.22	89.27	1.25	90.15	0.28
125	90.12	89.95	0.19	88.99	1.25	89.9	0.24

Therefore, it can be reasonably used as a benchmark for comparison when new efficiency techniques are developed specifically for inverter-fed machines. However, its use is still limited to some specifications of the inverter supply and can only be reliably applied to squirrel cage motors as discussed in section 5.3.

Table 5-3. Efficiency estimation results using the proposed NIEE-PWM-RMS, NIEE-PWM-HARM, IEC-TS 60034-2-3 and a direct method for the 45kW PWM inverter-fed motor.

Load (%)	DIRECT-PWM	NIEE-PWM-HARM	% Error	NIEE-PWM-RMS	% Error	IEC-TS 60034-2-3	% Error
25	82.57	83.78	1.47	83.69	1.36	83.66	1.32
50	89.06	89.43	0.41	89.33	0.30	89.57	0.57
75	90.98	90.75	0.25	90.59	0.43	91.12	0.15
100	91.03	90.79	0.26	90.56	0.52	91.31	0.31
110	90.85	90.62	0.25	90.36	0.54	91.22	0.41
115	90.93	90.53	0.44	90.26	0.74	91.15	0.24

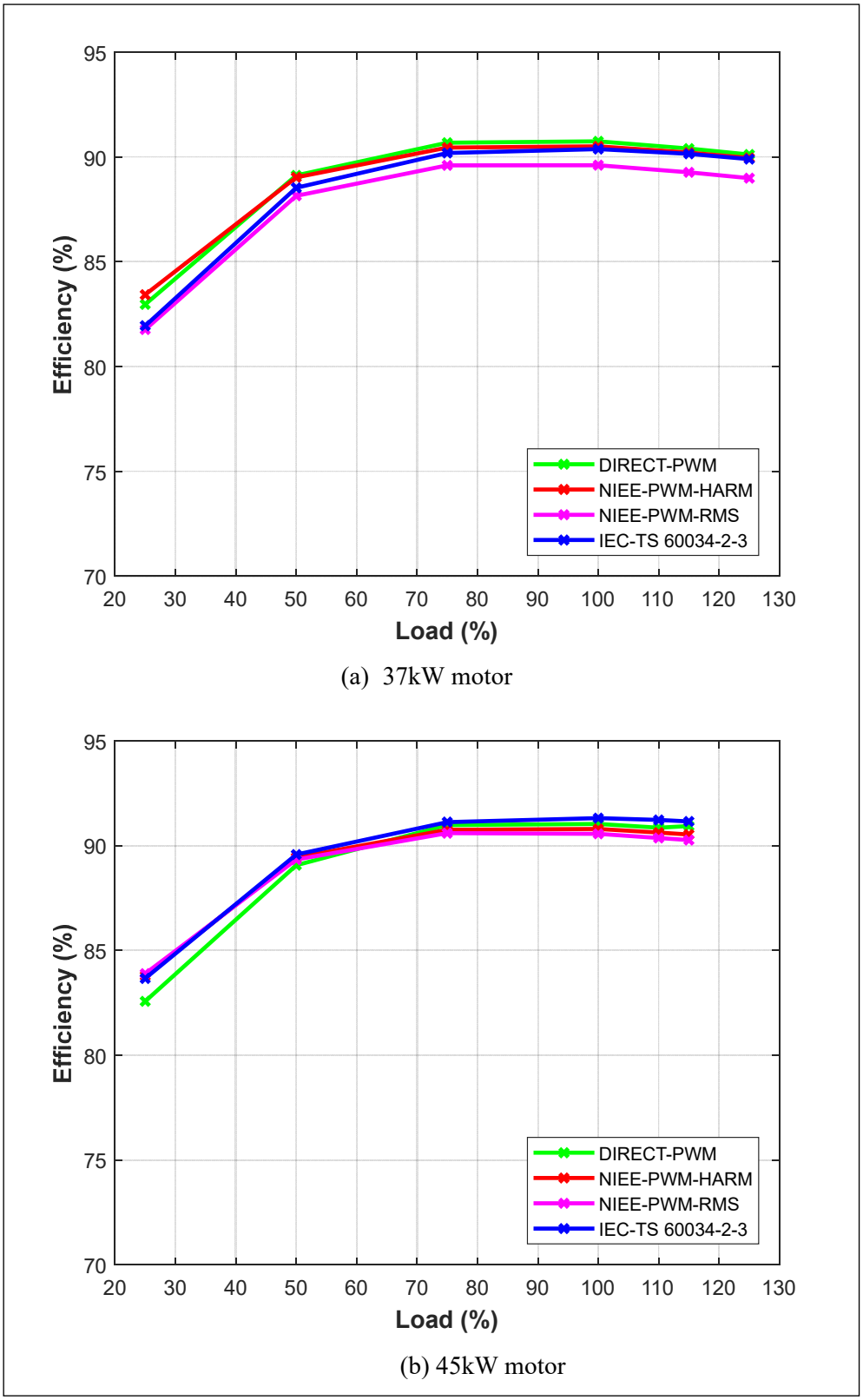

(a) 37kW motor

(b) 45kW motor

Figure 5-4. Efficiency estimates of the proposed NIEE-PWM technique, compared with the NIEE-PWM-HARM, IEC-TS 60034-2-3 and a direct method at different loading conditions.

Further analysis is added to section 5.5 against Figure 5.4 as follows:

The NIEE-PWM-HARM, NIEE-PWM-RMS and the IEC 60034-3-2 overestimates the efficiency of the 45kW motor slightly more than the 37kW motor at lower loading. This may be due to notable differences in the motor power factors at lower loads as discussed at the end of section 4.3.3 in Chapter 4 for the NIEE-PWM-HARM technique. The efficiencies from the NIEE-PWM-HARM technique are generally higher when compared to those from the NIEE-PWM-RMS technique across the two motors. This is because the NIEE-PWM-HARM technique only considers a finite number of harmonics in the computation of harmonic losses whereas the NIEE-PWM-RMS technique considers a holistic loss contribution by all harmonics. However, the two techniques are in better agreement for the 45kW motor than the 37kW motor. This effect can be caused by a slightly higher % error in the estimation of the rotor resistance parameter when using the NIEE-PWM-RMS technique for the 37kW motor. The estimation or even measurement of the motor parameters are prone to error when the motor is supplied by an inverter since rms values were derived from distorted supply waveforms.

To further substantiate the proposed non-intrusive efficiency estimation technique, Figure 5-5 shows the efficiency estimates obtained when the technique is applied to the fundamental components of the PWM inverter-fed motors. It can be seen in Figure 5-5 that the estimated efficiency results of this test are comparable to those obtained when the same motors are fed from pure sinusoidal supply at the same loading points. The percentage errors for the results obtained using NIEE-PWM fundamental component and the IEC 60034-2-1 Standard when compared to the direct method are shown Table 5-4 and Table 5-5 for the 37kW and 45kW PWM inverter-fed motors respectively.

The trend of efficiencies from the NIEE-PWM-FUNDAMENTAL and the IEC 60034-21 are in better agreement against the DIRECT-GRID for the 37kW motor than the 45kW motor. This discrepancy could be attributed to setup errors for 45kW motor when these methods were used. The IEC 60034-2-1 overestimates the efficiencies across the entire loading range while the NIEE-PWM-FUNDAMENTAL only overestimates the efficiencies at lower loading.

Table 5-4. Efficiency estimation results using the proposed NIEE-PWM-RMS technique, when applied to the fundamental components of a 37kW PWM inverter-fed motor, compared to the IEC-60034-2-1 Standard and a direct method when the same 37kW motor is fed from a sinusoidal supply.

Load (%)	DIRECT-GRID	NIEE-PWM-FUND	% Error	IEC 60034-2-1	% Error
25	84.98	86.00	1.20	85.66	0.80
50	90.27	90.51	0.27	90.57	0.33
75	91.37	91.48	0.13	91.51	0.15
100	91.10	91.30	0.22	91.29	0.21
115	90.74	90.89	0.16	90.90	0.18
125	90.30	90.58	0.31	90.55	0.28

Table 5-5. Efficiency estimation results using the proposed NIEE-PWM-RMS technique, when applied to the fundamental components of a 45kW PWM inverter-fed motor, compared to the IEC-60034-2-1 standard and a direct method when the same 45kW motor is fed from a sinusoidal supply.

Load (%)	DIRECT-GRID	NIEE-PWM-FUND	% Error	IEC 60034-2-1	% Error
25	85.08	86.70	1.91	87.36	2.68
50	90.45	91.05	0.66	91.63	1.30
75	91.82	91.86	0.05	92.51	0.75
100	91.72	91.62	0.10	92.37	0.71
110	91.64	91.38	0.28	92.18	0.59
115	91.56	91.26	0.32	92.06	0.55

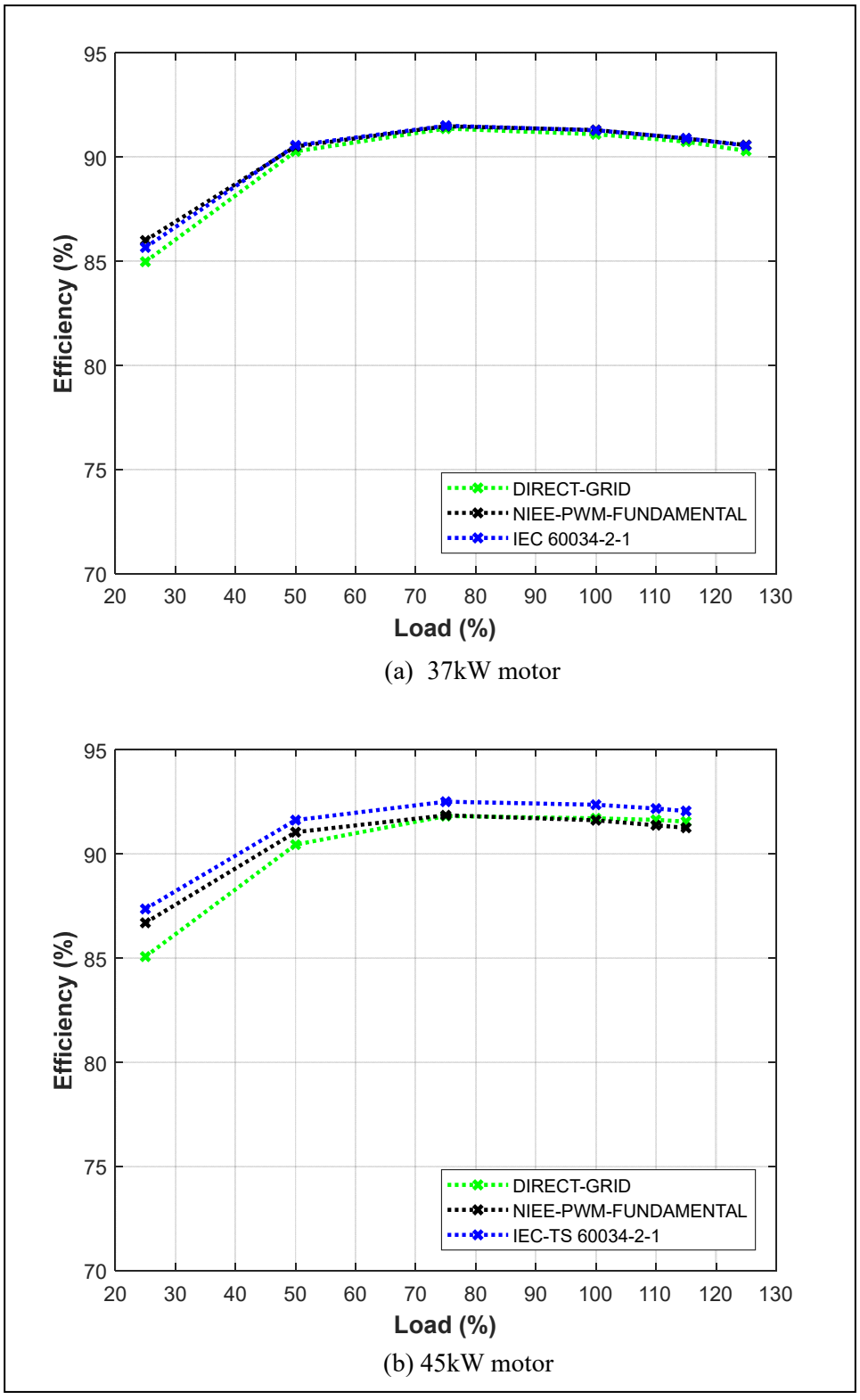

Figure 5-5. Efficiency estimates of the proposed NIEE-PWM-RMS technique using the fundamental components of a PWM-inverter motors compared with those obtained from IEC 60034-2-1 and a direct method when the motor is fed from a sinusoidal supply at different loading conditions.

Fig. 5.6 shows a comparison of the efficiency estimates of the proposed NIEE-PWM technique when applied to PWM and fundamental supply components of a PWM inverter-fed motor. The efficiency curves of NIEE-FUNDAMENTAL, NIEE-PWM-HARM and NIEE-PWM-RMS are shown. Their comparisons against direct measurement method are shown in Fig 5.4 and Fig 5.5. Here the aim is show that the efficiency is higher when the machine is supplied with the sinusoidal supply than when it is fed from the inverter.

The efficiency of a machine should generally be lower when the machine is fed from a PWM inverter compared to the same machine when supplied from a sinusoidal supply due to additional harmonic losses from the PWM inverter supply. This is confirmed in Figure 5-6 where the sinusoidal supply is represented by the fundamental component of the PWM inverter supply. In this case, the efficiency results due to NIEE-PWM-FUNDAMENTAL is higher than that presented by the NIEE-PWM-HARM and NIEE-PWM-RMS techniques for both the 37kW and the 45kW motors at different load points. The order of efficiencies for the three cases is generally correct, highest efficiencies from the NIEE-PWM-FUNDAMENTAL, followed by NIEE-PWM-HARM and then NIEE-PWM-RMS. However, larger margins between efficiencies from NIEE-PWM-HARM and NIEE-PWM-RMS are noticeable when using the 37kW motor than the 45kW motor. The reason could be attributed to inaccurate parameter estimation as discussed earlier.

Figure 5-7 and Figure 5-8 show comparisons of the total additional harmonic losses obtained from the NIEE-PWM-HARM, NIEE-PWM-RMS techniques and the IEC-TS 60034-2-3 Technical Specification for the 37kW and the 45kW motors respectively. In all cases, the total additional harmonic loss varies slightly with increase in motor load.

The magnitude of total additional harmonic losses depends on the assumptions from which they are obtained. The IEC-TS 60034-2-3 Technical Specification considers the constant additional harmonic losses as iron losses obtained from inverter-fed and sinusoidally fed induction motor at no load and assumes these to be constant across all loading points. This assumption accounts for the higher total harmonic losses of the IEC-TS 60034-2-3 than the NIEE-PWM-RMS and the NIEE-PWM-HARM techniques. The NIEE-PWM-RMS considers a holistic loss contribution by all harmonics while the NIEE-PWM-

HARM technique considers a finite number of harmonics (based on valid harmonic loss assumptions at certain harmonic orders) to ease the computational burden. The total harmonic loss slightly increases with increase in load due to the marginal increase in additional load dependent rotor and stray load losses.

The difference of the total harmonic losses between the NIEE-PWM-RMS and the NIEE-PWM-HARM techniques is larger on the 37kW motor than on the 45kW motor. This could be inherited from earlier discussions about a slightly higher % error in the estimation of the rotor resistance parameter in the case of the 37kW motor when estimated from PWM supply rms values.

The difference in the total harmonic loss magnitudes has shown no major effect on the overall efficiency of the motors due their small harmonic loss contribution compared to the fundamental loss as depicted in Figure 4-26 and Figure 4-27.

Table 5-6 provides a comparison of the hardware and computational requirements and response times for the IEC TS 60034-2-3 Technical Specification and the NIEE-PWM-HARM NIEE-PWM-RMS techniques in order to assess their implementation feasibility. It can be seen that whilst the IEC TS 60034-2-3 is highly intrusive, the processing of acquired data is not computationally intensive. However, the hardware implementation requires a fully furnished test rig with the listed hardware. The NIEE-PWM-HARM is computationally intensive following the requirements to process the parameter estimation optimization algorithms, harmonic regression analysis and harmonic loss analysis algorithms. However, this can be mitigated by taking advantage of the fast processing and parallelism of FPGA hardware architectures. The NIEE-PWM-RMS can be less computationally intensive since it does not perform any harmonic analysis. The response times of the NIEE-PWM-HARM and the NIEE-PWM-RMS can be almost in real time. The choice of NIEE-PWM-HARM or NIEE-PWM-RMS technique for non-intrusive efficiency estimation depends on the amount of analysis required.

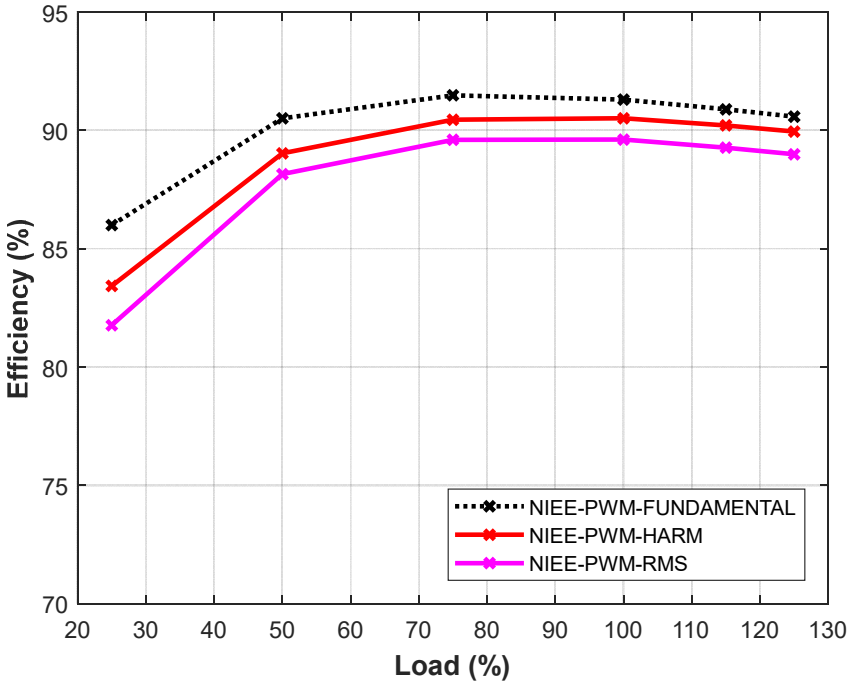

(a) 37kW motor

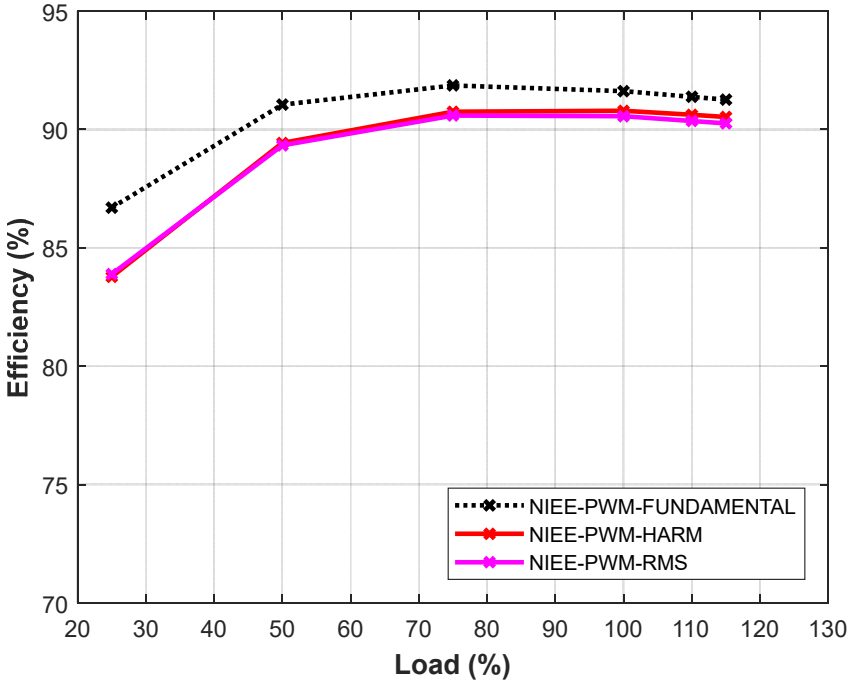

(b) 45kW motor

Figure 5-6. Comparison of the efficiency estimates of the proposed NIEE-PWM technique when applied to PWM and fundamental supply components of a PWM inverter-fed motor.

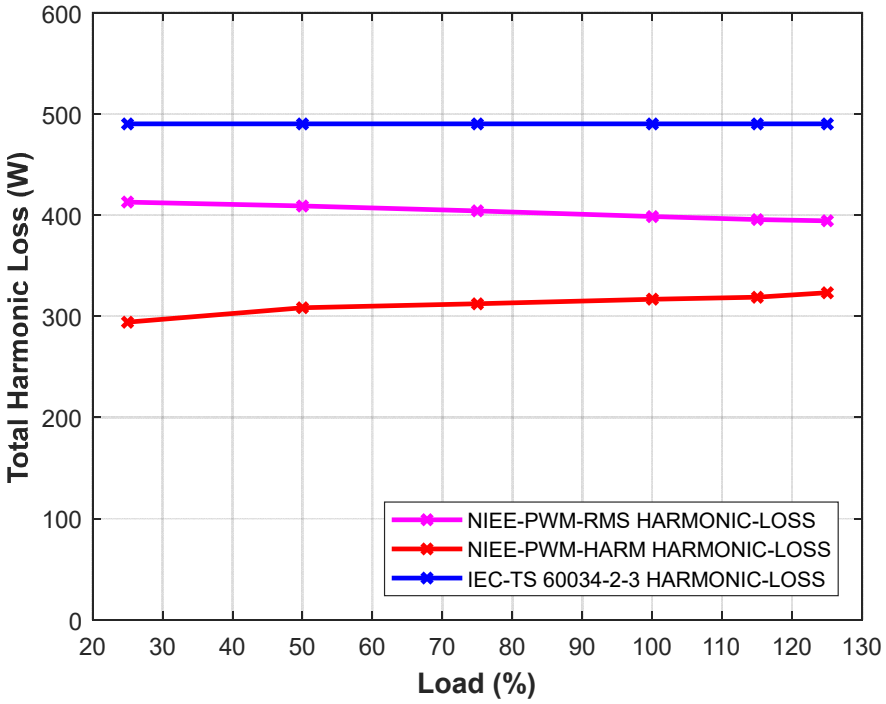

Figure 5-7. Comparison of the total harmonic losses obtained from the NIEE-PWM-RMS, NIEE-PWM-HARM and the IEC-TS 60034-2-3 Technical Specification for the 37kW motor.

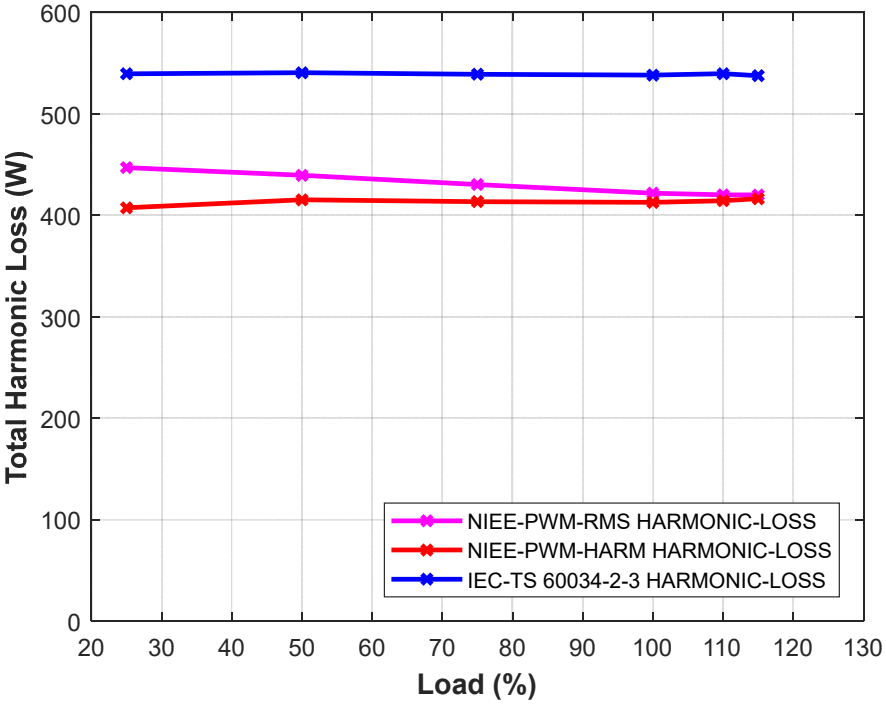

Figure 5-8. Comparison of the total harmonic losses obtained from the NIEE-PWM-RMS, NIEE-PWM-HARM and the IEC-TS 60034-2-3 Technical Specification for the 45kW motor.

Table 5-6. Comparison of the hardware and computational requirements and response times for the different techniques.

Method	Hardware Requirements	Computational Requirements	Response Time
IEC TS 60034-2-3	A test rig equipped with PWM inverter power supply, motor dynamometer assembly, test motors, data acquisition system, torque/speed sensors, voltage and current sensors, etc	Less computational requirements than NIEE-PWM-HARM and NIEE-PWM-RMS Techniques. Acquired machine data is processed off-line.	Almost immediate results during off-line processing.
NIEE-PWM-HARM	FPGA based hardware for parallel processing, parameter estimation optimization algorithms, harmonic regression analysis and harmonic loss analysis algorithms	More computational requirements than NIEE-PWM-RMS	Can be almost in real time due to the fast processing and parallelism of PGGA hardware architecture.
NIEE-PWM-RMS	FPGA based hardware for parallel processing of parameter estimation optimization algorithms and motor loss estimation	Less computational requirements than the NIEE-PWM-HARM	Can be almost in real time due to the fast processing and parallelism of PGGA hardware architecture. Can be better than NIEE-PWM-HARM

5.6. Error Analysis

The accuracy of the estimated efficiencies using the proposed NIEE-PWM-RMS technique and the IEC-TS 60034-2-3 Technical Specification were verified against the actual measurements of the direct method. However, the accuracy of the measured input values that are used to estimate efficiency still needs to be verified to ascertain their validity.

There are three types of errors associated with a typical experiment namely: methodological error, human error and instrument error. Methodological error is a result of errors in the testing procedure or methodology. Human errors are associated with inaccurate readings, incorrect calculations and misuse of instrumentation. Instrumentation error is a result of the accuracy margins of the instrumentation used in the acquisition of data.

Instrument error is the most common type of error in the efficiency estimation problem and is considered to be the main contributing factor in the measurement [16], [176]. The focus of this section will be on this type of error. Instrument error is calculated with three common evaluation techniques namely:

- Maximum Error Estimation (MEE)
- Worse Case Error Estimation (WCEE)
- Realistic Error Estimation (REE)

The MEE, which provides the maximum error is defined by:

$$\varepsilon_{\eta} = max\left|\frac{1\pm\varepsilon_{Po}}{1\pm\varepsilon_{Pi}}\right| - 1 = max\left|\frac{(1\pm\varepsilon_{T}).(1\pm\varepsilon_{S})}{1\pm\varepsilon_{Pi}}\right| - 1 \qquad (5\text{-}22)$$

where:

ε_{η} - is the relative error of the measured efficiency

ε_{Po} - is the relative error of the measured output power

ε_{Pi} - is the relative error of the measured input power

ε_{T} - is the relative error of the measured torque

ε_{S} - is the relative error of the measured speed

The relative error of the measured quantity is the ratio of absolute error to the true error and is usually found on the calibration certificate of the instrument. The relative errors for the transducers in question are stated below:

- Torque transducer: $\pm 0.2\%$
- Speed sensor: $\pm 0.05\%$
- Input power: $\pm 0.2\%$

Using the relative errors above in equation (5-22) gives the maximum measured efficiency error as:

$$\varepsilon_{\eta} = max\left|\frac{(1\pm 0.2\%).(1\pm 0.05\%)}{1\pm 0.2\%}\right| - 1 = \pm 0.45\%$$

The WCEE which handles separately the effect of each error on the measured efficiency based on an influence coefficient CI as shown in (5-23) [176].

$$\varepsilon_\eta = IC_T.\varepsilon_T + IC_S.\varepsilon_S + IC_{Pi}.\varepsilon_{Pi} \quad (5\text{-}23)$$

where:

IC_T - is the influence coefficient of torque transducer

IC_S - is the influence coefficient of speed transducer

IC_{Pi} - is the influence coefficient of input power

The influence coefficient for each parameter is calculated based on the perturbation method. The relative deviation of the output parameter is found for a known perturbation in an input parameter, for instance, torque as shown in (5-24) [176].

$$IC_T = \frac{\varepsilon_\eta}{\varepsilon_T} \quad (5\text{-}24)$$

The influence coefficient of the above input parameters for the direct method are given in [16] as: $IC_T = 1, IC_S = 1$ and $IC_{Pi} = 1.001$. Therefore, WCEE will be as follows:

$$\varepsilon_\eta = 1.(\pm 0.2\%) + 1.(\pm 0.05\%) + 1.001.(0.2\%) = \pm 0.45\%$$

The MEE and the WCEE are based on the maximum allowable error for each input parameter and thus produces almost similar output relative errors.

The REE assumes a uniformly distributed error for each input parameter and is a more realistic source of error. The relative distribution of the output parameter (efficiency) from REE is given by [176]:

$$\varepsilon_\eta = \sqrt{\sum (IC_T.\varepsilon_T)^2 + (IC_S.\varepsilon_S)^2 + (IC_{Pi}.\varepsilon_{Pi})^2} \quad (5\text{-}25)$$

The efficiency measurement error using the same influence coefficients is:

$$\varepsilon_\eta = \sqrt{\sum 1.(\pm 0.2\%)^2 + 1.(\pm 0.05\%)^2 + 1.001(\pm 0.2\%)^2}$$

$= \pm 0.29\%$

This error analysis serves to guarantee that the efficiency measurement using the direct method, from which the proposed NIEE-PWM-RMS technique efficiency estimate, and the IEC-60034-2-3 efficiency measurement are benchmarked, is performed within acceptable errors as presented above.

5.7. Repeatability Tests on Overall Efficiency

To ascertain the consistency of the efficiency estimation using the proposed NIEE-PWM-RMS technique three consecutive tests were performed on the 37kW and the 45kW motors at different load points. Table 5-7 indicates that the efficiency results were repeatable and consistent on both motors due to low (nearly zero) values of standard deviation, σ. This guarantees the reliability of the efficiency estimation techniques.

Table 5-7. Efficiency repeatability tests using the proposed NIEE-PWM-RMS technique on PWM inverter-fed motors.

NIEE-PWM-RMS - 37kW motor						
% Load	**25**	**50**	**75**	**100**	**115**	**125**
Run 1	81.7082	88.1370	89.6038	89.6142	89.2701	88.9766
Run 2	81.7041	88.1355	89.6033	89.6141	89.2698	88.9761
Run 3	81.7067	88.1365	89.6037	89.6142	89.2700	88.9764
$\bar{x}$	81.7063	88.1363	89.6036	89.6142	89.2700	88.9764
σ	0.0021	0.0008	0.0003	0.0001	0.0002	0.0003
NIEE-PWM-RMS - 45kW motor						
% Load	**25**	**50**	**75**	**100**	**110**	**115**
Run 1	83.7186	89.3480	90.6040	90.5710	90.3767	90.2775
Run 2	83.7169	89.3469	90.6029	90.5696	90.3751	90.2758
Run 3	83.7169	89.3469	90.6029	90.5696	90.3751	90.2758
$\bar{x}$	83.7175	89.3473	90.6033	90.5701	90.3756	90.2764
σ	0.0010	0.0006	0.0006	0.0008	0.0009	0.0010

5.8. Sensitivity Analysis

A sensitivity analysis of the 45kW motor using the NIEE-PWM-RMS technique was carried out to analyze the impact of rotor speed estimation error on the overall motor

efficiency. The graph in Figure 5-9 was derived from a linear regression which was performed on the data points. It can be seen that a worse case speed estimation error of 0.5% can only result in less than 2.5% error in efficiency. A good rotor speed accuracy of 0.1% result in efficiency error of less than 0.5%. This sensitivity analysis shows the robustness of the proposed efficiency estimation technique against small errors in speed estimation.

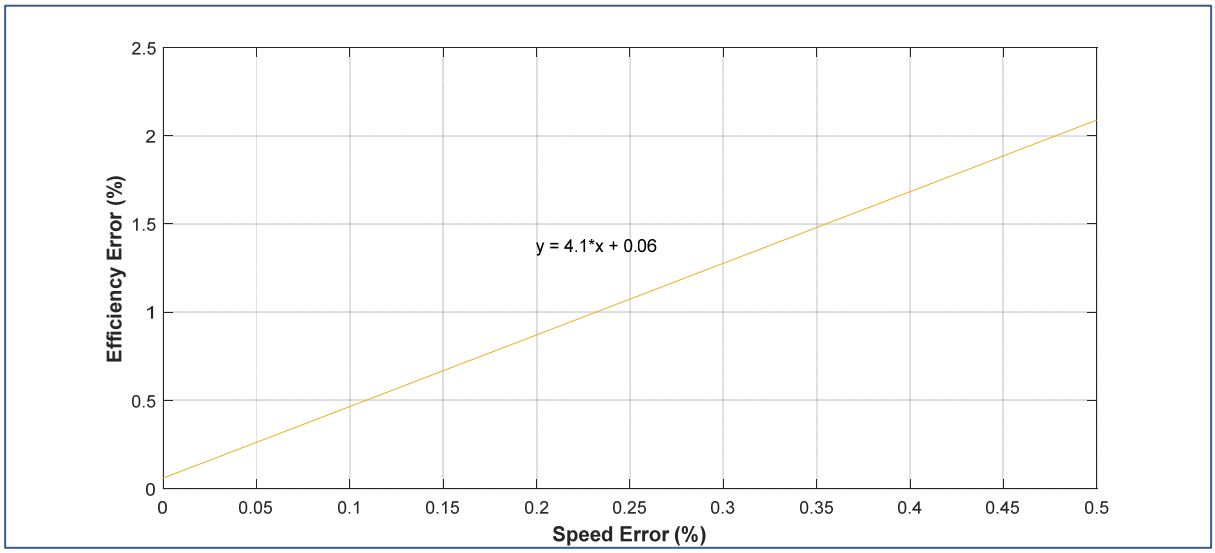

Figure 5-9. Sensitivity analysis of the 45kW motor using the NIEE-PWM-RMS technique

5.9. Concluding Remarks

A proposed non-intrusive efficiency estimation technique (NIEE-PWM-RMS) that does not depend on injected harmonic voltages but caters for a holistic harmonic loss is presented. This technique can estimate the motor efficiency within 2% error when tested on 37kW and 45kW PWM inverter-fed motors under normal loading conditions and can be used for both sinusoidal and inverter-fed machine efficiency estimation. The technique is compared to NIEE-PWM-HARM presented in Chapter 4, the IEC-TS 60034-2-3 Technical Specification. The overall estimated efficiency results agree to within 2% relative to direct measurement method.

The total additional harmonic losses vary only slightly with the changes in load based on the NIEE-PWM-RMS, NIEE-PWM-HARM and IEC-TS 60034-2-3 Technical Specification and the motors tested. Their magnitude and trend depend on the assumptions from which they are obtained and has shown no major effect on the overall efficiency of the motors due the small harmonic loss contribution compared to the fundamental loss.

Based on the tests conducted, the IEC-60034-2-3 Technical Specification measures the motor efficiency accurately and can be used as a benchmark when new efficiency estimation methods are tested specifically for inverter-fed machines. However, the Technical Specification still suffers implementation problems due its recommended use with specific attributes of the inverter supply such as switching frequency, DC bus voltage and its limited use to squirrel cage IMs.

The error analysis guarantees the efficiency measurement accuracy and repeatability tests confirm the reliability of the NIEE-PWM-RMS efficiency estimation solution.

Chapter 6

CONCLUSION AND RECOMMENDATIONS

6.1 Conclusion

This thesis has proposed non-intrusive efficiency estimation techniques applicable to inverter-fed induction machines. Prior to the development of proposed techniques, a detailed review and assessment of the efficiency estimation methods in terms of intrusiveness and applicability to inverter-fed machines was conducted. A review and analysis of the different rotor speed estimation techniques in terms of intrusiveness, relative accuracy and computational overhead when the motor is fed by an inverter supply was conducted. Based on the review, analysis and experimental results of the proposed efficiency estimation techniques presented, the following conclusions can be drawn:

6.1.1. Non-intrusive Efficiency Estimation Methods

A critical review of the efficiency estimation methods was conducted with specific assessment of their intrusiveness and use in inverter-fed machines. The quantification of additional losses due to inverter supply harmonics and the impact of the supply harmonics on the induction machine were explored. Following the consideration and analysis it can be concluded that the current and future trend in non-intrusive efficiency estimation of inverter fed motors focusses on segregation of motor losses based on equivalent circuits whose parameters are estimated by optimisation techniques that use limited measured values. Efficiency estimation errors at normal loads of within 1% and up to 1.2% based on PBIL using standard and iron loss equivalent circuits respectively have been reported [19]. An efficiency estimation error of 2% using BFA was reported in [70].

6.1.2. Rotor Speed Estimation

Following the analysis of the rotor speed estimation techniques for inverter-fed induction motors reported in literature and from the experimental verification, it can be concluded that the current spectrum-based speed estimation techniques coupled with advanced signal processing algorithms that fulfil the requirements of high frequency resolution, less computational time and applicable to non-stationary signals provide mature technology and are recommended for industrial use.

Motor current spectrum-based speed estimation is conveniently derived from the same data set that is used to estimate induction motor parameters in non-intrusive efficiency estimation, with sufficient accuracy (error less than 1%).

Accurate rotor speed estimates of within 0.05%, 0.33%, 0.55% and 0.55% error were obtained using vibration, rotor slot harmonic, MCSA and rotor eccentricity analysis respectively when tested on 250W, 37kW and 45kW inverter-fed motors. These results are quite comparable to those found in literature for the same speed estimation techniques. In general, the least intrusive speed estimation techniques provide less accuracy, less cost but more computational overhead depending on the signal processing techniques used specifically when the motor is supplied by the inverter.

The sensitivity results show that a small inaccuracy of 0.033 Hz in the measurement of the speed dependent harmonic frequency results in a small speed error (0.0431 rpm) when the RSH based speed estimation technique is used. This instills confidence in the use of this non-intrusive motor speed estimation technique due to its robustness especially when the motor current is infested with harmonics due to inverter supplies.

6.1.3. Non-intrusive Parameter Estimation and Harmonic Loss Analysis

A review of the equivalent circuit models suitable for non-intrusive parameter estimation of induction machines was presented. A PBIL algorithm was used to estimate the fundamental parameters of the induction motor equivalent circuit. The estimated parameters were compared to those obtained from IEC-60034-2-1 Standard and the results showed good agreement within 3.5% error using the equivalent circuit of Figure 4-2.

Harmonic rotor parameter estimation was performed using the BFO algorithm using harmonic magnitudes and phases. A Harmonic Regression Analysis (HRA) technique was used to extract the harmonic magnitude and phase from the supply voltage and current data. It is shown that the harmonic rotor resistance gradually increases with increase in harmonic frequency due to the decreasing conducting surface caused by skin effect. The harmonic rotor leakage reactance increases steeply with increase in harmonic frequency and becomes constant due to magnetic saturation.

The temperature estimation methodology adopted from [20] was employed to estimate machine operating temperature in order to correct the stator and rotor ohmic resistances.

A harmonic loss analysis is conducted using the harmonic parameters and the harmonic voltage and current data. It is observed that appreciable harmonic losses mainly occur at the *nth* order PWM sidebands. The total harmonic loss is dominated by the harmonic core losses which are almost constant across the entire loading range. The harmonic rotor and stray load losses seem to very marginally increase with increase in load. The harmonic stator loss remains marginally low.

The additional harmonic losses contribute an appreciable amount to the total motor losses but remain small compared to the fundamental loss. The total additional harmonic losses slightly increase with increase in the motor load.

The proposed techniques and harmonic loss analysis provide accurate efficiency estimates of within 1.5% error when compared to the direct method.

6.1.4. Non-intrusive Efficiency Estimation

A proposed non-intrusive efficiency estimation technique (NIEE-PWM-RMS) that does not depend on injected harmonic voltages but caters for a holistic harmonic loss is presented. This technique can estimate the motor efficiency within 2% error when tested on 37kW and 45kW PWM inverter-fed motors under normal loading conditions and can be used for both sinusoidal and inverter-fed machine efficiency estimation. The technique is compared to NIEE-PWM-HARM presented in Chapter 4, the IEC-TS 60034-2-3 Technical Specification. The overall estimated efficiency results agree to within 2% relative to direct measurement method.

The total additional harmonic losses vary only slightly with the changes in load based on the NIEE-PWM-RMS, NIEE-PWM-HARM and IEC-TS 60034-2-3 Technical Specification and the motors tested. Their magnitude and trend depend on the assumptions from which they are obtained and has shown no major effect on the overall efficiency of the motors due the small harmonic loss contribution compared to the fundamental loss.

Based on the tests conducted, the IEC-60034-2-3 Technical Specification measures the motor efficiency accurately and can be used as a benchmark when new efficiency estimation methods are tested specifically for inverter-fed machines. However, the Technical Specification still suffers implementation problems due its recommended use with specific attributes of the inverter supply such as switching frequency, DC bus voltage and its limited use to squirrel cage IMs.

The error analysis guarantees the efficiency measurement accuracy and repeatability tests confirm the reliability of the NIEE-PWM-RMS efficiency estimation solution.

6.2 Recommendations for Future Work

Based on the above conclusions, the following recommendations for further work can be made.

6.2.1. Parameter Estimation

Some recommendations for further work on parameter estimation are outlined below:

a) Use of single optimization technique to estimate both fundamental and harmonic parameters of the induction machines to improve computational efficiency.
b) Investigate on alternative harmonic parameter estimation techniques in order to compare the estimated results.
c) Qualification of the non-intrusive temperature estimation technique proposed in [20] and adopted in subsection 4.2.4.3 against measured temperature values and argue the non-concurrences against thermal air flow issues and strategic placement of thermocouples.

6.2.2. Non-Intrusive Efficiency Estimation

Some recommendations for further work on non-intrusive efficiency estimation of inverter-fed IMs are outlined below:

a) Investigate further to improve the determination of additional harmonic losses to improve the results obtained by the proposed techniques and the IEC-TS 60034-2-3.

REFERENCES

[1] *Energy Independence and Security Act (EISA),* US Department of Energy, United States, 2007.

[2] *Energy Policy Act (EPAct),* US Department of Energy, United States, 1992.

[3] *IEEE standard test procedure for polyphase induction motors and generators*, IEEE Standard 112-2017, IEEE Power Engineering Society, New York, NY.

[4] *Methods for determining losses and efficiency of rotating electrical machinery from tests*, IEC 34-2, International Electrotechnical Commission, Geneva, 1972.

[5] *Ecodesign for power drive systems, motor starters, power electronics and their driven applications – Energy efficiency indicators for power drive systems and motor starters*, IEC 61800-9-2, Geneva, 2017.

[6] *Specific test methods for determining losses and efficiency of converter-fed AC induction motors*, IEC-TS 60034-2-3, Geneva, 2013.

[7] M. Chirindo, M. A. Khan, and P. S. Barendse, "Considerations for non-intrusive efficiency estimation of inverter-fed motors," *IEEE Trans. Ind. Electron.,* vol. 63, no. 1, pp. 741-749, 2016.

[8] J. Hsu, J. Kueck, M. Olszewski, D. Casada, P. Otaduy, and L. Tolbert, "Comparison of induction motor field efficiency estimation methods," *IEEE Trans. Ind. Appl.*, vol. 34, no. 1, pp. 117–125, Jan./Feb. 1998.

[9] P. G. Cummings, W. D. Bowers, and W. J. Martiny, "Induction motor efficiency test methods," *IEEE Trans. Ind. Appl.*, vol. IA-17, pp. 253–272, May/June 1981.

[10] F. Ferreira and A. de Almeida, "Considerations on in-field induction motor load estimation methods," in *Proc. IEEE ICEM*, Vilamoura, Portugal, 2008, pp. 1-8.

[11] A. Wallance, A. Von Jouanne, E. Wiedenbrug, E. Matheson, and J. Douglass, "A laboratory assessment of in-service and non-intrusive motor efficiency testing methods," *Electr. Power Compon. Syst.*, vol. 29, no. 6, pp. 517–529, Jun. 2001.

[12] B. Lu, T. G. Habetler, and R. G. Harley, "A survey of efficiency-estimation methods of in-service induction motors," *IEEE Trans. Ind. Appl.*, vol. 42, no. 4, pp. 924-933, July/Aug. 2006.

[13] J. D. Kueck, "Development of a method for estimating motor efficiency and analyzing motor condition," in *Proc. IEEE PPIC.*, Portland, ME, USA, Jun. 1998, pp. 67–72.

[14] A. Dell'Aquila, L. Salvatore, and M. Savino, "A new test method for determination of induction motor efficiency," *IEEE Trans. Power Appl. Syst.*, vol. PAS-103, no. 10, pp. 2961–2973, Oct. 1984.

[15] J. S. Hsu and P. L. Sorenson, "Field Assessment of induction motor efficiency through air-gap", *IEEE Trans. Energy Convers.,* vol. 11, no. 3, pp. 489-494, 1996.

[16] B. Herndler, P. Barendse and M. A. Khan, "Considerations for improving the non-intrusive efficiency estimation of induction machines using the air gap torque method," *in Proc. IEEE IEMDC*, Niagara Falls, ON, Canada, 2011, pp. 1516-1521.

[17] B. Lu, C. Wenping; I. French, K. J. Bradley and T. G. Habetler, "Non-intrusive efficiency determination of in-service induction motors using genetic algorithm and air-gap torque methods," in *IEEE IAS Annual Meeting*, New Orleans, LA, USA, 2007, pp. 1186-1192.

[18] S. B. Lee and T. G. Habetler, "An online stator winding resistance estimation technique for temperature monitoring of line-connected induction machines," *IEEE Trans. Ind. Appl.*, vol. 39, no. 3, pp. 685-694, May/June 2003.

[19] C. S. Gajjar, M. A. Khan, and P. Barendse, "Analysis of non-intrusive efficiency estimation of Induction machines compared to IEEE 112B and IEC 34-2-1 standards", in *Proc. IEEE ECCE*, Pittsburgh, PA, Pennsylvania, 2014, pp. 294-301.

[20] A. G. Siraki, C. Gajjar, M. A. Khan, P. Barendse and P. Pillay, “An algorithm for non-intrusive *in situ* efficiency estimation of induction machines operating with unbalanced conditions,” *IEEE Trans. Ind. Appl.*, vol 48, no. 6, pp 1890-1900, Nov/Dec 2012.

[21] P. Pillay, V. Levin, P. Otaduy and J. Kueck, "In situ induction motor efficiency determination using the genetic algorithm," *IEEE Trans. Energy Convers.*, vol. 13, no. 4, pp. 326-333, Dec 1998.

[22] J. R. Gomez, E. C. Quispe, M. A. de Armas, P. R. Viego, "Estimation of induction motor efficiency in situ under unbalanced voltages using genetic algorithms," *in Proc. IEEE ICEM,* Vilamoura, Portugal, 2008, pp. 1-4.

[23] EASA, AEMT, “The effect of repair/rewinding on motor efficiency”, EASA/AEMT Rewind study and good practice to maintain motor efficiency, 2003. [Online]. Available: https://www.easa.com/sites/files/resource_library_public/EASA_AEMT_RewindStudy_1203-0115.pdf.

[24] *Motors and generators*, NEMA MG1-2003 Standard, National Electrical Manufacturers Association, Rosslyn, Virginia, 2003.

[25] B. S. Guru and H. R. Hiziroglu, *Electric machinery and transformers*, *3*rd ed. New York, NY, USA: Oxford Univ. Press, 2001, ch. 8.

[26] *Rotating electrical machines - Part 2-1: Standard methods for determining losses and efficiency from tests (excluding machines for traction vehicles)*, IEC 60034-2-1, Geneva, 2007.

[27] G. M. Hashem, and A. D. El-Koshariy, “Investigation of induction motor performance fed from PWM inverter,” in *Proc. IEEE MEPON*, El-Minia, Egypt, 2006, pp. 421-426.

[28] Ching-Yin Lee and Wei-Jen Lee, “Effects of non-sinusoidal voltage on the operation performance of a three-phase induction motor,” in *IEEE Trans. Energy Convers.*, vol. 14, no. 2, pp. 193-201, Jun.1999.

[29] *IEEE recommended practices and requirements for harmonic control in electrical power systems*, IEEE Std. 519-1992, New York, 1992.

[30] M. J. Melfi, "Quantifying the energy efficiency of motors fed by adjustable frequency inverters," in *Proc. IEEE PCIC*, Anaheim, CA, USA, 2009, pp. 1-7.

[31] A. Antonopoulos, G. Moree, J. Soulard, L. Angquist, and H. -P. Nee, "Experimental evaluation of the impact of harmonics on induction machines fed by modular converters," in *Proc. IEEE ICEM,* Berlin, Germany, 2014, pp. 768-775.

[32] S. R. Budi, and S. Shama, "A novel method of nine level inverter-fed induction motor drive", in *Proc. IEEE ICAETR*, Unnao, India, 2014, pp. 1-4.

[33] A. Abdel-Khalik, S. Ahmed, and A. Massoud, "Comparative evaluation of four quasi-square wave fed multiphase induction machines," in *Proc. 37th Annu. IEEE IECON*, Melbourne, VIC, Australia, 2011, pp. 3476-3481.

[34] E. M. Tsampouris, and A. G. Kladas, "Efficiency optimization considerations for standard induction motor fed by PWM inverter," in *Symp. 8th Int. IEEE ELECTROMOTION,* Lille, France, 2009, pp. 1-6.

[35] J. R. Dominguez, C. Mora-Soto, S. Ortega-Cisneros, J. J. R. Panduro, and G. L. Alexander, "Copper and core loss minimization for induction motors using high-order sliding-mode control," *IEEE Trans. Ind. Electron.*, vol. 59, no. 7, pp. 2877 – 2889, Jul. 2012.

[36] E. A. Klingshirn and H. E. Jordan, "Polyphase induction motor performance and losses on nonsinusoidal voltage sources," *IEEE Trans. Power App. Syst.*, vol. PAS-87, pp. 624-631, 1968.

[37] A. Khoobroo, M. Krishnamurthy, B. Fahimi, and W. Lee, "Effects of system harmonics and unbalanced voltages on electromagnetic performance of induction motors," in *Proc. 34th Annu. IEEE IECON*, Orlando, FL, USA, 2008, pp. 1173-1178.

[38] P. Phumiphak and C. Chat-uthai, "Non-intrusive method for estimating efficiency of inverter-fed induction motor using measured values," in *Proc. IEEE ICSET*, Singapore, 2008, pp. 580-583.

[39] S. Lee, and T. G. Habetler, "An online stator resistance estimation technique for temperature monitoring of line-connected induction machines," *IEEE Trans. Ind. Appl.*, vol. 39, no. 3, pp. 685-694, May 2003.

[40] F. Briz, M. W. Gegner, J. M. Guerrero, and A. B. Diez, "Temperature estimation in inverter-fed machines using a high-frequency carrier signal injection," *IEEE Trans. Ind. Appl.*, vol. 44, no. 3, pp. 799-808, May/Jun. 2008.

[41] M. C. Di Piazza, and M. Pucci, "Efficiency analysis in induction motor drives with discontinuous PWM and electrical loss minimization," in *Proc. IEEE ICEM,* Berlin, Germany, 2014 pp. 736-743.

[42] A. H. Eltom, and A. Demirbas, "Motor system energy efficiency in the nylon industry: A comparison of PWM and square wave inverters," in *Proc. IEEE IEMDC,* Miami, FL, USA, 2009, pp. 508-513.

[43] T. C. Green, C. A. Hernandez-Aramburo, and A. C. Smith, "Losses in grid and inverter supplied induction machine drives," *IEE Proc. Elect. Power Appl.*, vol. 150, no. 6, pp. 712-724, Nov. 2003.

[44] A. Boglietti, A. Cavagnino, L. Ferraris and M. Lazzari, "Skin effect experimental validations on induction motor squirrel cage parameters," in *Proc. 18th Conf., IEEE ICEM*, Vilamoura, Portugal, 2008, pp. 1-4.

[45] E. Schmidt, F. Mullner and H. Neudorfer, "Modelling and precalculation of additional losses of inverter fed asynchronous induction machines of traction drives," in *Proc. IEEE IEMDC*, Niagara Falls, ON, USA, 2011, pp. 533-538.

[46] W. H. Creer, D. W. Novotney and T. A. Lipo, "Determination of equivalent circuits for induction machines with skin effect using terminal characteristics," in *Elect. Mach. Power Syst*, vol. 10, no. 5-6, pp 379-394, Mar. 1985.

[47] H. Huiming, Y. Wang, Y. Qing, Z. Baofeng, and B. Baodong, "Effects of the PWM inverter parameters on the eddy current losses and thermal analysis of the flameproof induction motor," in *Proc. IEEE, ICEMS,* Beijing, China, 2011, pp. 1-6.

[48] K. Venkatesan and J. Lindsay, "Comparative study of the losses in voltage and current source inverter fed induction motors," *IEEE Trans. Ind. Appl.,* vol. IA-18, no. 3, pp. 240-246, May 1982.

[49] R. Kaczmarek, and M. Amar, "A general formula for prediction of iron losses under non-sinusoidal supply voltage waveform," *IEEE Trans. Magn.*, vol. 31, no. 5, pp. 2505-2509, Sep. 1995.

[50] Z. Gmyrek, A. Boglietti, and A. Cavagnino, "Estimation of iron losses in induction motors: calculation method, results, and analysis," *IEEE Trans. Ind. Electron.*, vol. 57, no. 1, pp. 161-171, Jan. 2010.

[51] A. Boglietti, A. Cavagnino, D. M. Ionel, M. Popescu, D. A. Staton, and S. Vaschetto, "A general model to predict the iron losses in pwm inverter-fed induction motors," *IEEE Trans. Ind. Appl.*, vol. 46, no. 5, pp. 1882-1890, Sep./Oct. 2010.

[52] M. Dems, and K. Komeza, "Performance characteristics of a high-speed energy-saving induction motor with an amorphous stator core," *IEEE Trans. Ind. Electron*, vol. 61, no. 6, pp. 3046-3055, Jun. 2014.

[53] W. Cao, K. J. Bradley, R. Magill, J. C. Clare, and P. W. Wheeler, "Comparison of stray load and inverter-induced harmonic losses in induction motors using calorimetric and harmonic injection methods," *IEEE Trans. Ind. Appl.*, vol. 46, no. 1, pp. 249-255, Jan./Feb. 2010.

[54] S. J. Salon, L. Ovacik, and J. F. Bailey, "Finite element calculation of harmonic losses in AC machine windings," in *Dig. 5th Biennial IEEE CEFC.*, Claremont, CA, USA, 1992, pp. TP25.

[55] K. Yamazaki and Y. Haruishi, "Stray load loss analysis of induction motor-comparison of measurement due to IEEE Standard 112 and direct calculation by finite-element method," *IEEE Trans. Ind. Appl.*, vol. 40, no. 2, pp. 543–549, Mar./Apr. 2004.

[56] V. S. Santos, *et al*., "Bacterial foraging algorithm application for induction motor field efficiency estimation under harmonics and unbalanced voltages," in *Proc. IEEE IEMDC,* Chicago, IL, USA, 2013, pp. 1108–1111.

[57] P. G. Cummings, "Estimating effect of system harmonics on losses and temperature rise of squirrel-cage motors," *IEEE Trans. Ind. Appl.*, vol. IA-22, no. 6, pp. 1121-1126, Nov. 1986.

[58] A. Siraki and P. Pillay, "An in-situ efficiency estimation technique for induction machines working with unbalanced supplies," *IEEE Trans. Energy Convers.*, vol. 27, no. 1, pp. 85–95, Mar. 2012.

[59] V. P. Sakthivel, R. Bhuvaneswari, and S. Subramanian, "Non-intrusive efficiency estimation method for energy auditing and management of in-service induction motor using bacterial foraging algorithm," *IET Elect. Power Appl.*, vol. 4, no. 8, pp. 579–590, Sep. 2010.

[60] V. P. Sakthivel, R. Bhuvaneswari, and S. Subramanian, "An accurate and economical approach for induction motor field efficiency estimation using bacterial foraging algorithm," *Measurement*, vol. 44, no. 4, pp. 674–684, May 2011.

[61] P. K. Sen and H. A. Landa, "Derating of induction motors due to waveform distortion," *IEEE Trans. Ind. Appl*., vol. 26, no. 6, pp. 1102–1107, Nov./Dec. 1990.

[62] L. Aarniovuori, L. I. E. Laurila, M. Niemela, and J. J. Pyrhonen, "Measurements and simulations of DTC voltage source converter and induction motor losses," *IEEE Trans. Ind. Electron.,* vol. 59, no. 5, pp. 2277-2287, May 2012.

[63] P. Nussbaumer, M. A. Vogelsberger, and T. M. Wolbank, "Exploitation of induction machine's high frequency behaviour for online insulation monitoring," in *Symp. 9th Int. IEEE SDEMPED,* Valencia, Spain, 2013, pp. 579-585.

[64] Z. Gao, T. G. Habetler, and R. G. Harley, "An online adaptive stator winding temperature estimator based on a hybrid thermal model for induction machines," in *Proc. IEEE IEMDC*, San Antonio, TX, USA, 2005, pp. 754–761.

[65] C. Kral, T. G. Habetler, R. G. Harley, F. Pirker, G. Pascoli, H. Oberguggenberger, and C. M. Fenz, "Rotor temperature estimation of squirrel-cage induction motors by means of a combined scheme of parameter estimation and a thermal equivalent model," *IEEE Trans. Ind. Appl.*, vol. 40, no. 4, pp. 1049–1057, Jul. 2004.

[66] Y. Wu and H. Gao, "Induction-motor stator and rotor winding temperature estimation using signal injection method," *IEEE Trans. Ind. Appl.*, vol. 42, no. 4, pp. 1038–1044, Jul./Aug. 2006.

[67] S. Lee, T. G. Habetler, R. G. Harley, and D. J. Gritter, "An evaluation of model-based stator resistance estimation for induction motor stator winding temperature monitoring," *IEEE Trans. Energy Convers.*, vol. 17, no. 1, pp. 7–15, Mar. 2002.

[68] L. M. Neto, J. R. Camacho, C. H. Salerno, and B. P. Alvarenga, "Analysis of a three-phase induction machine including time and space harmonics: the a, b, c reference frame," *IEEE Trans. Energy Convers.*, vol. 14, no. 1, pp. 80-85, Mar. 1999.

[69] A. R. Munoz, and C. L. Araya, "Magnetic vibration of three-phase induction motors supplied by inverters," in *Proc. IEEE ISIE*, Santiago, Chile, 1994, pp. 210-213.

[70] V. S. Santos, R. P. V. Felipe, J. R. G. Sarduy, N. A. Lemozy, A. Jurado, and E. C. Quispe, "Procedure for determining induction motor efficiency working under distorted grid voltages," *IEEE Trans., Energy Convers.*, vol. 30, no. 1, pp. 331-339, Mar. 2015.

[71] F. Tinazzi, M. Zigliotto, A. Boglietti, A. Cavagnino and M. Cossale, "Energy efficiency assessment for inverter-fed induction motors," in *Proc. IEEE PEMD*, Glasgow, UK, 2016, pp. 1-6.

[72] L. Wang, Y. Yan, Y. Hu, and X. Qian, "Rotational speed measurement using single and dual electrostatic sensors," *IEEE Sensors J.*, vol. 16, no. 3, pp. 1784-1793, 2015.

[73] F. J. T. E. Ferreira and F. J. P. Lopes, "Webcam-based tachometer for in-field induction motor load estimation," in *Proc. IEEE ICEM*, Lausanne, Switzerland, 2016, pp. 2380-2388.

[74] T. Wang, Y. Yan, L. Wang and Y. Hu, "Rotational speed measurement through image similarity evaluation and spectral analysis," in *IEEE Access*, vol. 6, pp. 46718-46730, 2018.

[75] M. Elloumi, L. Ben-Brahim and M. A. Al-Hamadi, "A survey of speed sensorless controls for IM drives," in *Proc. IEEE IECON*, Aachen, Germany, 1998, pp. 1018-1023.

[76] M. A. Gallegos, R. Alvarez and C. A. Nunez, "A survey on speed estimation for sensorless control of induction motors" in *Proc. IEEE CIEP*, Puebla, Mexico, 2006, pp. 1-6.

[77] R. P. Viera, C. C. Gastaldini, R. Z. Azzolin, and H. A. Grundling, "Sensorless sliding-mode rotor speed observer of induction machines based on a magnetizing current estimation," *IEEE Trans. Ind. Electron.*, vol. 61, no. 9, pp. 4573–4582, Sep. 2014.

[78] D. P. Marcetic, I. R. Krcmar, M. A. Gecic, and P. R. Matic, "Discrete rotor flux and speed estimators for high-speed shaft-sensorless IM drives," *IEEE Trans. Ind. Electron.*, vol. 61, no. 6, pp. 3099–3108, Jun. 2014.

[79] W. Sun, K. Liu, D. Jiang and R. Ou, "Zero synchronous speed stable operation strategy for speed sensorless induction motor drive with virtual voltage injection," in *Proc. IEEE, ECCE*, Portland, OR, USA, 2018, pp. 337-343.

[80] M. S. Zaky, M. K. Metwaly, H. Z. Azazi and S. A. Deraz, "A new adaptive SMO for speed estimation of sensorless induction motor drives at zero and very low frequencies," *IEEE Trans. Ind. Electron*., vol. 65, no. 9, pp. 6901-6911, 2018.

[81] S. M. Gadoue, D. Giaouris, and J. W. Finch, "Stator current model reference adaptive systems speed estimator for regenerating-mode low-speed operation of sensorless induction motor drives," *IET Elect. Power Appl.*, vol. 7, no. 7, pp. 597–606, Aug. 2013.

[82] J. Zhang, X. Wen and X. Gao, "A new speed estimation method for vector-controlled IMs," in *Proc. IEEE ICEMS*, Jeju, South Korea, 2018, pp. 1634-1638.

[83] Y. B. Zbede, S. M. Gadoue and D. J. Atkinson, "Model predictive MRAS estimator for sensorless induction motor drives," *IEEE Trans. Ind. Electron.,* vol. 63, no. 6, pp. 3511-3521, 2016.

[84] S. Das, R. Kumar, and A. Pal, "MRAS-based speed estimation of induction motor drive utilizing machines' d- and q-circuit impedances," *IEEE Trans. Ind. Electron.,* vol. 66, no. 6, pp. 4286-4295, 2019.

[85] W. Sun, J. Gao, Y. Yu, G. Wang and D. Xu, "Robustness improvement of speed estimation in speed-sensorless induction motor drives," *IEEE Trans. Ind. Appl.* vol. 52, no. 3, pp. 2525–2536, 2016.

[86] E. Zerdali, "Adaptive Extended Kalman filter for speed-sensorless control of induction motors," *IEEE Trans. Energy Convers.*, vol. 34, no. 2, pp. 789–800, 2019.

[87] E. Zerdali, R. Yildiz, R. Inan, R. Demir and M. Barut, "Adaptive fading extended Kalman filter based speed-sensorless induction motor drive," in *Proc. IEEE ICEM*, Alexandroupoli, Greece, 2018, pp. 1367-1373.

[88] A. J. Ellison and C. J. Moore, "Acoustic noise and vibration of rotating electric machines," in *Proc. IEE*, vol. 115, no. 11, pp. 1633-1640, Nov. 1968.

[89] S. E. Zouzou, M. Sahraoui, A. Ghoggal and S. Guedidi, "Detection of inter-turn short-circuit and broken rotor bars in induction motors using the Partial Relative Indexes: Application on the MCSA," *IEEE ICEM*, Rome, Italy 2010, pp. 1-6.

[90] W. T. Thomson and D. Morrison, "On-line diagnosis of stator shorted turns in mains and inverter fed low voltage induction motors," *IET PEMD*, Sante Fe, NM, USA, 2002, pp. 122-127.

[91] P. Phumiphak and C. Chat-uthai, "Induction motor speed measurement using motor current signature analysis technique," in *Proc. IEEE ICEMS*, Tokyo, Japan, 2009, pp. 1–5.

[92] P. Pillay and Z. Xu, "Labview implementation of speed detection for mains-fed motors using motor current signature analysis," in *IEEE Power Eng. Rev.*, vol. 18, no. 6, pp. 587–594, 1998.

[93] P. Phumiphak and C. Chat-uthai, "Non-intrusive method for induction motor field efficiency estimation using on-site measurement and modified equivalent circuit," in *Proc. IEEE, ICEMS*, Sapporo, Japan, 2012, pp. 1-5.

[94] R. Blasco, M. Sumner and G.M. Asher, "Speed measurement of inverter-fed induction motors using FFT and the rotor slot harmonics," in *Proc. IET Int. Conf. on Power Electron. Variable-Speed Drives*, London, U.K. 1994, pp 470-475.

[95] A. Ferrah, K. J. Bradley and G. M. Asher, "An FFT-based novel approach to noninvasive speed measurement in induction motor drives," *IEEE Trans. Instrum. Meas*. vol. 41, no. 6, pp. 797-802, Dec. 1992.

[96] K. D. Hurst and T. G. Habetler, "Sensorless speed measurement using current harmonic spectral estimation in induction machine drives," in *Trans. Power Electron.*, vol. 11, no. 1, pp. 66-73, 1996.

[97] J. Restrepo and P. Bowler, "Analysis of induction machine slot harmonics in the TF domain," in *Proc. IEEE ICDCS.*, Caracas, Venezuela, 1995, pp. 127–130.

[98] U. A. Orji, et al., "Non-intrusive induction motor speed detection," *EIT Electr. Power Appl.*, vol. 9, no. 5, pp. 388-396, 2015.

[99] Z. Gao, L. Turner, R.S. Colby and B. Leprettre, "A Frequency Demodulation Approach to Induction Motor Speed Detection," *IEEE Trans. Ind. Appl.* vol. 47, no. 4, pp. 1632–1642, 2011.

[100] A. Bellini, G. Franceschini, and C. Tassoni, "Monitoring of induction machines by maximum covariance method for frequency tracking," *IEEE Trans. Ind. Appl.,* vol. 42, no. 1, pp. 69-78, Jan./Feb. 2006.

[101] B. Ye, M. Cirrincione, M. Pucci and G. Cirrincione, "Sensorless control of induction motors by the MSA based MUSIC technique," in *Proc. IEEE ECCE*, Montreal, QC, Canada, 2015, pp. 2192-2199.

[102] M. Sahraoui, A. J. M. Cardoso, K. Yahia and A. Ghoggal, "The use of the modified Prony's method for rotor speed estimation in squirrel cage induction motors," in *Proc. IEEE SDEMPED*, Guarda, Portugal, 2015, pp. 455-460.

[103] M. Sahraoui, A. J. M. Cardoso, K. Yahia and A. Ghoggal, "The use of the modified Prony's method for rotor speed estimation in squirrel cage induction motors," *IEEE Trans. Ind. Appl.*, vol. 52. no. 3, pp. 2194-2202, 2016.

[104] S. Nandi, S. Ahmed and H. A. Toliyat, "Detection of rotor slot and other eccentricity related harmonics in a three-phase induction motor with different rotor cages," *IEEE Trans. Energy Convers*., vol. 16, no. 3, pp. 253-260, 2001.

[105] A. G. Yepes *et al.*, "Selection criteria of multiphase induction machines for speed-sensorless drives based on rotor slot harmonics," *IEEE Trans. Ind. Electron.*, vol. 63, no. 8, pp. 4663–4673, Aug. 2016.

[106] A. G. Yepes, J. Doval-Gandoy, F. Baneira, and H. Toliyat, "Speed estimation based on rotor slot harmonics in multiphase induction machines under open-phase fault," *IEEE Trans. Power Electron.*, vol. 33, no. 9, pp. 7980–7993, Sep. 2018.

[107] B. W. Williams, J. K. Goodfellow, T. C. Green, "Sensorless speed measurement of inverter driven squirrel cage induction motors," in *Proc. IET Conf. Power Electron Variable-Speed Drive*, London, UK, 1991, pp. 297-300.

[108] T. C. Green, B. W. Williams and D. S. Schramm, "Noninvasive speed measurement of inverter driven induction motors," in *Proc. IEEE IAS*, Seattle, WA, USA, 1990, pp. 395-398.

[109] A. Gharakhani and P. Pillay, "An *in-situ* efficiency estimation technique for induction machines working with unbalanced supplies," *IEEE Trans. Energy Convers.*, vol. 27, no. 1, pp. 85–95, Mar. 2012.

[110] D. M. McNamara, B. Enayati and A.K. Ziarani, "Sensorless speed measurement of induction motors using adaptive frequency-tracking algorithm," in *Proc. IEEE IECON*, Orlando, FL, USA, 2008, pp. 1919-1924.

[111] C. P. Salomon *et al*, "Induction motor efficiency evaluation using a new concept of stator resistance," *IEEE Trans. Instrum. Meas*., vol. 64, no. 11, pp. 2908-2917, 2015.

[112] M. Arkan, "Sensorless speed estimation in induction motor drives by using the space vector angular fluctuation signal," *EIT Electr. Power Appl.*, vol. 2, no. 2, pp. 113–120, 2008.

[113] C. Wang, Z. Zhou, P. J. Unsworth, and T. O. Farrell, "Sensorless speed measurement of induction machines using short time Fourier transformation," *IEEE-SPEEDHAM*, Ischia, Italy, 2008, pp. 1114–1119.

[114] X. Song, J. Hu, J. Zhang, "Eccentricity harmonics detection-based speed estimation approach in a sensorless induction motors," *IEEE-CYBER*, Shenyang, China, 2015, pp. 1405-1410.

[115] D. Shi, P. J. Unsworth, and R. X. Gao, "Sensorless speed measurement of induction motor using hilbert transform and interpolated fast fourier transform," *IEEE Trans. Instrum. Meas.*, vol. 55, no. 1, pp. 290–299, Feb. 2006.

[116] X. Song, Z. Wang, S. Li and J. Hu, "Sensorless speed estimation of an inverter-fed induction motor using the supply-side current," *IEEE Trans. Energy Convers.*, vol. 34, no. 3, pp. 1432–1441, 2019.

[117] M. Al-Badri, P. Pillay, P. Angers, "A novel in situ efficiency estimation algorithm for three-phase induction motors operating with distorted unbalanced voltages," in *Proc. IEEE-ECCE*, Milwaukee, WI, USA, 2016, pp. 1-5.

[118] S. M. Gadoue, D. Giaouris, and J. W. Finch, "Stator current model reference adaptive systems speed estimator for regenerating-mode low-speed operation of sensorless induction motor drives," *IET Elect. Power Appl*., vol. 7, no. 7, pp. 597–606, Aug. 2013.

[119] R. Supangat, N. Ertugrul, W. Soong, D. A. Gray, C. Hansen and J. Grieger, "Estimation of the number of rotor slots and rotor speed in induction motors using current, flux or vibration signature analysis," in *AUPEC*, Melbourne, 2006.

[120] P. Pillay and Z. Xu, "Motor current signature analysis," in *Proc. IEEE IAS Annu. Meeting*, San Diego, CA, USA, 1996, vol. 1, pp. 587–594.

[121] J. Murimi, "Development of an induction motor condition monitoring test jig and fault detection strategies," M.S. thesis, Dept. Elect. Eng., Univ. of Cape Town, Cape Town, 2016.

[122] M. Dlamini, "Development of a specialised test rig for assessing the efficiency of large industrial induction machines," M.S. thesis, Dept. Elect. Eng., Univ. of Cape Town, Cape Town, 2014.

[123] M. Al-Badri, P. Pillay and P. Angers, "A novel in situ efficiency estimation algorithm for three-phase induction motors operating with distorted unbalanced voltages," *IEEE Trans. Ind. Appl.*, vol. 53, no. 6, pp. 5338-5347, 2017.

[124] M. Hafner, M. Popescu, A. Boglietti and A. Cavagnino, "Analytic modelling of inverter-fed induction machines—A practical approach for matching measurement and simulation data," in *Proc. IEEE ICEM*, Berlin, Germany, 2014, pp. 58–64.

[125] A. Boglietti, R. Bojoi, A. Cavagnino and L. Ferraris, "No-load operations of induction motors under PWM supply," in *Proc. IEEE. ISIE*, Bari, Italy, 2010, pp. 1383–1388.

[126] E. Levi, A. Lamine and A. Cavagnino, "Impact of stray load losses on vector control accuracy in current-fed induction motor drives," *IEEE Trans. Energy Convers*., vol. 21, no. 2, pp. 442-450, 2006.

[127] A. Boglietti, A. Cavagnino, L. Ferrraris and M. Lazzari, "Induction motor equivalent circuit including the stray load losses in the machine balance," *IEEE Trans. Energy Convers*., vol. 23, no. 3, pp.796-803, 2008.

[128] K. Yamazaki et al., "A novel equivalent circuit involving stray load loss and harmonic torques for high speed induction motors driven by inverters," in *Proc. IEEE IEMDC*, Niagara Falls, ON, Canada, 2011, pp. 902-907.

[129] M. N. Ansari, A. Dalal and P. Kumar, "Analysis of stray loss and its determination with equivalent circuit for double cage rotor induction motor", in *Proc. IEEE INDICON*, Mumbai, India, 2013, pp. 1-6.

[130] G. R. Slemon, "Modelling of induction machines for electric drives," *IEEE Trans. Ind. Appl.*, vol. 25, no. 6, pp. 1126–1131, Nov./Dec. 1989.

[131] S. Yamamura, AC motors for high-performance applications: analysis and control. New York, NY, USA: Marcel Dekker, 1986.

[132] M. Carraro and M. Zigliotto, "Automatic parameter identification of inverter-fed induction motors at standstill", *IEEE Trans. Ind. Electron*., vol. 61, no. 9, pp. 4605-4613, 2014.

[133] A. M. Alturas, S. M. Gadoue, B. Zahawi and M.A. Elgendy, "On the identifiability of steady-state induction machine models using external measurements", *IEEE Trans. Energy Convers.*, vol. 31, no. 1, pp. 251-259, 2016.

[134] A. V. Ivanov-Smolenski, *Electrical machines, vol. 2*. Moscow, Russia: Mir, 1984.

[135] R. Krishnan and F. C. Doran, "Study of parameter sensitivity in high performance inverter-fed induction motor drive system," *IEEE Trans. Ind. Appl*., vol. IA-23, no. 4, pp. 623-635, 1987.

[136] H. Rasmussen, M. Knudsen and M. Tonnes, "Parameter estimation of inverter and motor model at standstill using measured currents only," in *Proc. IEEE ISIE*, Piscataway, NJ. USA, 1996, pp. 331-336.

[137] T. Stefanski and L. Zawarczynski, "Parameter identification of mathematical model of inverter drive hydraulic pump with induction motor," in *Proc. IEEE MMAR*, Miedzyzdroje, Poland, 2017, pp. 959-964.

[138] J. A. Riveros, A. G. Yepes, F. Barrero, J. D-G. B. Bogado, O. Lopez, M. Jones and E. Levi, "Parameter identification of multiphase induction machines with distributed windings – Part 2: Time domain techniques," *IEEE Trans. Energy Convers*., vol. 27, no. 4, pp. 1067-1077, 2012.

[139] J. Koupeny, S. Lucke and A. Mertens, "Extended observer-based simultaneous online parameter estimation of inverter-fed squirrel-cage induction machines considering the influence of current and speed measurement errors," in *Proc. IEEE ECCE*, Karlsruhe, Germany, 2016, pp. 1-10.

[140] T. Iwasaki and T. Kataoka, "Application of an Extended Kalman filter to parameter identification of an induction motor," *in Proc. IEEE IAS*, San Diego, CA, USA, pp. 248-253.

[141] D. Bhowmick, M. Manna and S. K. Chowdhury, "Estimation of equivalent circuit parameters of transformer and induction motor from load data," *IEEE Trans. Ind. Appl.*, vol. 54, no. 3, pp. 2784-2791, 2018.

[142] D. Bhowmick, M. Manna and S. K. Chowdhury, "Improved equivalent circuit parameter estimation of induction motor using H-G diagram and PSO," in *Proc. IEEE CALCON*, Kolkata, India, 2017, pp. 443-447.

[143] D. Bhowmick, M. Manna and S. K. Chowdhury, "Online estimation and analysis of equivalent circuit parameters of three phase induction motor using particle swarm optimization," in *Proc. IEEE PIICON*, Bikaner, India, 2016, pp. 1-5.

[144] P. Nangsue, P. Pillay and S. E. Conroy, "Evolutionary algorithms for induction motor parameter determination," *IEEE Trans. Energy Convers.*, vol.14, no. 3, pp. 447-453, 1999.

[145] A. Accetta, F. Alonge, M. Cirrincione, F. D`ppolito, M. Pucci and A. Sferlazza, "GA-based off-line parameter estimation of the induction motor model including magnetic saturation and iron losses," in *Proc. IEEE ECCE*, Cincinnati, OH, USA, 2017, pp. 2420-2426.

[146] S. A. Lima, C. A. C. Wengerkievicz, N. J. Batistela, N. Sadowski, P. A. da Silva and A. Y. Beltrame, "Induction motor parameter estimation from manufacturer data using genetic algorithms and heuristic relationships," in *Proc. IEEE COBEP*, Juiz de Fora, Brazil, 2017, pp. 1-6.

[147] S. C. Sabharwal, "Methodology for estimating performance characteristics of three phase induction motor operating direct-on-line or with six pulse inverter," in *Proc. IEEE PEDES*, New Dehli, 2006, pp. 1-4.

[148] J. Li, J. Dang, Feng Bu, and J. Wang, "Analysis and improvement of the bacterial foraging optimization algorithm," *J. Comput. Sci. Eng.*, vol. 8, no. 1, pp. 1-10, 2014.

[149] K. M. Passino, "Biomimicry of bacterial foraging for distributed optimization and control," *IEEE Control Syst. Mag.*, vol. 22, no. 3, pp. 52-67, 2002.

[150] S. Baluja, "An empirical comparison of seven iterative and evolutionary function optimization heuristics," Carnegie Mellon University, Pittsburg, PA, USA, Tech. Rep. CMU-CS-95-193, 1995.

[151] J. Greene, "A role for simple, robust black-box optimisers in the evolution of engineering systems and artefacts," in *Proc. 2nd Int. GALESIA,* Sheffield, U.K., Sep. 1997, pp. 427-432.

[152] E. Hughes, "Optimisation using population based incremental learning (pbil)," in *IEE Colloquium on Optimisation in Control: Methods and Applications*, 1998.

[153] NCSS, "Harmonic regression," in *NCSS Statistical Software*, 2019, Kaysville, Utah, USA: NCSS, LCC., 2019, ch. 460, pp. 460-1–460-10. [Online]. Available: http://ncss.com/software/ncss.

[154] A. J. Zavala and A. R. Messina, "Dynamic harmonic regression approach to wind power generation forecasting," in *IEEE PES T&D-LA*, Morelia, Mexico, 2016, pp. 1-6.

[155] M. Lamichi, J.Balcells, M. Corbalan and E. Griful, "Nonlinear loads model for harmonics flow prediction, using multivariate regression," in *IEEE Trans. Ind. Electron.*, vol. 64, no. 6, pp. 4820-4827, 2017.

[156] O. Dordevic, M. Jones and E. Levi, "Analytical formulas for phase voltage rms squared and THD in PWM multiphase systems," in *IEEE Trans. Power Electron.*, vol. 30, no. 3, pp. 1645-1656, 2015.

[157] F. P. Marafao, S. M. Deckmann and J. A. G. Marafao, "Power factor analysis under nonsinusoidal and unbalanced systems," in *Proc. IEEE ICHQP*, Rio de Janeiro, Brazil, 2002, pp. 266-271.

[158] W. Marc Grady and R. J. Gilleskie, "Harmonics and how they relate to power factor," in *Proc. EPRI PQA*, San Diego, CA, 1993, pp. 1-8.

[159] L. Monjo, H. Kojooyan-Jafari, F. Corcoles and J. Pedra, "Squirrel-cage induction motor parameter estimation using a variable frequency test," *IEEE Trans. Energy Convers.*, vol. 30, no. 2, pp. 550-557, 2015.

[160] H. Van Khang, W. Pawlus and K. G. Robbersmyr, "Identification of parameters and harmonic losses of a deep-bar induction motor," in *IEEE-ICIST,* Da Nang, Vietnam, 2017, pp. 194-199.

[161] T. M. Undeland and N. Mohan, "Overmodulation and loss considerations in high-frequency modulated transistorized induction motor drives," *IEEE Trans. Power Electron.*, vol. 3, no. 4, pp. 447-452, 1988.

[162] S. Lee, J. Kim, D. An and J. Hong, "Equivalent circuit considering the harmonics of core loss in the squirrel-cage induction motor for electrical power steering application," *IEEE Trans. Magn.*, vol. 50, no. 11, pp. 1-4, 2014.

[163] N. Mohan, T. Underland and W. Robbins, Power electronics. John Wiley & Sons, Inc, 2nd ed., 1995.

[164] S. Das, A. Biswas, S. Dasgupta, et al., "Bacterial foraging optimization algorithm: theoretical foundations, analysis, and applications," in *Foundations of Computational Intelligence*, vol. 3, 2009, Berlin, Heidelberg: Springer, pp. 23-55.

[165] P. Indarack, S. Douangsyla, C. Joochim, A. Kunakorn, M. Kando and V. Kinnares, "A harmonic loss calculation of PWM-fed induction motors using loss factor characteristics," *IEEE TECON*, Chiang Mai, Thailand, 2004, pp. 236-239.

[166] S. Khomfoi, V. Kinnares and P. Viriya, "Influence of PWM characteristics on the core losses due to harmonic voltages in PWM fed induction motors," in *IEEE Proc. PES*, Singapore, Singapore, 2000, pp. 365-369.

[167] S. Khomfoi, V. Kinnares and P. Viriya, "Investigation into core losses due to harmonic voltages in PWM fed induction motors," IEEE PEDS, Hong Kong, Hong Kong, 1999, pp. 104-109.

[168] K. Bradley, W. Cao, J. Clare and P. Wheeler, "Predicting inverter-induced harmonic loss by improved harmonic injection," *IEEE Trans. Power Electron.*, vol. 23, no. 5, pp. 2619-2624, 2008.

[169] R. Antonello, F. Tinazzi and M. Zigliotto, "Energy efficiency measurements in IM: The non-trivial application of the norm IEC 60034-2-3:2013," in *Proc. IEEE-WEMDCD*, Torino, Castello del Valentino, Italy, 2015, pp. 248-253.

[170] A. Boglietti, A. Cavagnino, M. Cossale, A. Tenconi and S. Vaschetto, "Efficiency determination of converter-fed induction motors: Waiting for the IEC 60034-2-3 standard," in *Proc. IEEE-ECCE*, Colorado, CO, USA, 2013, pp. 230-237.

[171] E. B. Agamloh, S. Peele and J. Grappe, "An experimental evaluation of the effect of voltage distortion on the performance of induction motors," in *Proc. IEEE-PPIC*, Portland, OR, USA, 2012, pp. 1-7.

[172] E. B. Agamloh, "Power and efficiency measurement of motor-variable-frequency drive systems," in *IEEE Trans. Ind. Appl*., vol. 53, no. 1, pp. 766-773, 2017.

[173] M. Al-Badri, P. Pillay and P. Angers, "A novel full-load efficiency estimation technique for induction motors operating with unbalanced voltages", in *Proc. IEEE-IEMDC*, Coeur d'Alene, ID, USA, 2015, pp. 35-40.

[174] A. K. Ziarani and A. Konrad, "A method of extraction of nonstationary sinusoids," *Signal Processing*, vol. 84, pp. 1323-1346, 2004.

[175] H. Olsson, K. J. Astrom, C. C. de Wit, M. Gafvert, and P. Lischinsky, "Friction models and friction compensation," *European Journal of Control*, vol. 4, no. 3, pp. 176-95, 1998.

[176] B. Lu, W. Cao, T.G Habetler, "Error analysis of motor-efficiency estimation and measurement," in *Proc. IEEE PESC*, Orlando, FL, USA, 2007.

A. APPENDIX A

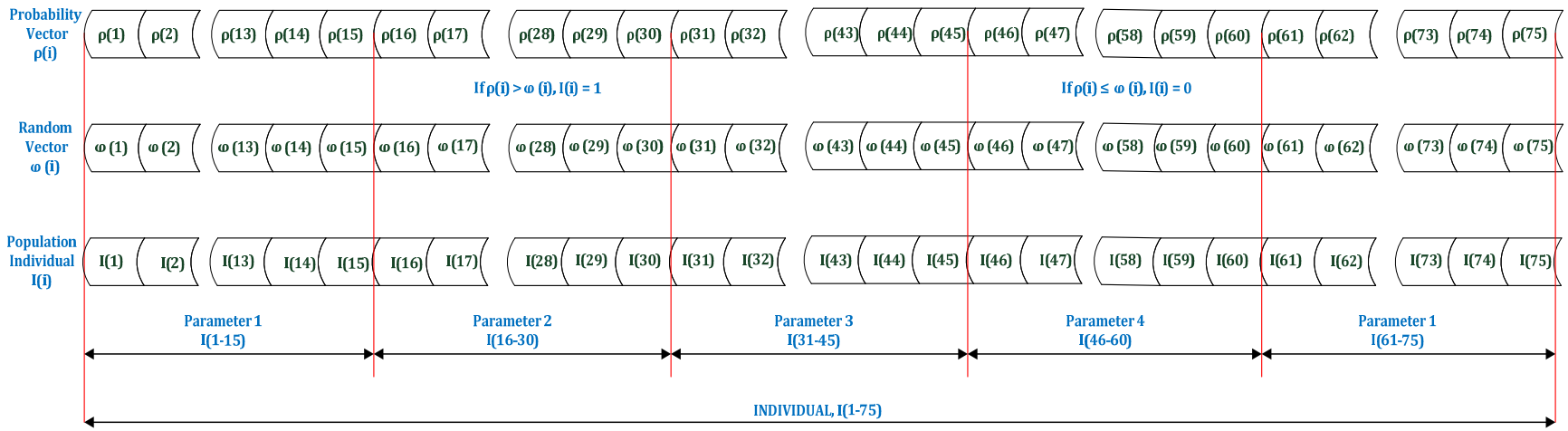

Figure A-1. Generating a population individual.

B. APPENDIX B

Table B-1. Speed estimation test results using different analysis techniques for the 37kW and 45kW inverter-fed IMs.

250W Motor (Grid and Inverter Supply)									
				Analysis Method					
Pwr	**Measured (rpm)**	**Vibration (rpm)**	**|Error| (%)**	**RSH (rpm)**	**|Error| (%)**	**MCSA (rpm)**	**|Error| (%)**	**REH (rpm)**	**|Error| (%)**
Grid	2955.653	2956.100	0.015	2955.500	0.005	2956.100	0.015	2951.700	0.134
Inv.	2956.093	2957.500	0.048	2946.400	0.328	2939.900	0.548	2939.900	0.548

Table B-2. Speed estimation test results using different analysis techniques for the 37kW and 45kW inverter-fed IMs.

37kW Motor (Inverter Supply)							
		Analysis Method					
% Load	**Measured (rpm)**	**RSH (rpm)**	**|Error| (%)**	**MCSA (rpm)**	**|Error| (%)**	**REH (rpm)**	**|Error| (%)**
25	1493.2169	1493.1999	0.0011	1490.5920	0.1758	1490.476	0.1836
50	1487.0195	1486.9351	0.0057	1489.1640	0.1442	1489.200	0.1466
75	1480.5651	1480.1239	0.0298	1483.440	0.1942	1481.7900	0.0827
100	1473.5015	1473.931	0.0291	1479.150	0.3833	1476.0720	0.1744
125	1469.1745	1469.1772	0.0002	1467.7020	0.1002	1468.9200	0.0173
150	1466.1825	1466.1681	0.0010	1469.1360	0.2014	1467.4860	0.0889

45kW Motor (Inverter Supply)							
		Analysis Method					
% Load	**Measured (rpm)**	**RSH (rpm)**	**|Error| (%)**	**MCSA (rpm)**	**|Error| (%)**	**REH (rpm)**	**|Error| (%)**
25	1493.7452	1493.0518	0.0464	1490.5920	0.21110	1490.3760	0.2256
50	1487.9918	1487.3793	0.0412	1487.7300	0.01760	1488.9480	0.0643
75	1481.9305	1481.5868	0.0232	1483.4400	0.10190	1483.2240	0.0873
100	1475.4689	1476.4283	0.0650	1477.7160	0.15230	1474.6380	0.0563
110	1472.6645	1472.4820	0.0124	1474.8600	0.14910	1468.9200	0.2543

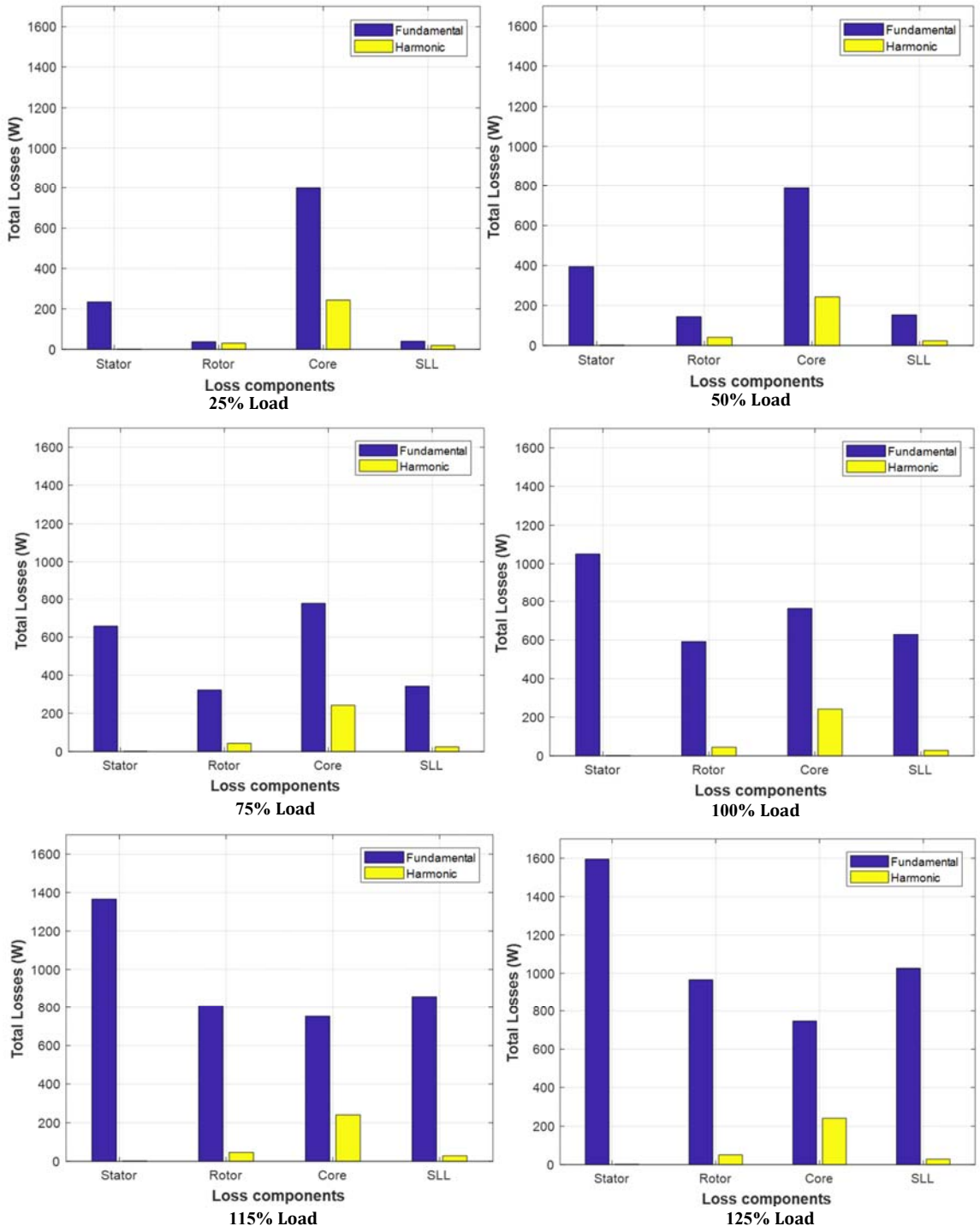

Figure B-1. Segregation of harmonic losses compared to the fundamental loss at different load points for the 37kW motor using NIEE-PWM-HARM technique.

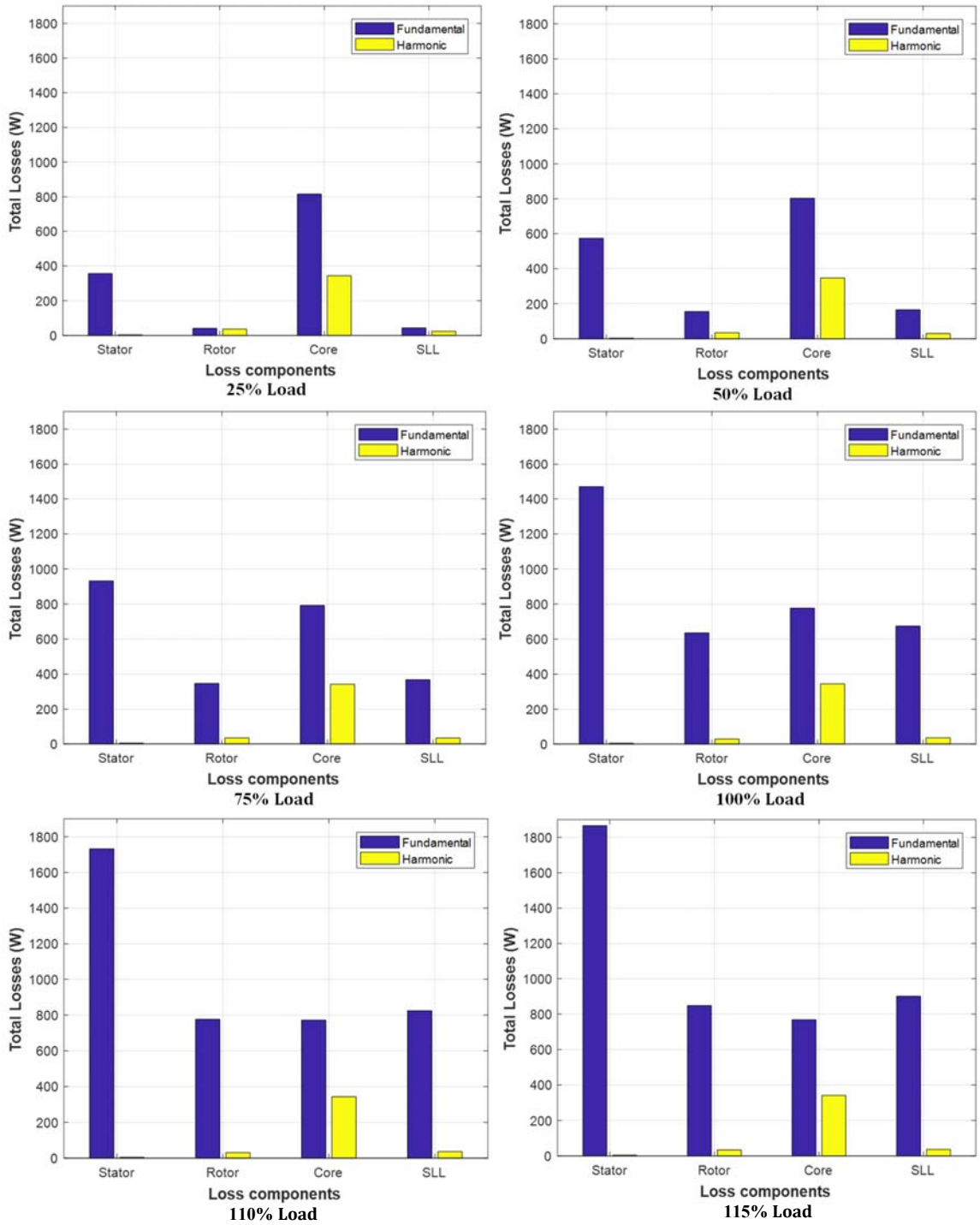

Figure B-2. Segregation of harmonic losses compared to the fundamental loss at different load points for the 37kW motor using NIEE-PWM-HARM technique.

Table B-3. Segregation of harmonic losses at different load points for the 37kW motor using NIEE-PWM-HARM technique.

% Load	Stator Harmonic Loss (W)	Rotor Harmonic Loss (W)	Core Harmonic Loss (W)	Stray-Load Harmonic Loss (W)	Total Harmonic Loss (W)
25	1.8175	30.4044	243.2967	18.5852	294.1038
50	2.1185	40.745	242.8202	22.7227	308.4064
75	2.2924	43.1854	242.1519	24.6568	312.2865
100	2.4276	44.7962	241.9196	27.6965	316.8399
115	2.533	46.3763	241.7248	28.1425	318.7766
125	2.5971	50.5476	241.582	28.4478	323.1745

Table B-4. Segregation of harmonic losses at different load points for the 45kW motor using NIEE-PWM-HARM technique.

% Load	Stator Harmonic Loss (W)	Rotor Harmonic Loss (W)	Core Harmonic Loss (W)	Stray-Load Harmonic Loss (W)	Total Harmonic Loss (W)
25	3.2301	36.0788	343.933	24.1518	407.3937
50	3.7441	34.6475	346.925	29.9094	415.226
75	4.059	34.2332	341.8476	33.3385	413.4783
100	4.2527	27.9534	344.7093	35.8267	412.7421
110	4.305	30.6863	343.3449	36.0134	414.3496
115	4.3242	33.6495	341.6867	36.6883	416.3487

Table B-5. Comparison of losses and efficiency errors among the different techniques at different load points for the 37kW motor.

Technique	Load (%)	Total Fundamental Loss (W)	Total Harmonic Loss (W)	Total Loss (W)	Efficiency (% Error)
NIEE-PWM-RMS	25	1606.700	483.300	2090.000	1.45
	50	2021.600	479.700	2501.300	1.09
	75	2718.100	474.200	3192.300	1.19
	100	3759.700	465.000	4224.700	1.26
	115	4592.500	456.800	5049.300	1.25
	125	5197.500	450.500	5648.000	1.25
NIEE-PWM-HARM	25	1605.100	294.104	1899.204	0.56
	50	1970.300	308.406	2278.706	0.10
	75	2587.400	312.287	2899.687	0.25
	100	3516.400	316.840	3833.240	0.26
	115	4264.700	318.777	4583.477	0.22
	125	4811.000	323.175	5134.175	0.19
IEC-TS 60034-2-3	25	1585.555	484.808	2094.644	1.23
	50	1956.135	467.854	2445.439	0.66
	75	2598.302	436.191	3042.358	0.54
	100	3551.125	392.128	3927.235	0.41
	115	4256.060	369.578	4635.879	0.28
	125	4826.803	345.758	5161.773	0.24

Table B-6. Comparison of losses and efficiency errors among the different techniques at different load points for the 45kW motor.

Technique	Load (%)	Total Fundamental Loss (W)	Total Harmonic Loss (W)	Total Loss (W)	Efficiency (% Error)
NIEE-PWM-RMS	25	1782.500	488.500	2271.000	1.36
	50	2248.700	479.500	2728.200	0.30
	75	3028.000	468.900	3496.900	0.43
	100	4203.300	460.500	4663.800	0.52
	115	4774.100	459.900	5234.000	0.54
	125	5065.500	460.600	5526.100	0.74
NIEE-PWM-HARM	25	1854.300	407.390	2261.690	1.47
	50	2292.400	415.230	2707.630	0.41
	75	3028.200	413.980	3442.180	0.25
	100	4142.400	412.740	4555.140	0.26
	115	4687.300	414.350	5101.650	0.25
	125	4965.300	416.350	5381.650	0.44
IEC-TS 60034-2-3	25	1713.065	539.491	2276.104	1.32
	50	2100.042	540.509	2659.065	0.57
	75	2764.716	539.015	3316.920	0.15
	100	3755.703	538.118	4306.577	0.31
	115	4214.237	539.552	4790.943	0.41
	125	4489.956	537.627	5042.665	0.24

```
function harmonic_loss_estimation()
 clc
 %% load harmonic data
data = load('harmonic_data_file');
 %% machine data structure
data.Voltage = data.Harm_Voltage;
data.Current = data.Harm_Current;
data.PF = data.Harm_PF;
data.Speed = data.Speed;
data.Harm_Order = data.Harm_Order;
data.Pfw_config = 1;
data.T_amb = T_amb;
data.slip_rated = slip_rated;
data.Rr_material = rotor_material;
data.V_rated = voltage_rated;
data.I_rated = current_rated/sqrt(3);
data.PF_rated = PF_rated; %rated power factor
data.Pin_rated = 3*data.V_rated*data.I_rated*data.PF_rated;
data.P_fw_rated = 0.012*data.Pin_rated;
data.K_fw = data.P_fw_rated/((speed_rated*2*pi/60)^2);

%% Initialise harmonic parameter values
Rm_values = zeros(1,length(data.Harm_Order)-1);
Rr_values = zeros(1,length(data.Harm_Order)-1);
Xr_values = zeros(1,length(data.Harm_Order)-1);
% Fundamental parameters from separate algorithm or measured
fund_parameters = [Rs,Xs,Xm,Rm,Rr];
B = core_loss_constant; % core loss constant from harmonic loss curve
f = data.Freq(1); % operating frequency
```

```
Pcore = 0; % initialise harmonic core loss
 %% calculate total harmonic core loss
for k=2:length(data.Harm_Order)-1
   Pcr(k) = 3*((B*data.Voltage(k)^2)/(data.Harm_Order(k)*f)^0.32)/1000;
   Pcore = Pcore + Pcr(k);
end
  %% harmonic parameter estimation
for harm_index = 0:(length(data.Harm_Order)-2)
   Rm_values(harm_index+1) = ((data.Voltage(harm_index+2))^2)/(Pcore/3);
   fund_parameters_bfo = [Rs,Xs,Xm,Rm_values(harm_index+1),Rr];
    %% get harmonic parameters
   [BFO_solution] = BFO(data, Rr_material, harm_index+2, fund_parameters_bfo);
    Rr_values(harm_index+1) = BFO_solution(1);
    Xr_values(harm_index+1) = BFO_solution(2);
end
 Rm_values = abs(Rm_values');
Rr_values = abs(Rr_values');
Xr_values = abs(Xr_values');


%% upload harmonic parameters to data structure
data.Rm = Rm_values;
data.Rr = Rr_values;
data.Xr = Xr_values;
 %% perform fundamental and harmonic loss analysis
for harm_indx = 0:(length(data.Harm_Order)-1)
   if ~harm_indx
     [P_fund] = fundamental_loss_analysis(data,fund_parameters);
   else
     P_harm(harm_indx) = harmonic_loss_analysis(data,fund_parameters,harm_indx+1);
   end
```

```
end
 %% initialise harmonic loss variables
Ph1_Loss_Tot = zeros(1,1);  %  harmonic loss
Ph1_CuS = zeros(1,1);       %  harmonic stator loss
Ph1_CuR = zeros(1,1);       %  harmonic rotor loss
Ph1_C = zeros(1,1);         %  harmonic core loss
Ph1_SLL = zeros(1,1);       %  harmonic stray load loss loss
 %% obtain segregation of harmonic losses
for i = 1:(length(data.Harm_Order)-1)
   Ph1_CuS = Ph1_CuS + P_harm(i).CuS;
   Ph1_CuR = Ph1_CuR + P_harm(i).CuR;
   Ph1_C = Ph1_C + P_harm(i).C;
   Ph1_SLL = Ph1_SLL + P_harm(i).SLL;
   Ph1_Loss_Tot = Ph1_Loss_Tot + P_harm(i).P_Loss_Tot;
end
 eff_fund = 100*(data.Pin(1) - P_fund.P_Loss_Tot)/data.Pin(1); % fundamental efficiency
eff = 100*(data.Pin(1) - (P_fund.P_Loss_Tot+Ph1_Loss_Tot))/data.Pin(1); % efficiency
```

```
%%-------------------------------------------------------------------------------------------------------
% Rolando Gonzales
% Bayesian Institute for Research on Development
% (http://www.bayesgroup.org)
% November, 2015
% Adapted by Mathews Chirindo
% January 2020
% Bacterial Foraging Algorithm function
%%-------------------------------------------------------------------------------------------------------
function [solution] = BFO(machine_data, rotor_material,harm_indx,PBIL_params)
 % (1)Initialization
n  =  2;          % Dimension of search space
S  = 60;          % Number of bacteria in the colony
Nc = 25;          % Number of chemotactic steps
Ns =  4;          % Number of swim steps
Nre=  4;          % Number of reproductive steps
Ned=  2;          % Number of elimination and dispersal steps
Sr =S/2;          % The number of bacteria reproductions (splits) per generation
Ped=0.5;          % The probability that each bacteria will be eliminated/dispersed
c(:,1)=0.05*ones(S,1);   % the run length unit (the size of the step taken in each run or
                                  tumble)
 % Initial positions
for m=1:S
   B(1,:,1,1,1)= 10*rand(S,1)';
   B(2,:,1,1,1)= 10*rand(S,1)';
 end
 %% Loops
% (2) Elimination-dispersal loop
for l = 1:Ned
   % (3) Reproduction loop
   for k = 1:Nre
```

```
    % (4) Chemotaxis (swim/tumble) loop
    for j=1:Nc
      % (4.1) Chemotatic step
      for i=1:S
        % (4.2) Fitness function
        J(i,j,k,l) = fitnessBFO(B(:,i,j,k,l),machine_data,rotor_material,harm_indx,
                    PBIL_params);
        % (4.3) Jlast
        Jlast=J(i,j,k,l);
        % (4.4) Tumble
        Delta(:,i) = unifrnd(-1,1,n,1);
        % (4.5) Move
        B(:,i,j+1,k,l)=B(:,i,j,k,l)+c(i,k)*Delta(:,i)/sqrt(Delta(:,i)'*Delta(:,i));
        % (4.6) New fitness function
        J(i,j+1,k,l)=fitnessBFO(B(:,i,j+1,k,l),machine_data,rotor_material,harm_indx,
                     PBIL_params);
        % (4.7) Swimming
        m=0; % counter for swim length
        while m < Ns
          m=m+1;
          if J(i,j+1,k,l)<Jlast
            Jlast=J(i,j+1,k,l);
            B(:,i,j+1,k,l)=B(:,i,j+1,k,l)+c(i,k)*Delta(:,i)/sqrt(Delta(:,i)'*Delta(:,i)) ;
J(i,j+1,k,l)=fitnessBFO(B(:,i,j+1,k,l),machine_data,rotor_material,harm_indx,PBIL_params);
          else
            m=Ns;
          end
        end
        J(i,j,k,l)=Jlast; %???
      end % (4.8) Next bacterium
      x = B(1,:,j,k,l);
```

```
        y = B(2,:,j,k,l);

    end % (5) if j < Nc, chemotaxis
    % (6) Reproduction
    % (6.1) Health
    Jhealth=sum(J(:,:,k,l),2);     % Set the health of each of the S bacteria
    [Jhealth,sortind]=sort(Jhealth);% Sorts bacteria in order of ascending values
    B(:,:,1,k+1,l)=B(:,sortind,Nc+1,k,l);
    c(:,k+1)=c(sortind,k);         % Keeps the chemotaxis parameters with each bacterium at
                                       the next generation
    % (6.2) Split the bacteria
    for i=1:Sr % Sr??
        B(:,i+Sr,1,k+1,l)=B(:,i,1,k+1,l); % The least fit do not reproduce, the most fit ones
                                              split into two identical copies
        c(i+Sr,k+1)=c(i,k+1);
    end
  end % (7) Loop to go to the next reproductive step
  % (8) Elimination-dispersal
    for m=1:S
      if  Ped>rand % % Generate random number
        B(1,:,1,1,1)= 50*rand(S,1)';
        B(2,:,1,1,1)= .2*rand(S,1)';
       %   B(3,:,1,1,1)= .2*rand(S,1)';
      else
        B(:,m,1,1,l+1)=B(:,m,1,Nre+1,l); % Bacteria that are not dispersed
      end
    end
end
%% Results
      reproduction = J(:,1:Nc,Nre,Ned);
```

```
        [jlastreproduction,O] = min(reproduction,[],3);  % min cost function for each
bacterial
        [Y,I] = min(jlastreproduction);
        pbest = B(:,I,O(I,:),k,l);
        solution = pbest;
%%-------------------------------------------------------------------------------------------------------
% Fitness test function
%%-------------------------------------------------------------------------------------------------------
function J = fitnessBFO(v, machine,rr_material,harmonic_indx,fund_base_params)
%% fundamental parameters
R1 = fund_base_params(1);
X1 = fund_base_params(2)*1i;
Xm = fund_base_params(3)*1i;
Rm = fund_base_params(4);
R2 = fund_base_params(5);
%% v is a vector with two estimated harmonic parameters
R2_harm = v(1);
X2_harm = v(2)*1i;
if rr_material
  machine.rr_material = 234.5;   %  copper
else
  machine.rr_material = 225;     %  Aluminium
end
 %% getting values for fitness test
machine.T_FL_rated = FL_temp_rated; %full load temperature rated
machine.T_amb = T_amb;
machine.slip_rated = slip_rated;
 Rsll = 0.018*R2 * (1-machine.slip_rated)/machine.slip_rated;
 Freq = machine.Freq(1);
n_sync = 30*Freq;
slip = (n_sync - machine.Speed(1))/n_sync;
```

```
V_harm = machine.Voltage(harmonic_indx);
I_harm = machine.Current(harmonic_indx);
Angle_harm = acos(machine.PF(harmonic_indx));
Harm_Order = machine.Harm_Order(harmonic_indx);
%% calculated harmonic impedance
Z_harm_cal = (V_harm/(I_harm/sqrt(3)))*(cos(Angle_harm) + 1i*sin(Angle_harm));

index = harmonic_indx-1;
 %% harmonic slip for harmonics of interest
if mod(index,2)
  slip_harm = (Harm_Order+(1-slip))/Harm_Order;
 else
   slip_harm = (Harm_Order-(1-slip))/Harm_Order;
 end

Rsll_harm = Harm_Order^0.8*Rsll;
Zs = R1 + (Harm_Order*X1);
Zr = R2_harm + (R2_harm*(1-slip_harm)/slip_harm) + Rsll_harm + X2_harm;
Zm = (Rm*(Harm_Order*Xm))/(Rm+(Harm_Order*Xm));
%% estimated harmonic impedance
Z_harm_est = Zs + ((Zm*Zr)/(Zm+Zr));
%% minimum J fitness
J = abs((Z_harm_est/ Z_harm_cal)-1)^2;

%%-------------------------------------------------------------------------------------------------------------
% Fundamental loss analysis function
%%-------------------------------------------------------------------------------------------------------------
 function [P] = fundamental_loss_analysis(M_data,PBIL_base_prms)
%% fundamental parameters
R_1 = PBIL_base_prms(1);
X_1 = PBIL_base_prms(2)*1i;
```

```
X_m = PBIL_base_prms(3)*1i;
R_m = PBIL_base_prms(4);
R_2 = PBIL_base_prms(5);
 %%  initialise loss variables
P.P_Loss_Tot = zeros(1,1);
P.CuS = zeros(1,1);
P.CuR = zeros(1,1);
P.C = zeros(1,1);
P.SLL = zeros(1,1);
P.FW = zeros(1,1);

X_2 = X_1;
Frequency = M_data.Freq; % operating frequency
Speed = M_data.Speed;  % operating speed
n_sync1 = 30*Frequency(1); % synchronous speed
s = (n_sync1 - Speed(1))/n_sync1;
V_ph = M_data.Voltage(1);
Rssl = 0.018*R_2*(1-M_data.slip_rated)/M_data.slip_rated;
%% motor impedances
Z_s = R_1 + X_1;
Z_r = R_2 + (R_2*(1-s)/s) + Rssl + X_2;
Z_m = (R_m*X_m)/(R_m+X_m);
%% motor admittances
Ys = 1/Z_s;
Yr = 1/Z_r;
Ym = 1/Z_m;
%% motor currents
Is = abs((V_ph*Ys*(Ym+Yr))/(Ys+Ym+Yr));
Is = Is*sqrt(3);
Ir = abs((V_ph*Ys*Yr)/(Ys+Ym+Yr));
Im = abs((V_ph*Ys*Ym)/(Ys+Ym+Yr));
```

```
Pm_loss = (Im^2)*(real(Z_m));

%% friction and windage loss
if M_data.Pfw_config
  P_FW = (M_data.K_fw*((M_data.Speed(1)*2*pi/60)^2));
else
  P_FW = 0.012 * M_data.Pin(1);
end
%% motor losses
P.CuS = 1.5*((Is^2)*(R_1));
P.CuR = 3*((Ir^2)*(R_2));
P.C = 3*(Pm_loss);
P.SLL = 3*((Ir^2)*(Rssl));
P.FW = P_FW;
P.P_Loss_Tot = P.CuS + P.CuR + P.C + P.SLL + P.FW;

%%-------------------------------------------------------------------------------------------------------------
% Harmonic loss analysis function
%%-------------------------------------------------------------------------------------------------------------
 function [Ph] = harmonic_loss_analysis(h_data,fund_b_prms,h_index)
 %% fundamental parameters
R_1 = fund_b_prms(1);
X_m = fund_b_prms(3)*1i;
R_2 = fund_b_prms(5);
 %% initialise loss variables
Ph.P_Loss_Tot = zeros(1,length(h_data.Current));
Ph.CuS = zeros(1,length(h_data.Current));
Ph.CuR = zeros(1,length(h_data.Current));
Ph.C = zeros(1,length(h_data.Current));
Ph.SLL = zeros(1,length(h_data.Current));
```

```
%% getting data for harmonic loss analysis
Frequency = h_data.Freq; % operating frequency
Speed = h_data.Speed;  % operating speed
Rsll = 0.018*R_2*(1-h_data.slip_rated)/h_data.slip_rated;
 n_sync1 = 30*Frequency(1);  % synchronous speed
s = (n_sync1 - Speed(1))/n_sync1;  % slip
V_ph = h_data.Voltage(h_index);
Is = h_data.Current(h_index);
Harm_Order = h_data.Harm_Order(h_index);
R_m =h_data.Rm(h_index-1);
R2_rn = h_data.Rr(h_index-1);
X2_harm = h_data.Xr(h_index-1);
 %% harmonic slip for harmonics of interest
index = h_index-1;
 if mod(index,2)
   slip_harm = (Harm_Order+(1-s))/Harm_Order;
 else
    slip_harm = (Harm_Order-(1-s))/Harm_Order;
 end

Rsll_harm = Harm_Order^0.8*Rsll;
 %% harmonic impedance
Z_r = R2_rn + (R2_rn*(1-slip_harm)/slip_harm) + Rsll_harm + X2_harm;
Z_m = (R_m*(Harm_Order*X_m))/(R_m+(Harm_Order*X_m));
 %% harmonic currents
I_ph = Is/sqrt(3);
Ir = abs(I_ph*(Z_m/(Z_m+Z_r)));
%% harmonic losses
Ph.CuS = 1.5*((Is^2)*(R_1));
Ph.CuR = 3*((Ir^2)*(R2_rn));
Ph.C =  3*((26.98*V_ph^2)/(Harm_Order*Frequency(1))^0.32)/1000;
```

```
Ph.SLL = 3*((Ir^2)*(Rsll_harm));
Ph.P_Loss_Tot = Ph.CuS + Ph.CuR + Ph.C + Ph.SLL;
```